ACOUSTIC SENSING FOR METAL TRANSFER MODE AND PENETRATION STATE CLASSIFICATION OF GMAW USING ARTIFICIAL NEURAL NETWORKS

An investigation of the acoustic response of GMAW's capabilities within machine learning-based weld quality monitoring

By

Anders Bidstrup

Master thesis
M.Sc. Manufacturing Technology
Aalborg University

AALBORG UNIVERSITY
STUDENT REPORT

MAIN REPORT

AALBORG UNIVERSITY
STUDENT REPORT

Study Board of Industry and Global Business Development
Fibigerstræde 16
DK - 9220 Aalborg Øst
Tlf. 99 40 93 09
ift@m-tech.aau.dk
www.en.ses.aau.dk

Title:
Acoustic sensing for metal transfer mode and penetration state classification of GMAW using artificial neural networks

Semester:
VT-4

Project period:
February 2017 - June 2017

ECTS:
30

Anders Bidstrup

Supervisors:
Simon Bøgh
Casper Schou

Censor:
Peter Vangsø Jeberg

Pages: *79*
Appendix: *29*
Enclosures: *2 pcs.*

Synopsis

This report covers a study of the acoustic response of GMAW's capabilities within machine learning-based weld quality monitoring. Initially it is determined to train an artificial neural network, ANN, to classify two metal transfer modes - globular transfer and short-circuit transfer - and three penetration states - lack of penetration, full penetration and excessive penetration - based on related work. To do so, 1166 features are extracted for each window of acoustic signal consisting of a range of temporal-, spectral shape-, harmonic- and perceptual features as well as statistical features from a wavelet packet decomposition.
Classification data is produced in a robotic GMAW cell by provoking the desired classification states. The acquired data is then preprocessed and input to a function made to train 110 ANN configurations for 15 combinations of window size and overlap using both gradient descent with adaptive learning rate, GDA, and scaled conjugate gradient, SCG, descent.
Based on the trained ANNs it was concluded that classification of the three penetration states was possible for ANNs trained using SCG and partially possible if they are trained using GDA. Furthermore, the results for whether classification of metal transfer mode is possible were inconclusive but showed a tendency of correct prediction.

Preface

This report documents the project composed by Anders Bidstrup at the 4^{th} semester on the master program in Manufacturing Technology at Aalborg University during the period from the 1^{st} of February 2017 to the 2^{nd} of June 2017.

This being the master thesis, the author has to demonstrate his/her ability to solve industrial or scientific problems within manufacturing engineering and technology. To accomplish this, research is done on a problem combining concepts within the fields of digital signal processing, machine learning and welding where the acoustic signal of gas metal arc welding's capabilities within weld quality monitoring is investigated.

Reading guide Through the report source references in the form of the Harvard method will appear and these are all listed at the back of the report. References from books, homepages or the like will appear with the last name of the author and the year of publication in the form of [Author, Year].

Figures and tables in the report are numbered according to the respective chapter. In this way the first figure in chapter 3 has number 3.1, the second number 3.2 and so on. Explanatory text is found under the given figures and tables. Figures without references are composed by Anders Bidstrup.

Dansk resumé

I denne rapport er der foretaget et studie af MIG/MAG-svejsnings akustiske respons med henblik på at fastslå dets evner inden for kvalitetsmonitorering af svejsning.

Baseret på et litteraturstudie, er det indledningssvist bestemt, at et neuralt netværk skal trænes til at klassificere to typer af materialeoverførsel - dråbeoverførsel og kortslutningsoverførsel - og tre gennembrændingsniveauer - mangelfuld gennembrænding, fuld gennembrænding og overdreven gennembrænding. For at gøre dette er 1166 karakteristika udregnet for hvert vindue af et akustisk signal. Disse karakteristika består af en række tidsmæssige-, spektrale-, harmoniske- og perceptuelle karakteristika såvel som statistiske karakteriska fra en *wavelet packet decomposition*.

Klassifikationsdataen er produceret ved hjælp af en MIG/MAG robotcelle ved at fremprovokere de ønskede klasser. Den opsamlede data er herefter pre-processeret og brugt som input i en funktion til træning af de neurale netværk. Denne træner 110 forskellige neurale netværk for 15 kombinationer af vinduesstørrelse og overlap ved brug af både *gradient descent with adaptive learning rate*, GDA, og *scaled conjugate gradient descent*, SCG.

Baseret på de trænede neurale netværk blev det konkluderet, at klassifikation af de tre gennembrændingsniveauer er muligt ved brug af neurale netværk optimeret med SCG. Samtidig er det konkluderet, at samme klassifikation er delvis mulig ved brug af neurale netværk optimeret med GDA. Derudover var resultaterne ufyldestgørende for, hvorvidt klassifikation af materialeoverførsel er mulig. De trænede neurale netværk viste dog en tendens til at kunne forudsige de korrekte klasser.

Table of contents

Nomenclature

Abbreviations:

Abbr.	Explanation
AAU	Aalborg University
GMAW	Gas metal arc welding
GTAW	Gas tungsten arc welding
SMAW	Shielded metal arc welding
CTWD	Contact tip to work piece distance
WFS	Wire feed speed
MK	Associate Professor Morten Kristiansen
GP	Geoffrey Peeters
ADC	Analogue to digital converter
DAC	Digital to analogue converter
DSP	Digital signal processing
FFT	Fast fourier transform
PSD	Power spectral density
IFFT	Inverse fast fourier transform
MFC	Mel frequency cepstrum
DCT	Discrete cosine transform
MFCC	Mel frequency cepstrum coefficients
ZCR	Zero crossing rate
GDA	Gradient descent with adaptive learnin rate
SCG	Scaled conjugate gradient
FS	Feature scaling
TH	Threshold
PCA	Principle component analysis
IIR	Infinite impulse response
FIR	Finite impulse response
ANN	Artificial neural network
VI	Virtual instrument
KISS	"Keep it simple and sequential"
WPD	Wavelet packet decomposition
GD	Gradient descent
SCG	Scaled conjugate gradient descent
BC	Best configuration
ACC	Accuracy

Symbols:

Symbol	Explanation	Unit
T	Period	-
f	Frequency	Hz
N	Number of...	-
SPL	Sound pressure level	dB
P	Pressure	Pa
U	Voltage	V
I	Current	A
t	Time	s
L	Litre	L
s	Second	s
min	Minute	min
m	Meter	m
mm	Millimetre	mm
σ	Standard deviation	-
n	Number of..	-
h	Hypothesis	-
x	Input	-
y	Output	-
J	Cost function	-
θ	Parameters/weights	-
a	Activation of neuron	-
z	Neural input	-
g	Sigmoid function	-
Sm	Softmax function	-
L	Total number of layers	-
K	Number of neurons in previous layer	-
I	Number of neurons in current layer	-
$\mathcal{L}$	Likelihood	-
P	Probability	-
δ	Neural error	-
Δ	Partial derivative accumulator	-
D	ANN partial derivative matrix	-
λ	Regularisation constant	-
(1)	Class 1	-
(2)	Class 2	-
(3)	Class 3	-
w_{size}	Window size	s
w_o	Overlap	%

Introduction

In turn with the rise of the global market, the pressure for western manufacturers to perform has increased. The entry of manufacturing companies based in countries with lower production costs has lowered the prices of products and forced western manufacturing companies to either relocate, outsource parts of their production or in other ways reduce their production cost. Consequently business philosophies have surfaced to aid in the fight for competitiveness often focusing on eliminating waste in the form of time and materials leading to an increased demand for process monitoring and control.

In order to perform control of a process effectively a monitoring model of the given system is developed to produce reference values for the process stability. Developing this model can be time consuming requiring extensive knowledge about the given process as well as about general process modelling within the fields the given process. The alternative comes with the rise of machine learning. Through mathematical algorithms a computer can automate the process modelling making a previously tedious and expensive task doable with data analytics and programming as the only prerequisites for a wide range of applications.

As one of the primary joining processes, welding plays a significant role in the manufacturing industry. Especially gas metal arc welding, henceforth GMAW, has due to its capability for automation, versatility, speed and low cost found its place as the most used welding process in industry. Therefore it would be advantageous for the industry to be able to monitor and control the GMAW process. However, the process involves many sources of variance making the traditional modelling method ineffective and has over the years therefore lead to the use of machine learning. As early as around year 2000 papers document that voltage and current monitoring in combination with machine learning algorithms made it possibly to identify penetration status in GMAW [Di et al., 2000] [Feng et al., 2002]. Alongside the continuous improvement of technology the feature space started to include more process features including features based on human sense mimicking. It is intuitively understandable that welders rely on their sight and touch to perform a job. This has inspired researches to develop machine vision for welding applications to monitor aspects such as the molten pool of material [Baskoro et al., 2011], seam geometry [Xiuping et al., 2014] etc. Less intuitively is the fact that welders' performance rely on their auditory sense, which was not properly investigated until a study by Joseph Tam and Jan Huissoon in 2005, which proved a correlation [Tam and Huissoon, 2005]. Consequently research regarding the use of the acoustic signal of welding processes for quality monitoring has surfaced.

In this report the acoustic response of GMAW's capabilities in machine learning-based weld quality monitoring is investigated.

1 Welding theory

In this chapter basic welding theory and an explanation of the GMAW process is presented. Furthermore *ISO-5817: Welding - Fusion-welded joints in steel, nickel, titanium and their alloys (beam welding excluded) - Quality levels for imperfections* is presented alongside an explanation of how the process variance is controlled in manual GMAW.

1.1 The GMAW process

In this section the basics of GMAW is presented.

1.1.1 Equipment and terminology

In order to explain how GMAW works, it is necessary to be familiar with the general equipment used in the process and its related terms. The following list of equipment is provided alongside figure 1.1 to provide an idea of the setup.

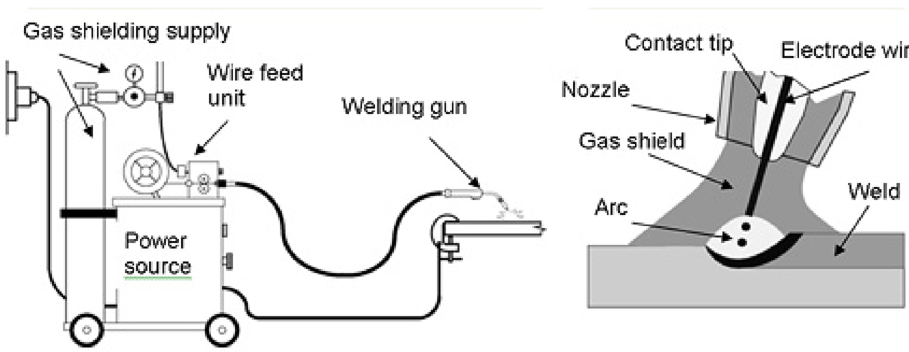

Figure 1.1: The required setup to perform gas metal arc welding [Hera, 2017].

- **Arc**
  An electric arc is a heat generating electrical discharge between an anode and catode separated by a layer of gas.
- **Work piece**
  The work pieces of a welding process are the pieces of metal to be joined and function as the catode in the creation of the electric arc.
- **Electrode wire**
  The electrode wire serves as both the anode in the creation of the electric arc and as the filler material of the weld.
- **Weld**
  The weld refers to the created joint between two work pieces.

- **Gas shield**
  The gas shield is provided to protect the molten weld pool from mainly oxygen and water vapour.
- **Welding gun**
  The welding gun is what the welder controls during the welding process, hereby determining the position of the weld as well as when to activate and deactivate gas flow and wire feed.
- **Nozzle**
  The end of the welding gun is denoted the nozzle. It supplies the wire electrode as well as the gas for the gas shield.
- **Wire feed unit**
  The wire feed unit supplies the welding gun with a continuous flow of electrode wire.
- **Gas shielding supply**
  The gas shielding supply supplies the welding gun with a continuous flow of shielding gas.
- **Power source**
  The power source supplies the electric current needed to create the arc.

To gain an understanding as to how the equipment works together to produce a weld, a process description is given.

1.1.2 Process description

In order for a weld to be generated during GMAW, an arc needs to be struck. This happens by providing the work piece with an electric current and creating contact with the wire electrode fed by the welding gun. The heat generated by the arc melts the wire electrode which causes a material transfer to take place. Since the arc also heats up part of the work piece a molten weld pool is created consisting of both work piece and filler material. Once cooled, the filler material has melted together with part of each work piece hereby creating the joint known as a weld.

As suggested by the name, the process includes the use of gas. To be specific, an inert or semi-inert gas is used to shield the molten weld pool mainly from oxygen and water vapour. The gas is provided by an external supply, feeding it to the welding gun that through the nozzle creates the wanted atmosphere around the weld.

1.1.3 Types of welds

When speaking of types of welds, the topic can be divided into two areas - joint type and weld groove type.

The joint type refers to how the two work pieces are going to be joined and is because of this rarely an aspect to be changed after the product design is fixed. A selection of the most common joint types is shown on figure 1.2.

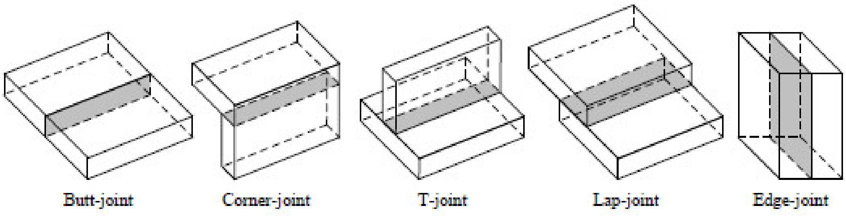

Figure 1.2: A range of joint types in welding [Kristiansen, 2007].

Some of the joint types shown on figure 1.2 are either classified as or can be made as a groove weld. A groove weld indicates that there is a groove to be filled during the welding process, see figure 1.3 A, and is the counterpart to the fillet weld where no groove is present as indicated on figure 1.3 B.

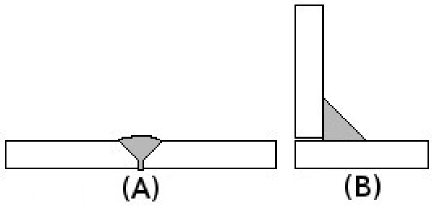

Figure 1.3: (A) A groove weld and (B) a fillet weld.

A joint type as butt weld is always a groove weld. However, the simple square groove is not always sufficient for the task at hand. To cope with more situations multiple groove types are available and are shown in figure 1.4.

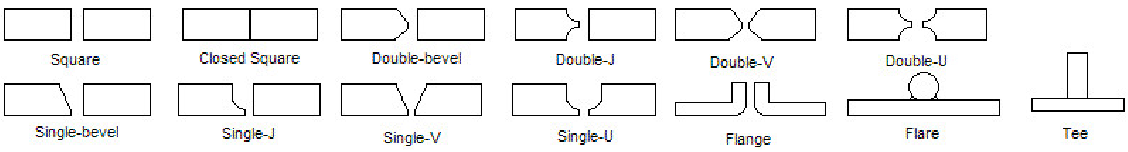

Figure 1.4: A range of weld groove types [Wikiwand, 2017].

Each type of groove has a range of suitable applications making it necessary to investigate and conclude on what type of groove is most suitable for the given job.

1.1.4 Oscillation

During a weld it is sometimes necessary to perform an oscillation pattern. In the case of no oscillation the welder simply welds in a straight line along the weld axis. When an oscillation pattern is applied, variation in the gun position takes place along the weld axis. To illustrate the concept, a range of oscillation patterns are shown on figure 1.5.

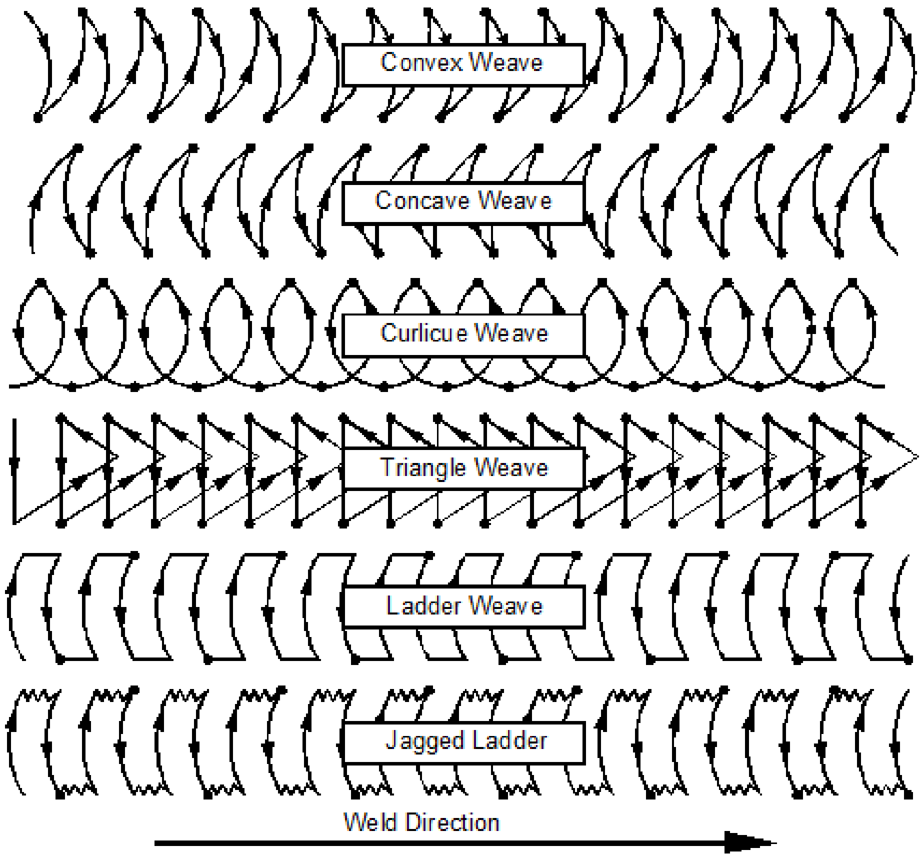

Figure 1.5: A range of oscillation patterns [Marlow, 2012].

The patterns shown on figure 1.5 indicate the attack point of the welding gun along a weld, going from the left and following the arrowed line. As the oscillation patterns on the figure indicate, the possibilities when it comes to choosing an oscillation pattern are endless and each have different results. Which pattern to choose is highly situational and should be investigated prior to any weld.

1.1.5 Metal transfer modes

In GMAW the wire melts and thereby transfers metal to the work piece. Depending on the input parameters the way of transferring material is different. Three overall transfers modes are considered and explained in this section based on an article from *The Fabricator* [FMA communications, 2008].

Short-circuit transfer mode

In short-circuit transfer mode the wire is allowed to reach the work piece without melting even though an arc is established. Once the wire is in contact with the work piece, the system is short-circuited causing the arc to extinguish and the wire to heat up and undergo pinching, see figure 1.6 (A). The pinching involves a necking process of the wire which eventually ends up with a molten piece of wire being transferred to the work piece and an arc being established, see figure 1.6 (B).

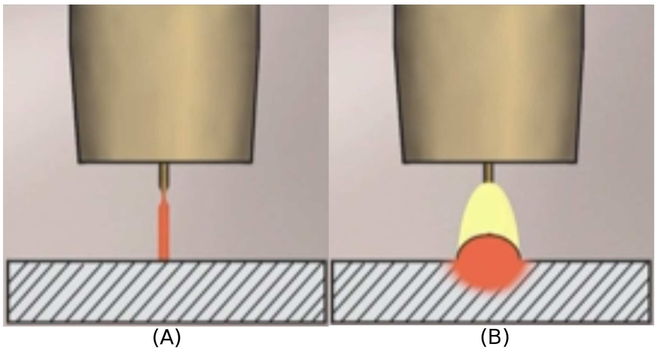

Figure 1.6: Short-circuit GMAW with (A) illustrating the contact, heat build-up and pinching of the wire and (B) illustrating the arc and molten transferred material on the work piece [Wall Mountain Company, 2002].

This mode is generally enabled when using a voltage below 22 V [Wall Mountain Company, 2002].

Globular transfer mode

In contrast to short-circuit transfer mode, the arc is always active in globular transfer mode. In this case the heat of the arc causes the wire to melt before getting into contact with the work piece. Consequently globs of molten wire material breaks off and is transferred to the work piece as shown on figure 1.7.

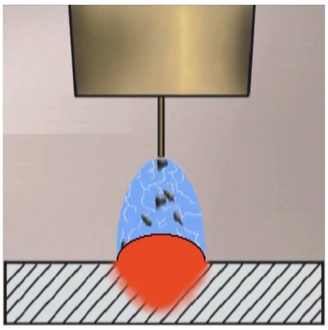

Figure 1.7: Globular transfer with molten globs of wire material being transferred to the work piece through the arc [Wall Mountain Company, 2002].

The globs are usually larger than the diameter of the wire and can exit the arc resulting in excessive spatter. This mode is generally enabled when using a voltage of more than 22 V, a current of less than the transition current specified in the article by *The Fabricator* and a shielding gas consisting of either 100 % CO_2 or an argon and CO_2 mix is used [Wall Mountain Company, 2002].

Spray transfer mode

Similar to globular transfer, spray transfer does not result in contact between wire and work piece. The metal is still transferred in globs but in the case of spray transfer these are usually smaller than the diameter of the wire and more frequent, see figure 1.8. Furthermore the globs are restricted to the arc reducing spatter.

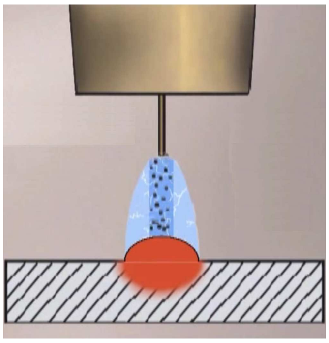

Figure 1.8: Spray transfer with molten globs being transferred to the work piece through the arc [Wall Mountain Company, 2002].

The difference compared to globular transfer lies in the choice of shielding gas and current. Although the mode is enabled using a voltage of more than 22 V, a current above the transition current specified in the article by *The Fabricator* and requires the use of an argon and CO_2 mix shielding gas with an argon content of more than 80 % [Wall Mountain Company, 2002].

1.1.6 Control parameters

In order to monitor and control GMAW it is required to have an understanding as to which parameters affect the process. This report uses the classification of parameters derived by Associate Professor Morten Kristiansen, henceforth MK, at AAU in appendix L: *taxonomy of generic information model* of his PhD thesis from 2007 [Kristiansen, 2007]. From these parameters a sub-set, which contains suitable controlling parameters, is chosen and the conclusion as to which to consider in this project is presented.

In figure 1.9 a part of the set of parameters derived by MK is shown.

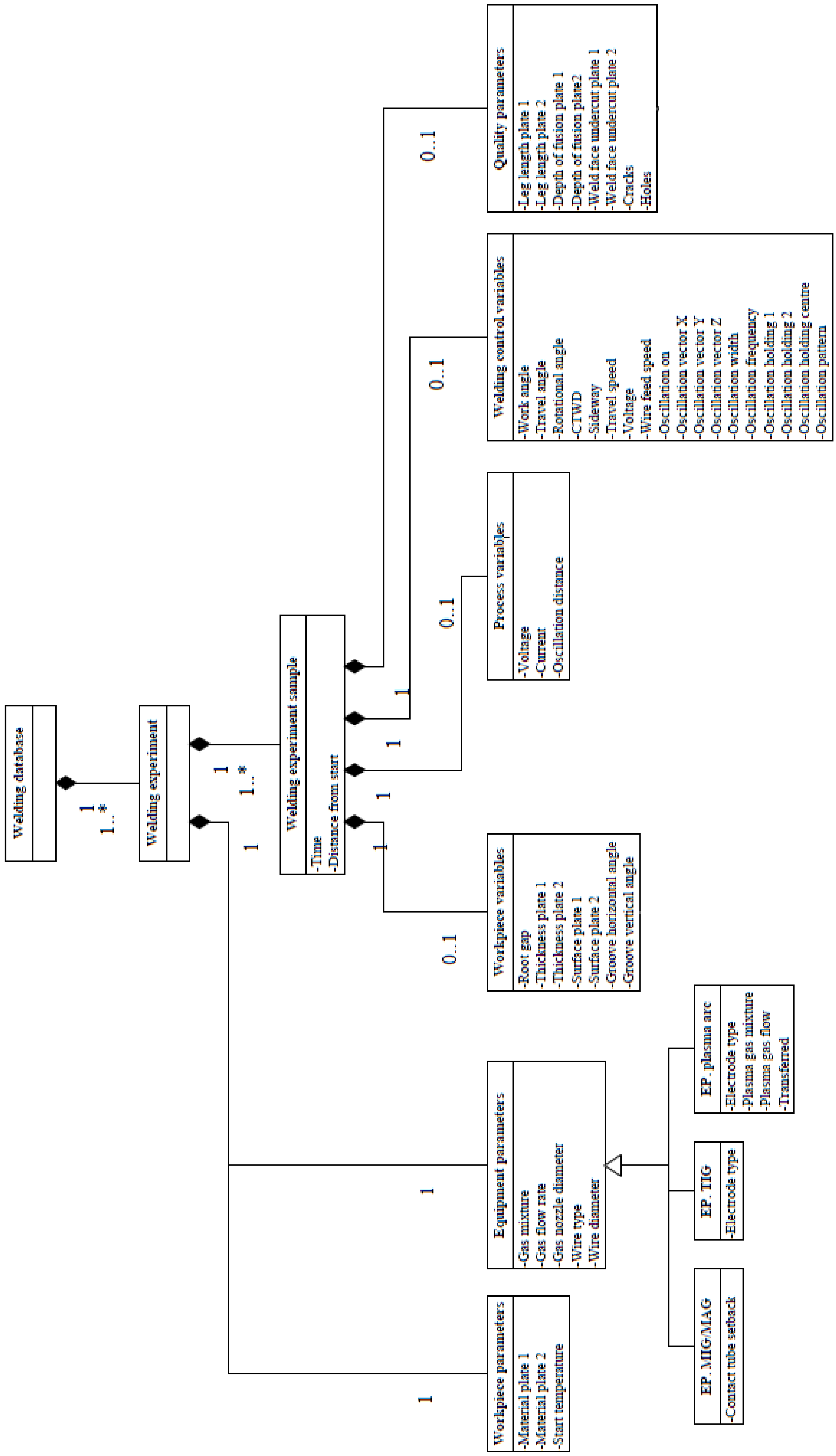

Figure 1.9: Part of the set of welding parameters derived by MK [Kristiansen, 2007].

As indicated on figure 1.9, the parameters are split up into six main groups

- **Work piece parameters**
  The constant parameters throughout the work piece.

- **Equipment parameters**
  The parameters that describe the used equipment.

- **Work piece variables**
  The parameters that vary along the weld axis.

- **Process variables**
  The parameters to be measured throughout the process.

- **Welding control variables**
  The parameters used to control the weld.

- **Quality parameters**
  The parameters that indicate the quality of the weld.

Inspecting the total set of parameters it is clear that some are more suitable for controlling the system. Initially all parameters contained in *Work piece parameters*, *Equipment parameters* and *Work piece variables* are disregarded with the exclusion of gas flow rate. The remaining parameters are determined prior to a welding task and require either design or equipment changes, which is the basis for the assessment to disregard them as control parameters. Furthermore, both the *process variables* and *quality parameters* are disregarded as direct control parameters. The *process variables* in the case of MK are parameters to be measured throughout the process and are thereby, much like the *quality parameters*, a consequence of the other parameters contained in the entire six groups. However, due to this nature these parameters are potential candidates for process monitoring.

Through the elimination of parameters, the following sub-set is proposed:

- Work angle
- Travel angle
- Rotational angle
- CTWD
- Sideway
- Travel speed
- Voltage
- Wire feed speed
- Gas flow rate
- Oscillation on
- Oscillation vector X
- Oscillation vector Y
- Oscillation vector Z
- Oscillation width
- Oscillation frequency
- Oscillation holding 1
- Oscillation holding 2
- Oscillation holding centre
- Oscillation pattern

To provide further understanding of the parameters they are explained individually.

Angles

In the sub-set three angles appear - work-, travel- and rotational angle. An overview of these can be seen on figure 1.10.

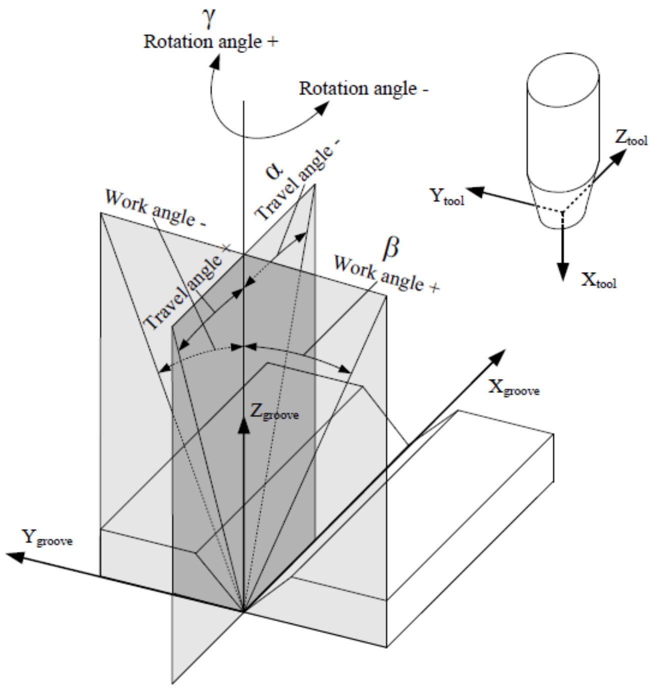

Figure 1.10: An overview of the angles and axes found in a weld [Kristiansen, 2007].

As indicated on figure 1.10, the axis along the weld is denoted X_{groove}, the axis along the width of the work piece is denoted Y_{groove} and the axis perpendicular to the plane defined by X_{groove} and Y_{groove} is denoted Z_{groove}. Using this terminology the angles can now be explained.

The work angle is defined as the angle between Z_{groove} and Y_{groove}, the travel angle is defined as the angle between Z_{groove} and X_{groove} and the work angle is the rotation around Z_{groove}.

Contact tube to work piece distance

The contact tube to weld distance, henceforth CTWD, is the distance from the contact tube to the weld.

Sideway

The sideway is the line onto which the welding guns point of attack is. Should it be necessary to change the point of attack, it moves along this line.

Travel speed

The speed at which the welder moves the weld gun along the weld axis.

Voltage

The voltage set on the welding equipment.

Wire feed speed

The speed at which the wire is fed to the welding gun.

Gas flow rate

The rate at which the gas flows to the welding gun.

Oscillation on

A binary parameter to define whether an oscillation pattern is chosen. If set to 0, the remaining parameters in the control parameter set are disregarded.

Oscillation parameters

The rest of the parameters in the control parameter set are used to define the nature of the oscillation pattern chosen for the process.

1.2 Quality of a weld

In this section the possible imperfections of a weld is presented alongside an introduction to how the quality of a weld is determined in practice and how control is performed in practice in manual welding.

1.2.1 Welding imperfections

Whether the quality of a weld is satisfactory is ultimately determined by whether the weld lives up to the set of specifications given by the customer in the form of aesthetic or functional requirements. Both of these aspects are evaluated according to the presence of welding defects or imperfections. Because of this ISO-5817 exists to aid in determination of the quality level of a weld. [DanskStandard, 2014].

The standard specifies four groups of guidelines in regards to quality checking. The groups are enumerated and named as follows:

- 1.0 Surface imperfections
- 2.0 Internal imperfections
- 3.0 Imperfections in joint geometry
- 4.0 Multiple imperfections

For reference, each guideline is specified by a number preceded by the group number, e.g. *2.12: Lack of fusion* being the 12^{th} internal imperfection. A short description of each group of guidelines is given with examples from the standard. For further elaboration on the specific guidelines, the author refers to the standard.

Surface imperfections

This group contains the guidelines for imperfections on the surface. In order to provide a graspable introduction to these a grouping of imperfections is made. The grouping resulted in the imperfections being divided into surface cracks, surface pores, end-geometry imperfections and penetration imperfections.

In terms of surface cracks and pores the names are self-explanatory. Furthermore it is specified that the presence of surface cracks is not permitted under any circumstance while pores can be allowed in some cases based on the wanted quality level and pore size.

In relation to surface cracks and pores, the set of guidelines for end-geometry imperfections is more extensive. These are all related to improper geometric parameters of the weld such as undercuts, excess weld material or overlapping as illustrated on figure 1.11 A, B and C respectively.

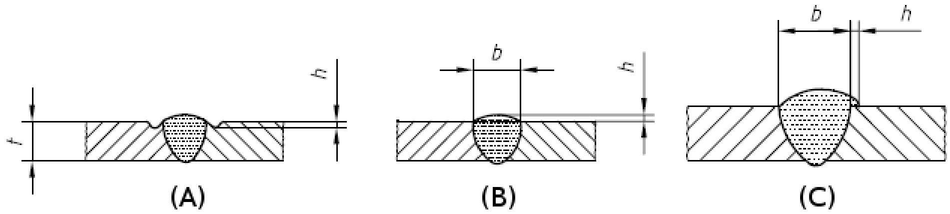

Figure 1.11: The imperfections (A) *1.7 Undercut*, (B) *1.9 Excess weld metal (butt weld)* and (C) *1.13 Overlap* from ISO 5817 [DanskStandard, 2014].

Next are the penetration imperfections. These guidelines specify the quality levels for the weld penetration and contain the situations of lack of fusion, incomplete root penetration and burn through, among others.

Besides the mentioned surface imperfections contained in the derived groups there are three additional guidelines. The first is denoted *1.22 Stray arc* and refers to whether there has been a stray arc during the weld, i.e. an arc that strikes outside the weld groove resulting in a local change of material structure. The second is denoted *1.23 Spatter* and refers to the presence of spatter on the surface of the material. Lastly there is the imperfection *1.14 Temper colour* which refers to discolouration of the material around the weld.

Internal imperfections

Within this group are the imperfections regarding the internal structure of the weld. As for surface perfections a grouping is made with the result of three groups being made.

The first group contains the guidelines for internal cracks. The standard specifies that visible cracks are not allowed under any circumstance while micro cracks, i.e. cracks only visible under a microscope, can be permitted depending on parent metal crack sensitivity.

The second group contains the guidelines for porosity, cavities and inclusions. In regards to porosity it specifies the quality levels for the type of pores, their geometry and their pattern. Similarly the quality levels for cavities and inclusions are based on geometry. In addition to geometry, the included material is also of concern when classifying inclusions.

Lastly the third group contains internal penetration imperfections. The two imperfections found in this group are lack of fusion and internal lack of penetration. As the names suggest, lack of fusion is the situation where the filler material is not fused together with the work piece whereas internal lack of penetration is the situation where the weld does not go deep enough into the weld groove.

Imperfections in joint geometry

Within this group are the imperfections regarding the joint geometry. More specifically it contains guidelines for work piece misalignment or incorrect root gaps for fillet welds.

Multiple imperfections

Lastly this group provides guidelines for the case of multiple imperfections.

1.2.2 Quality inspections

Generally quality control is divided into two groups - non-destructive, henceforth NDT, and destructive, henceforth DT. An overview of popular NDTs and DTs is given in appendix A.

1.3 Discussion

Based on the presented welding theory and the purpose of this report, it is determined that square grooved butt-joint welds is to be investigated in this project. The decision is based on the simplicity of the joint design and the assessment that it is suitable for the extraction of evidence regarding the research topic of machine learning driven quality monitoring based on acoustic emission.

In order to select a fitting set of quality parameters a study of which imperfections have a unique acoustic response should be performed. Based on these results, adequate quality tests can be determined through the methods listed in appendix A.

Signal Theory 2

In this chapter the basics of digital signals, acoustic data and digital signal processing, henceforth DSP, is presented.

2.1 Digital signals

In order to perform monitoring, output data is to be obtained from a range of sensors. Although the purpose for the report is to monitor and control the process through acoustic data, other signals can be used to aid the process. Based on their vital role in the stability of the process and influence on the generated sound during GMAW, see chapter 4, current and voltage could be acquired to help understand the process and indicate changes.

The equipment required to acquire the voltage, current and sound have one thing in common which is that they convert an analogue signal to a digital signal. An introduction to the distinction of analogue and digital signal as well as the terminology used for digital signals and the possible pitfalls of the acquisition is presented in appendix B. Based on the information presented in the appendix, key features to be aware of during the data acquisition is the bit resolution and sample frequency. The resolution should be chosen so that its full range is utilised without the equipment capping. Furthermore the sample frequency should be chosen so that the desired frequencies to be observed can be extracted.

2.2 Acoustic data

As the primary output of the welding process in this project the acoustic signal needs to be captured and processed to identify discriminative features. In this section the digital representation of sound is presented.

2.2.1 Sound

To gain an understanding of what equipment to use in acoustic data acquisition it is required to understand sound. The information presented in this section is based on the lecture notes from Gerald Penn from University of Toronto [Penn, 2010].

Sound is defined as a mechanical wave moving through a given medium and created by the vibration of an object. The medium can be anything, i.e. metal, water, gasses, and, as in the case of this report, air. The energy produced by the arc sets the particles of the surrounding air in motion making them oscillate between compressions and rarefactions as indicated by figure 2.1.

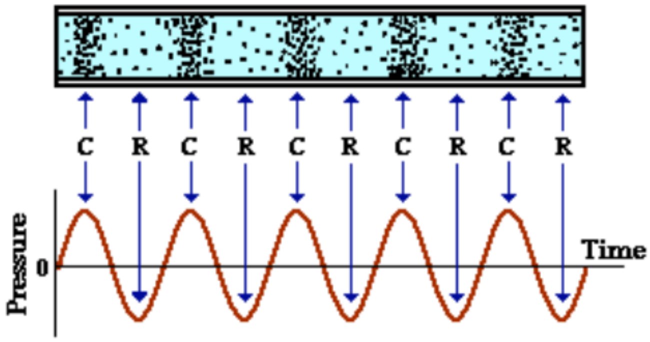

Figure 2.1: A sound wave in a medium. The alternation between compression and rarefactions within the air is indicated by C and R respectively [Penn, 2010].

The wave illustrated on figure 2.1 is called a longitudinal wave. Furthermore it should be noted that sound can be represented by a single or combination of sine functions as indicated by the pressure-time graph on figure 2.1.

To describe a wave the frequency and amplitude should be known. The frequency of the wave is the amount of complete back-and-forth motions, i.e. periods, is present in the medium per unit of time. It is denoted f and has the unit Hz. Depending on the mechanism to pick up the sound different frequency ranges can be measured. In the case of the human ear the audible frequency range is said to be between 20 Hz and 20 000 Hz [BBC, 2014]. The human ear is simply not capable of picking up signals outside this range, however sound in the non-audible range for humans still exist. Commonly the domain with frequencies below 20 Hz is denoted infra sound whereas the domain above 20 000 Hz is denoted ultra sound.

As for the amplitude, it is the work done to generate the energy that sets the particles in motion and is shown as the displacement from equilibrium on an amplitude-time graph [Penn, 2010].

The intensity of sound is measured in decibel, dB. It is presented on a logarithmic scale and tells the ratio for comparing two sounds in intensity. For an interpretable unit a fixed pressure of $2 \cdot 10^5$ is defined as the reference for 0 dB, P_0, which corresponds to the threshold of hearing [Penn, 2010]. Using this reference the absolute sound pressure, P, can be calculated as 20 $log_{10}(P/P_0)$. For reference table 2.1 shows a list of sound intensities.

Intensity	Reference
0 dB	Threshold of hearing
20 dB	Quiet living room
40 dB	Refrigerator
60 dB	Normal conversation
90 dB	Passing motorcycle
100 dB	Somebody shouting
110 dB	Loud rock concert
120 dB	Pain threshold

Table 2.1: Reference activities for levels of sound intensity [Penn, 2010].

2.3 Digital signal processing

Seeing as a signal is a quantity varying in time, it is in some cases necessary to extract features from the data to describe the signal. One of these cases could be to effectively distinguish between two signals, e.g. in certain machine learning algorithms. For the distinction to be made it is elementary that discriminating features are extracted from the signals which is why understanding how to synthesise, transform and analyse these is key. Being aspects of the field of DSP this section aims to present sufficient information as to how this is performed.

2.3.1 Segmenting

In DSP assignments the basic operation of *segmenting* is often used when analysing signals whose characteristics vary over time. By expressing the signal as a series of segments with their own properties, a piece-wise understanding of the signal is obtained. To perform the segmentation, the concept of *windowing* is introduced.

Windowing

The process of windowing is performed by letting a window pass through a signal in the time domain by using a so-called *window function*. A window function is defined by being real-valued within a finite range of inputs and zero-valued outside the given range. By applying this function on a signal, a segment is cut and scaled through the values specified in the real-valued part of the window. In order to perform windowing, three parameters need to be considered - type, length and overlap.

The type of window is determined by the shape and magnitude of the values applied to the signal during the window length. Two typical windows are shown in figure 2.2.

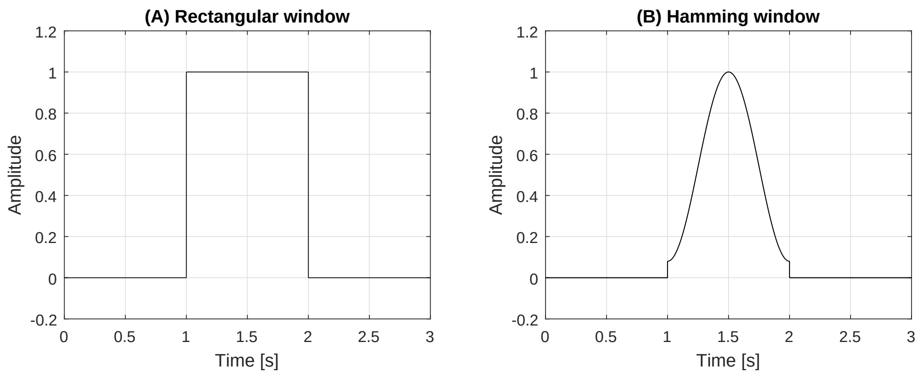

Figure 2.2: A (A) rectangular and (B) Hamming window in the time frame going from $t = 1$ to $t = 2$.

For both graphs the window function is set to have its effect between $t = 1$ and $t = 2$. On figure 2.2 (A) a rectangular window is shown. As indicated it has the value zero outside the window space and a constant value of one during the length of the window. Employed on a signal it merely cuts out a segment of the signal since the data is scaled equally by a factor of one throughout the window. Alternatively a Hamming window is shown on figure 2.2 (B). This type of window has a bell shape with the tails ending in a value of 0.08. By doing so, every part of the window has a weight in contrast to having the tails reaching zero. With the curve at the top of the graph and the tails decreasing on either side, the function weights the data in the center of the window the most, while moving away from the center to either side entails a decrease in the weight of the data. Determining the type of window to use depends on applications and should be considered before each DSP operation where a window function is used.

The length of the window is as the name suggests how long the window should be. Having the signal as samples, the length is defined as how many samples are included in the window. The choice of length entails different results when doing DSP so careful consideration should be taken before a decision is made.

Besides the type of length of the window, *overlapping* may be introduced. The overlap is a parameter to determine how much of the previous window should be included in the current window and is denoted in percent. Examples of overlap is seen in figure 2.3.

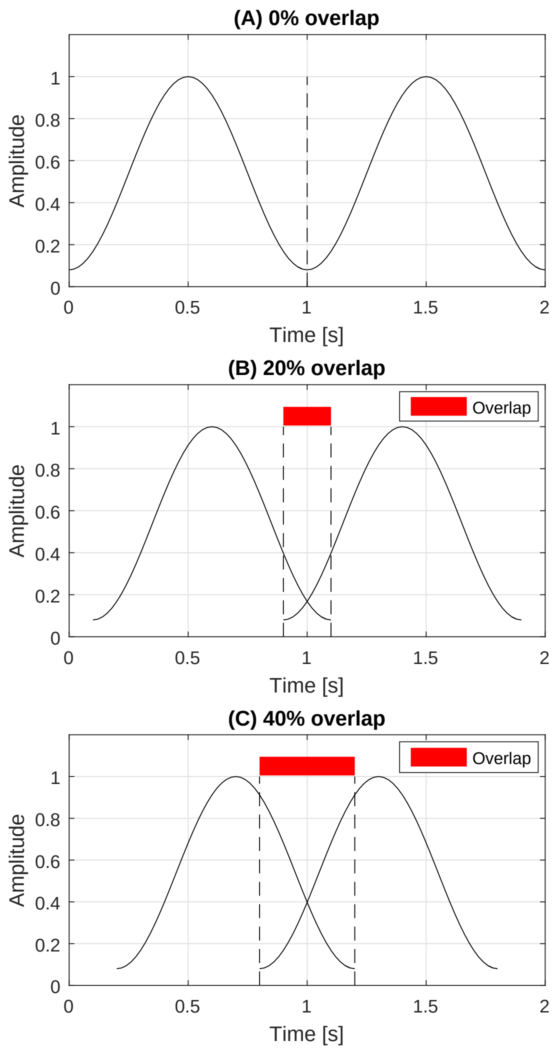

Figure 2.3: Two consecutive Hamming windows with an overlap of (A) 0%, (B) 20% and (C) 40%.

Illustrated on figure 2.3 are two consecutive Hamming windows with 0%, 20% and 40% overlap respectively. Moving the window through a signal using an overlap has an averaging effect since an amount of data from the previous window is included in the current one - an effect which can be beneficial in DSP operations.

Lastly the choice of window length and overlap defines the amount of segments the signal is split into, denoted n_w, the effect of which is specific to the DSP operation in progress.

2.3.2 Signal domains

In the field of DSP so-called domains exist the most common of which being time domain and frequency domain. The transition between domains occur through signal transforms and each domain provides a set of features to be extracted.

Time domain

When acquiring a signal it is obtained as a set of values through time as mentioned in section 2.1, i.e. the signal is captured in the time-domain. A signal in the time domain is usually presented as a time series as seen in figure 2.4.

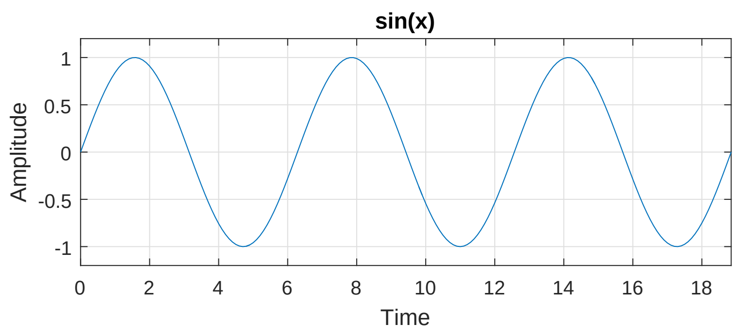

Figure 2.4: sin(x) in the time domain.

Having a signal in the time-domain allows analysis of specific values, e.g. through descriptive statistics, and time-dependent features, i.e. temporal features. Having a signal in the time domain makes it possible to spot trends in the data and allows for pinpointing moments in time where specific situations occur. However, it does not present an overview of which frequencies are present in the signal, which can aid in the description and synthesising of signals. To gain this information a transformation is made to transfer the signal to the frequency domain.

Frequency domain

Transforming a signal from time-domain to frequency-domain happens through a spectral decomposition. The idea behind this builds on the assumption that any signal can be expressed as a combination of sine functions with different frequencies. The way of determining the frequencies of these sine functions is done by performing a discrete fourier transform or the more computationally efficient version called *fast fourier transform*, henceforth FFT. The result of this is a complex-valued function of frequency. Taking the square magnitude of the function provides values that describe how much power of a given frequency bin is present in the signal. The set of these powers is called the power spectral density, henceforth PSD, and is plotted in what is known as a power spectrum or periodogram which can be described through e.g. peak analysis or spectral shape descriptors.

Along with any sampled signal comes the disadvantage of it being imperfect and being a finite set of data. Consequently the calculated PSD is an estimation riddled with noise. Due to this Peter D. Welch developed a method to reduce the effect of the noise in a trade-off with frequency resolution [Welch, 1967]. Instead of calculating the PSD for the entire data set, it is subjected to windowing, usually with a Hamming window, before creating a series of periodograms that averaged make up the *Welch's power spectral density estimate*. An example of a Welch power spectrum is given in figure 2.5.

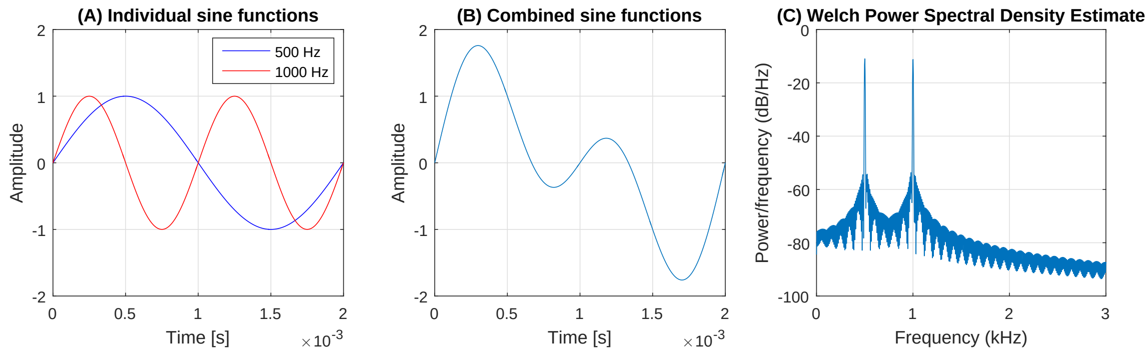

Figure 2.5: (A) Two sine functions that are combined to the signal in (B) for which the Welch power spectral density is shown in (C).

In this example two sine waves are combined - one with a frequency of 500 Hz and one with a frequency of 1000 Hz, see figure 2.5 (A), to make up the signal on figure 2.5 (B). Using Welch's method, the power spectrum in figure 2.5 (C) is derived. As indicated by the peaks in power the graph clearly identify the frequencies of 500 Hz and 1000 Hz as dominating and of equal power in the signal, which is consistent with the analysed function.

In the case where it is necessary to transform the data back to the time-domain an *inverse fast fourier transform*, henceforth IFFT, can be used.

Time-frequency-domain

Lastly, methods of showing the signal in both the time- and frequency-domain exist. One method is by segmenting the signal in time, calculating the periodograms and plotting them on a time-frequency graph known as a *spectrogram*. This method can be used when the frequencies of the signal vary over time as in e.g. a *chirp*. The change in a chirp can either be that the frequency increases, up-chirp, or decreases, down-chirp. To illustrate the principle of a spectrogram an example of an up-chirp is presented in figure 2.6.

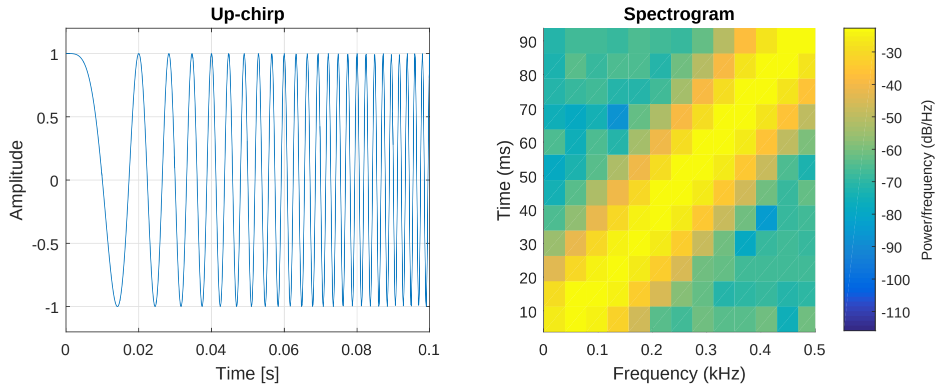

Figure 2.6: (A) The time-domain signal of an up-chirp going from 0 Hz to 500 Hz within 0.1 second and (B) its corresponding spectrogram.

In the example shown on figure 2.6, an up-chirp is generated with a start frequency of 0 Hz at $t = 0$ and an end frequency of 500 Hz at $t = 0.1$, see figure 2.6 (A). To illustrate the change in frequency the corresponding spectrogram is calculated and presented in figure 2.6 (B) where it is clear that the frequency increases linearly through time from 0 Hz to 500 Hz in the specified time span, which is consistent with the analysed function.

As the case for the transformation back to time domain, an IFFT for each segment of time can be performed.

2.3.3 Digital filtering

When obtaining or synthesising a signal the data is not always as expected. It can be riddled with noise or have certain frequencies that is not desired for the given process at hand. Therefore preprocessing of the data is used to modify the data to be more useful. The process of doing so often requires a form of filtering. The filtering can be done either as an analogue or digital process, but since digital filtering is not subject to the same restrictions as analogue filtering it is decided to only consider digital filters in this report. For an introduction to the the basics of filtering, see appendix C.

2.3.4 Feature extraction

Being able to transform a signal between time- and frequency domain as well as implementing digital filters provide the basics of DSP. To better understand how to discriminate between signals, this section presents an introduction to feature extraction. It should be noted that only instantaneous features, i.e. *short-time features*, are presented since global features are assessed to not provide a beneficial effect to the machine learning aspect of this project.

This section is based on the work of Geoffroy Peeters, henceforth GP, [Peeters, 2004] in which a large set of audio features is presented. To illustrate the feature extraction process and the necessary transforms, the author propose the figure seen on figure 2.7.

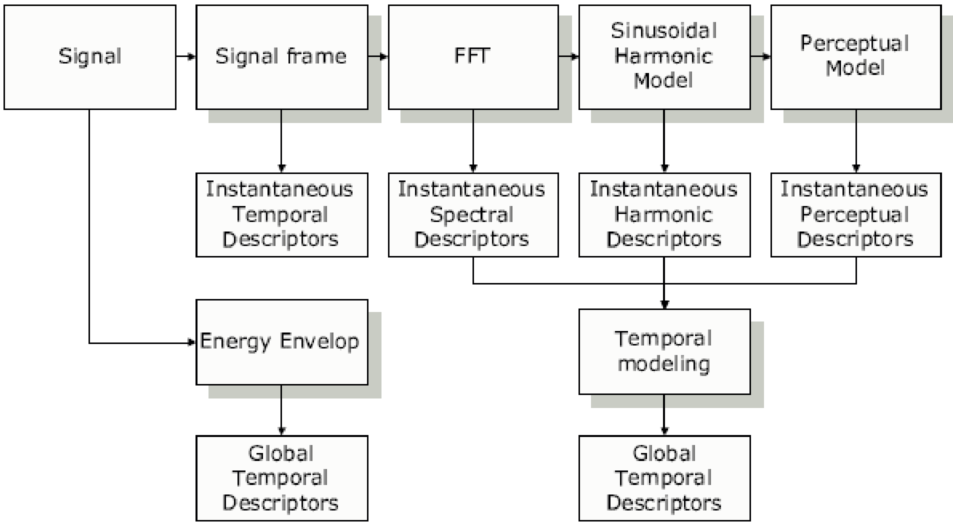

Figure 2.7: An overview of the feature extraction process presented in [Peeters, 2004]

As indicated by figure 2.7, GP classifies the features in the following groups:

- Temporal features
- Spectral shape features
- Harmonic features
- Perceptual features

Furthermore a range of energy features are considered in both the harmonic analysis and from the signal frame. Note that global temporal descriptors can be extracted from both the energy envelope and temporal modelling. These are not presented in this section as it focuses on the extraction of instantaneous features. From figure 2.7 the feature extraction process is as follows:

1. The original signal is segmented into frames
2. Temporal features are extracted
3. FFT is performed on each segment
4. Spectral shape features are extracted
5. A sinusoidal harmonic model is derived
6. Harmonic features are extracted
7. A perceptual model is derived
8. Perceptual features are extracted

By performing these steps both the time domain and frequency domain are well covered and provides features known to be useful in speech recognition.

Temporal features

Temporal features are extracted from the time-series data of a signal segment. Due to intuitive sense of the type of data and the fact that no transformation is necessary the majority of temporal features are relatively simple to extract and understand compared to spectral features. One range of features focus on the distribution of the amplitudes in a signal segment through descriptive statistics. Others are time-dependent and involve calculating the frequency of which an event occurs such as the zero-crossing rate, henceforth ZCR, which measures the amount of time the signal crosses zero within the signal segment.

Spectral shape features

Once the FFT has been performed on the signal, the frequency spectrum of the signal segment is found. Similarly to the descriptive statistics used in the time domain, the spectral shape can be described through similar features. Examples of these features are the spectral centroid, spectral spread and spectral skewness. Furthermore spectral temporal features can be extracted by comparing the spectrum of consecutive signal segments through e.g. normalised cross-correlation.

Harmonic features

Using the spectrum of the signal segment harmonic features can be extracted. These include calculating the fundamental frequency, noisiness and inharmonicity of the signal.

Perceptual features

A perceptual model of the signal can be derived through e.g. *mel-frequency cepstrum*, henceforth MFC [cryptography, 2012]. To obtain the MFC, the spectrum for a signal is calculated and subjected to a *mel filterbank*, which is a set of 20-40 triangular filters spaced using the mel-scale. After applying the mel filterbank, the energy for each filter is computed as the sum of powers. Taking the logarithm to the filterbank energies and performing the DCT results in what is denoted the *mel-frequency cepstral coefficients*, henceforth MFCC, which have shown promising results for auditory weld quality monitoring as mentioned in chapter 4.

2.3.5 Discussion

In this section the focus of feature extraction has been on audio. However, the features serve as general descriptors for signals and can be used for e.g. current and voltage data.

Deriving a perceptual model such as the MFC allows for the extraction of features which refer more to the way a human perceives sound. Seeing as the inspiration from this report comes from the fact that welders use their auditory sense to determine process stability [Tam and Huissoon, 2005], extracting perceptual features seems promising and should be investigated.

Machine learning overview 3

In this chapter an overview of machine learning is given. Specifically a classification of algorithms is presented alongside a general introduction to how a hypothesis is trained and evaluated.

3.1 Machine learning algorithms

In machine learning algorithms, i.e. mathematical procedures, are used to automatically build models. This means that for a given problem it is necessary for the user to determine what the final model should predict and based on what type of data. Once determined, a suitable algorithm is chosen after which the model is trained, evaluated and evaluated.

Machine learning dates back to around year 1950 and countless algorithms have been developed from then to now [Marr, 2016]. Consequently the selection of algorithms has become inconceivable and lacks proper grouping - a task made cumbersome by the trend of developing task-specific algorithms. However, individuals have tried to group the algorithms and for the case of this project, the method of representation follows Dr. Jason Brownlee's classification [Brownlee, 2013]. He proposes a grouping based on style and similarity both of which are presented in appendix D. Although extensive, the list is not exhaustive but provides insight into the possibilities of the field.

3.2 Training an algorithm

Once an algorithm is chosen it is used to train a model. Depending on the algorithm the training process may vary and all cases are not presented in this section. However the process presented in this section is widely used and presents the general approach of model training via machine learning algorithms.

Generally the training process consists of the following steps:

1. Determine hypothesis
2. Determine cost function
3. Minimise cost function

This section is inspired by the Stanford University course *Machine Learning* led by Andrew Ng [Ng, 2017].

3.2.1 Determining the hypothesis

The *hypothesis* is the function or model, $h(x)$, that maps the input, denoted x, to the output, denoted y. In other words, it is the model to be trained to make the best possible prediction or mapping based on the training data. Determining the hypothesis depends on the chosen algorithm and multivariate linear regression is used as an example in this report to illustrate the process. The related hypothesis is:

$$h_\theta(\mathbf{x}) = \sum_{i=0}^{n} \theta_i x_i \mid x_0 = 1$$

with the θ's all being constant parameters or *weights*, n being the number of features used and the convention of x_0 being set to one. It should be noted that the hypothesis is subscripted based on weight notation which is why it in this case is subscripted with a θ.

3.2.2 Determining the cost function

The *cost function* is denoted J and is defined differently based on the data provided. In labelled data generally it is an expression of the difference between the hypothesis' prediction and the training data output, while for unlabelled data the algorithms use more specific cost functions. Continuing the case of multivariate linear regression the cost function can be set to the half the sum of squared differences:

$$J(\boldsymbol{\theta}) = \frac{1}{2m} \sum_{i=1}^{m} (h_\theta(x^{(i)}) - y^{(i)})^2$$

with m being the number of training examples.

3.2.3 Minimising the cost function

With the cost function determined the next step is to minimise. By minimising the cost function in relation to the weights, the hypothesis is trained to predict the output with the smallest error. For this the *gradient descent* method can be used but more advanced optimisation methods can be implemented if necessary. The formula is written as:

$$\underset{\boldsymbol{\theta}}{\text{minimise}}\, J(\boldsymbol{\theta}) = \frac{1}{2m} \sum_{i=1}^{m} (h_\theta(x^{(i)}) - y^{(i)})^2$$

and functions by updating all weights simultaneously using a specified learning rate, α, in the direction of the negative gradient of the cost function in a given point. It should be noted that the direction of negative gradient is always orthogonal to the contour line at the point in which it is computed. This may cause a zig-zag phenomenon in the optimisation problem, which in some cases may lead to slower convergence. The updating formula is:

$$\theta_j = \theta_j - \alpha \frac{\delta}{\delta \theta_j} J(\boldsymbol{\theta})$$

Assuming the learning rate was chosen correctly, a local or global optimum is reached over the course of a finite amount of iterations depending on the initial guess of the weights and the convexity of the problem.

When working with gradient descent one should be aware of the impact of the learning rate and differently scaled features.

Gradient descent learning rate

In regards to the learning rate it is important to choose the right value. The influence of α is shown on figure 3.1.

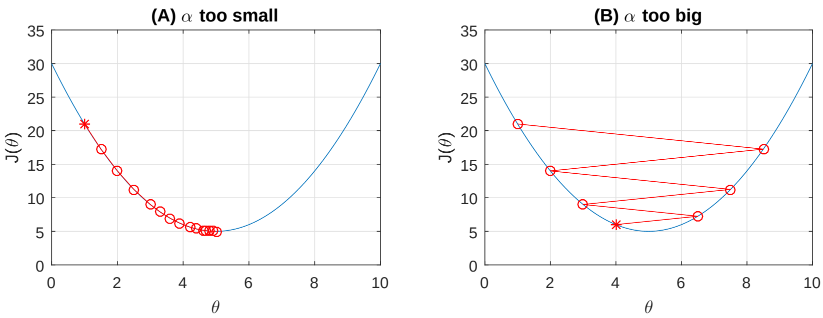

Figure 3.1: The iterations of a minimisation task with the asterisk marking the starting value. Examples of (A) slow convergence due to small α and (B) divergence due to large α.

Choosing a learning that is too small results in slow convergence as seen on figure 3.1 (A) and should be made larger to improve performance. Having the learning rate too large will cause the function to diverge and thereby never reach the optimum as indicated on figure 3.1 (B). Therefore choosing the learning rate should be done with care.

Feature scaling

When the used features are on different scales attention should also be paid. An increasing degree of difference between the scales of two features increase the rate of convergence for the minimisation. To handle this e.g. *feature scaling* can be used. The principle of this is to make the scales similar by scaling them to be in in the same range. An example of this could be through the following formula:

$$x_{fs}^{(i)} = \frac{x^{(i)} - min(\mathbf{x})}{max(\mathbf{x}) - min(\mathbf{x})}$$

with x_{fs} denoting the feature scaled input. By using this formula for the input, they are all converted to the range of 0 to 1, which may improve the rate of convergence and prediction accuracy compared to the raw state.

3.2.4 Overfitting vs underfitting

When training a model it is important to handle the problem of *overfitting* and *underfitting*. The problem is illustrated for a housing price example in figure 3.2.

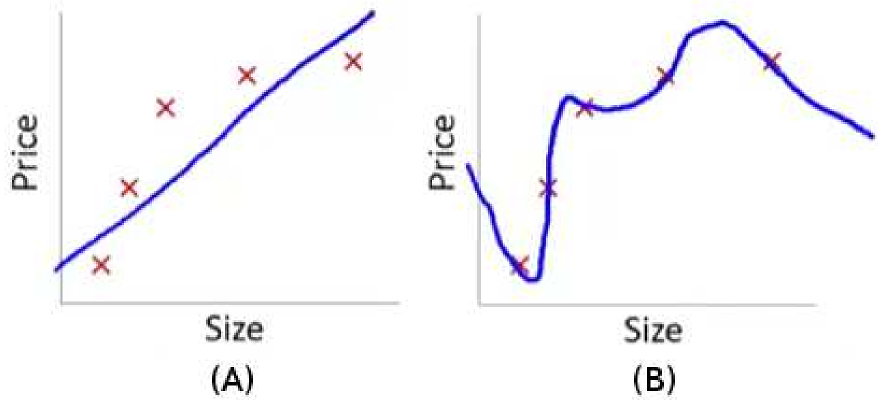

Figure 3.2: Exmaples of (A) underfitting and (B) overfitting on a housing price example [Ng, 2017].

On figure 3.2 (A) the case of underfitting is shown. As indicated the fit is a bad match since it does not accurately predict the price for the training data. On figure 3.2 (B) the case of overfitting is shown. Here the hypothesis accurately predicts the price in the exact point of the training data but fails to model the tendency of the data making it inaccurate on cases different from the training data. To combat this regularisation is used.

Regularisation

Regularisation is a term added to the cost function and included in the optimisation process to combat fitting errors. The term is:

$$\lambda \sum_{j=1}^{N} \theta_j^2$$

with λ being the regularisation constant and N being the amount of features. It should be noted that the summation starts at $j = 1$ since the parameter θ_0 should not be scaled. As indicated by the term, it multiplies the squared sum of weights by a value of λ to control the effect of them on the hypothesis. By using a large value of λ the weights assume small values and hereby makes the hypothesis less prone to overfitting. Using a too large value however, causes the hypothesis to become a constant. Because of this regularisation can be used to reduce fitting errors, but λ should be chosen carefully.

3.3 Evaluating hypothesis

Once the hypothesis is trained to fit the training data there is a method of evaluating its performance. It consists of testing the hypothesis on data not in the data set. One way of obtaining test data is to split the acquired data set into a training set and a test set. The hypothesis is then trained on the training set and tested on the remaining data set to provide a measure of performance. However, only training on one data set may lead to overfitting.

To better secure the performance of a hypothesis the data set can be split into three section - *training set*, *test set* and *validation set*. By having three sets another loop in the optimisation can be implemented. In the case of doing polynomial regression the outer loop could choose the degree of the polynomial. In this case the procedure is as follows:

1. Optimise the weights for each polynomial degree on the training set
2. Calculate the error of the hypotheses on the validation set
3. Choose the degree of polynomial based on lowest validation error
4. Calculate the error of the hypothesis on the test set

Making the outer loop decide the degree of polynomial results in a better generalised fit which then, similarly to the method with two sets, can be used to calculate a performance measure on the data from the test set. A rule of thumb for the splitting of the data is to use 60%, 20% and 20% of the original data set to create the training-, validation- and test set respectively.

Other evaluating tactics exist to determine the performance of the hypothesis and proposed actions to improve it looking into bias and variance cases as well as learning curves.

3.4 Discussion

Based on the knowledge presented in this report it seems fitting to use a supervised classification algorithm for the quality monitoring of GMAW.

4 Related work

Researchers have investigated the acoustic response of welding processes since the 1940's. During the years of research it has been concluded that the primary influences on the sound generated during GMAW are the arc behaviour, molten pool dynamics, droplet transfer, shielding gas and welding equipment [Saini and Floyd, 1998] [Grad et al., 2003]. In short this means that the arc stability can be measured in the sound which suggests that welding defects caused by or causing instability of the arc can be detected. Since the transfer mode of a GMAW process affects the voltage and current signal, and in turn the arc, it is possible to detect which transfer mode is active during the weld as investigated by E. H. Cayo and S. C. Absi Alfaro in 2008 [Cayo and Alfaro, 2008].

So far the majority of research focus on identifying the penetration state on flat butt welds with a process generally consisting of data acquisition, feature extraction, dimensionality reduction and algorithm choice.

Data acquisition
Since the inspiration for investigating the acoustic signal of welding has its roots within human hearing sense mimicking there is a wide agreement to use microphones with a frequency range within the hearing range of humans, i.e. 20 Hz - 20 000 Hz.

Feature Extraction
In order to train a given machine learning algorithm, a range of features must be extracted from the acoustic data. These features can be found within any of the signal domains, i.e. time domain, frequency domain etc., and a definitive answer as to which to use is not available. Therefore different combinations of features are investigated often without limiting to one domain. If gas tungsten arc welding, henceforth GTAW, and shielded metal arc welding, henceforth SMAW, are considered as well, multiple suggestions as to which features to use can be found. These suggestions range from simpler solutions using statistical features from the original time domain signal [A.Sumesh et al., 2015] or from the nodes of a wavelet packet decomposition [Wang et al., 2011] to more comprehensive solutions using multiple features from both time-, frequency-, MFC- and geometry domain [Bi et al., 2010]. The three mentioned papers all succeeded in using their respective features to classify penetration status which consequently leads to the conclusion that the acoustic signal of GMAW, GTAW and SMAW indeed can be used for penetration state classification.

Dimensionality reduction
The use of dimensionality reduction is seen in the article by Shujuan Bi, Hu Lan, Hongyan Zheng and Lijun Liu from 2010, PCA is used to eliminate redundant features from a larger set of descriptive parameters [Bi et al., 2010]. In the similar case for GTAW a

large set of features extracted from a wavelet decomposition is reduced using a generic algorithm [Wang et al., 2011]. In both cases the authors managed to produce models with an accuracy of 85 % or higher.

Algorithm choice

Since there is no direct answer as to which machine learning algorithm to use for GMAW monitoring, a wide range of examples can be found. Examples include artificial neural networks [Bi et al., 2010] [Wang et al., 2011] [Lv et al., 2013] and Hidden Markov Models [Na et al., 2013] as well as decision trees such as J48 and Random Forest [A.Sumesh et al., 2015]. All proposed algorithms provide an accuracy of more than 70 %.

5 Problem specification

Throughout chapter 1, chapter 2, chapter 3 and chapter 4 the problem of developing a quality monitoring system for robotic GMAW based on sound is presented. Consequently it is decided to look into the transfer modes and penetration state of square grooved butt welds. A model is to be trained using the acoustic emission of the process leading to the decision of using a supervised classification algorithm.

Chapter 2 and chapter 4 presents a range of temporal-, spectral-, harmonic- and perceptual features to extract which may prove useful in the classification process. Especially the use of perceptual features are of interest since these are extracted from a model closely resembling the way sound is perceived by humans. Furthermore, research has shown that the use of descriptive features from the nodes of a wavelet packet decomposition is useful in the classification of the penetration state of a weld. Lastly chapter 3 and chapter 4 suggests that a range of algorithms can train models able of prediction penetration state with an accuracy greater than 70 %. Based on its documented ability to predict the penetration state of GMAW and its versatility it is decided to further investigate the use of an artificial neural network, henceforth ANN, in penetration state monitoring as well as metal transfer mode monitoring leading to the following hypothesis and sub-hypotheses:

> $\mathbf{h}_1$: It is possible to monitor GMAW using an artificial neural network trained on labelled acoustic data
>
> > $\mathbf{h}_{1.1}$: *It is possible to identify the penetration state of GMAW through its acoustic emission using an artificial neural network*
> >
> > $\mathbf{h}_{1.2}$: *It is possible to identify the metal transfer mode of GMAW through its acoustic emission using an artificial neural network*

To specify the problem further a range of delimitations are determined:

- **The use of oscillation patterns is not considered**
  - Investigating the process of welding with oscillation patterns is not considered for this project.
- **Other gasses than Mison 18 are not considered**
  - Mison 18 is available and suitable for the project. Other gasses could be used but including these in the investigation is beyond the scope of this report.
- **Other metals than steel are not considered**
  - Other metals could be used but including these in the investigation is beyond the scope of this report.

- **Other wire materials or types are not considered**
  - Other wire materials and types could be used but including these in the investigation is beyond the scope of this report.
- **Other type of welds or grooves are not considered**
  - Other types of welds or grooves could be investigated but including these in the investigation is beyond the scope of this report.
- **Other types of weld geometries are not considered**
  - Other types of weld geometries could be investigated but including these in the investigation is beyond the scope of this report.

6 Method

In order to either accept or reject the hypotheses in chapter 5, evidence is produced to support the claims. The method developed to do so consists of the following steps:

- Specify the type of ANN
- Modify the current experimental setup
- Perform experiments
- Analyse data
- Extract features
- Train ANN
- Evaluate performance

Each point is elaborated further in this chapter.

Specify the type of ANN

The first step of testing the hypotheses is to specify the type of ANN and fully understand the structure, hypothesis, cost function and training method.

Modify the experimental setup

To gain an understanding of the limitations and usage of the existing setup, an analysis of the current hardware and software is required. Once understood, a data acquisition system must be made so that the voltage, current and sound can be logged at an appropriate rate and quality.

Perform experiments

Once the algorithm is specified and the data acquisition system is implemented, experiments can be made. The settings of the process are specified and preventive actions to reduce variance are applied to ensure the quality of the experiments. Afterwards experiments are performed to obtain data for each classification case.

Analyse data

The acquired data from the experiments is labelled so that it can be used for supervised learning. In the process of doing so unwanted sections of the data are removed in an attempt to reach maximum prediction accuracy. If further preprocessing of the data is required, this should also be performed before feature extraction.

Extract features

Having the labelled data available, the feature extraction can begin. Which features to include should be considered and how to extract them presented. Once determined the data can be segmented according to a specific type and length of window with as well as the size of the overlap, after which the chosen features can be extracted. Once completed, the feature vectors for each segment is given the label of the data from which the segment is cut, consequently leading to two matrices for each hypothesis - an input feature matrix, $\mathbf{x}$, and a labelled output matrix, $\mathbf{y}$.

Train ANN

Using the input and output matrix found during the feature extraction, the ANNs can be trained. Before doing so it should be considered whether normalisation would boost the prediction accuracy of the model.

Evaluate performance

Having trained the neural networks confusion matrices are used to provide an overview of the accuracy of the classifier. Lastly the evaluation of the ANNs is used to assess whether the hypotheses are accepter or rejected.

7 The artificial neural network

In this chapter the choice of neural network is presented including elaboration on the choice of optimisation method and cost function.

Specifically the type of network used is a backpropagation network using a cross-entropy cost function. For a detailed description of the general structure and functionality of the specified ANN, see appendix E.

Structure

Generally no guideline for the structure of a neural network is given. Therefore different structures should be analysed during training and the best network configuration chosen.

Choice of optimisation

It is assessed that the use of gradient descent is sufficient for the ANN training performed in this project. The method is simple to implement and a popular choice of optimisation method for neural networks. However, as explained in chapter 3, the choice of learning rate of the optimisation method is crucial to the performance of the method. Therefore the introduction of an adaptive learning rate is used. This is done by implementing a punishment/reward-system based on the performance of the optimisation. Specifically if the newest cost exceeds the previous cost by a pre-defined ratio, the newly calculated weights are disregarded, the step size is decreased and the weights are recalculated. Should the newest cost not exceed the previous cost the step size is increased. This method is known as gradient descent with adaptive learning rate, henceforth GDA.

Alternatively the use of *scaled conjugate gradient descent*, henceforth SCG, could be investigated. This optimisation method is not learning rate dependent and proven to increase convergence rate [Moeller, 1991]. The main improvement lies in the fact that where the gradient descent can only take steps in the orthogonal direction of the contour line, see chapter 3, the SCG can step in any direction. By doing so, the optimum can be reached without the zig-zag steps performed in gradient descent and possibly handle non-convex problems more effectively.

Choice of cross-entropy

A commonly known cost function is the mean square error, see chapter 3, proven to work perform well for linear regression. However, for the case of logistic regression, such as the case of ANNs using sigmoid activation functions, the cost function would be *non-convex* due to the degree of non-linearity [Ng, 2017]. This means that the cost has multiple local minima and in that way does not guarantee convergence to the global minimum. To counteract this, *cross-entropy* is used, since it produces a convex optimisation problem [Ng, 2017]. Based on its known effect in logistic regression, cross-entropy is a popular choice of cost function in neural networks. This is done despite the fact that the multiple logistic regressions performed in an ANN makes the optimisation problem non-convex. However, based on its popular usage, it is chosen to use cross-entropy in this project.

The specific type of cross-entropy used in this report is based on the use of a *Softmax* output activation function. In order to function properly, the labelled data should be *one-hot encoded* as explained in appendix E.

Experimental setup and data collection 8

In this chapter the experimental setup and the modification made to perform the required data acquisition is presented.

8.1 Experimental setup

To perform robotic GMAW AAU has provided a cell with the necessary equipment. Onto this equipment a range of sensors have been implemented and a data acquisition system is developed. To provide an understanding of the complete setup, this section initially presents the robotic GMAW equipment followed by a presentation of the hardware and software of the data acquisition system.

8.1.1 The robotic GMAW setup

The setup is shown on figure 8.1.

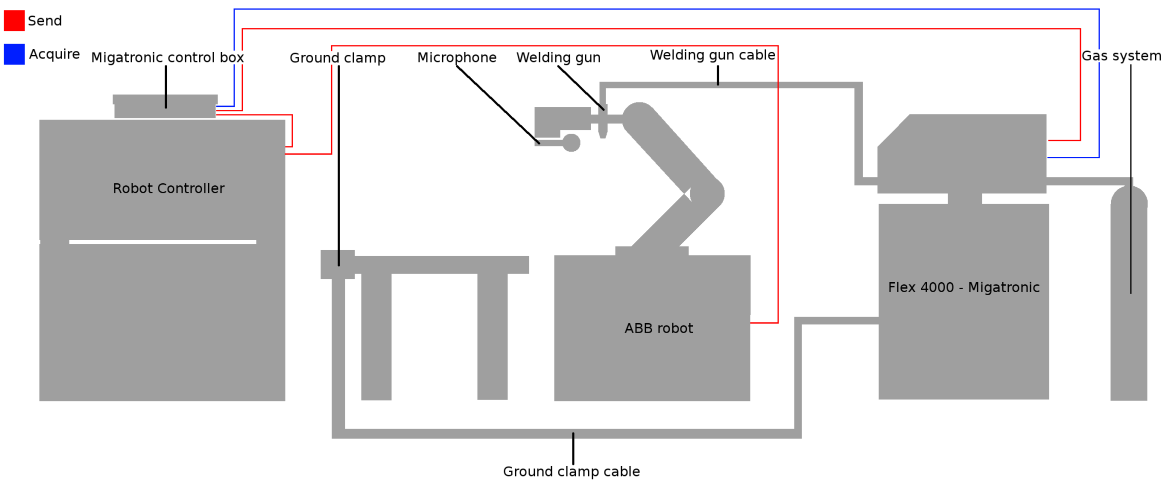

Figure 8.1: The available setup at Aalborg University.

As indicated on the figure the equipment consists of the following items:

- Gas system
- Flex 4000 Migatronic welding equipment
- Welding gun + cable
- Ground clamp + cable

- Robot controller
- Migatronic control box
- ABB robot
- Microphone
- Welding fixture

The gas system, Flex 4000 Migatronmic welding equipment, welding gun, welding gun cable, ground clamp and ground clamp cable are connected as specified in section 1.1. The gripper of the ABB robot holds the welding gun and is equipped with a stand for the microphone. Control of the robot and welding equipment happens through the robot controller which sends the signals directly to the robot and indirectly to the welding equipment through the Migatronic control box. Furthermore the Migatronic control box acquires the actual voltage and current of the welding equipment at a sample rate of 1 Hz.

To provide deeper understanding of the equipment each module is described in detail.

Welding equipment

The welding equipment is provided by Migatronic and is of the type Flex 4000 [Migatronic, 2017]. It can deliver a wire freed speed of 1 - 24 $\frac{m}{min}$, a current of 5 - 500 A and sets the voltage automatically. Inside a drum of 1.2 mm rutile flux-cored wire [welding, 2013] is mounted and the machine is fed gas from an external source.

Gas system

The gas system consists of a gas cylinder, a regulator and a manometer. In the gas cylinder there is Mison 18 [AGA, 2015] which is a gas consisting of primarily ≈18 % CO_2 and ≈82 % argon. Going from the cylinder to the welding equipment, the gas passes through a regulator onto which a manometer is mounted. On the regulator the flow of gas can be changed and the actual flow is measured and shown on the manometer.

ABB robot

The robot is made by ABB and is of type IRB 140 [ABB, 2017]. It has 6 degrees of freedom allowing it to control the work-, travel- and rotational angle as well as perform the required movement for the process. It is controlled through a supplied robot controller that reads RAPID programs. A hand held pendant is used to perform online programming and alternatively programs can be written on a computer and send to the controller via FTP connection. The robot controller also communicates with the Migatronic control box. The controller enables the user to move the robot to a different point in space with a specified speed and an option to specify rounding of path between separate movements is available. Furthermore it has specific inputs for welding denoted as *seam*-, *weld*- and *weave* data is specified.

In the case of this report both seam- and weave data is disregarded leaving the weld data in which the WFS, voltage and travel speed of the weld is specified.

The robot is mounted with a gripper to hold the welding gun and has an attachment onto which a microphone can be mounted, see figure 8.2.

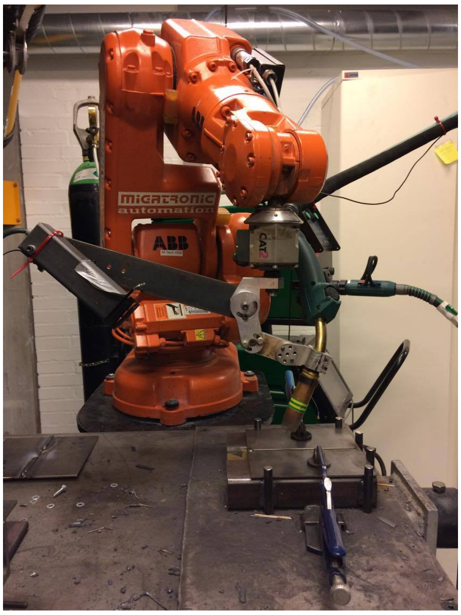

Figure 8.2: The ABB robot holding the welding gun and the attachment to the gripper holding a microphone.

Migatronic control box

The Migatronic control box sends and acquires signals from the welding equipment and communicates to the robot controller. The terminals of the control box are explained in the data sheet, see enclosure A. The box controls the welding equipment by activating WFS, gas flow, voltage and current once triggered. The signal for WFS and current ranges from 0 - 10 V and translates to a WFS of 0 - 24 $\frac{m}{min}$ or current of 0 - 400 A. The signal for voltage also ranges from 0 - 10 V and translates to an actual voltage of 0 - 100 V. Lastly the control box has terminals which output the measured voltage and current of the welding equipment.

Microphone

The microphone is from *Projects unlimited* and is of type AOM-6738P-R [unlimited, 2006]. The sensitivity of the microphone is stable between 20 Hz and 2 000 Hz after which its stability decreases going towards 20 000 Hz. However, it allows the acquisition of the frequencies in the human auditory range. Extra features of the microphone include being omnidirectional, meaning it can capture sound from all directions, and having distortion-free response.

Welding fixture

The welding fixture was designed and produced as part of this project and is shown on figure 8.3.

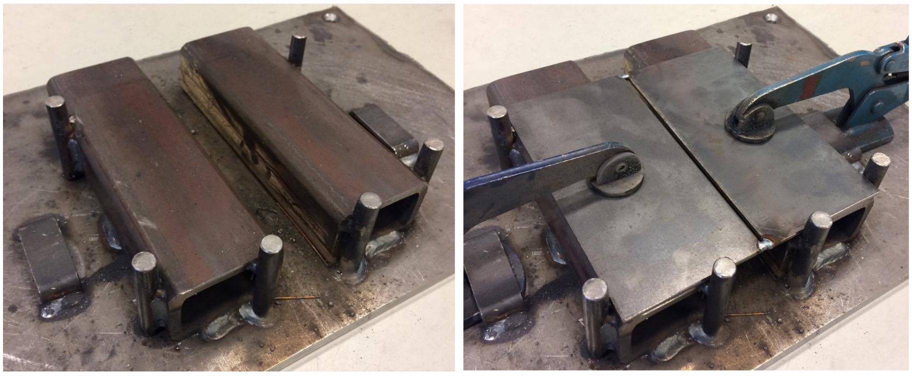

(A) (B)

Figure 8.3: The welding fixture.

As shown on figure 8.3 (A), the fixture consists of two section of a square pipe welded to a plate onto which six circular stops are welded to guide the work pieces. It is designed to leave a gap of 2 mm between two work pieces of 75 mm width. Onto the plate is also welded two sections of a U-pipe to allow welding clamps to secure the plates once on the fixture, see figure 8.3 (B). The entire fixture is fixed to the work table with two bolts in countersunk holes to secure its position in case of dis- and reassembly.

8.1.2 The data acquisition setup

It is decided to acquire both voltage, current and sound from the process. Sound is acquired from the microphone while voltage and current is acquired both from the Migatronic control box and newly installed sensors on the welding equipment. The low sample frequency of the measurement of voltage and current in the Migatronic control box makes the signal unable to effectively capture the characteristic events of the voltage and current as explained in chapter 4. Therefore a voltage probe and current sensor is installed on the equipment and sampled at a higher frequency.

The full data acquisition setup is shown on figure 8.4.

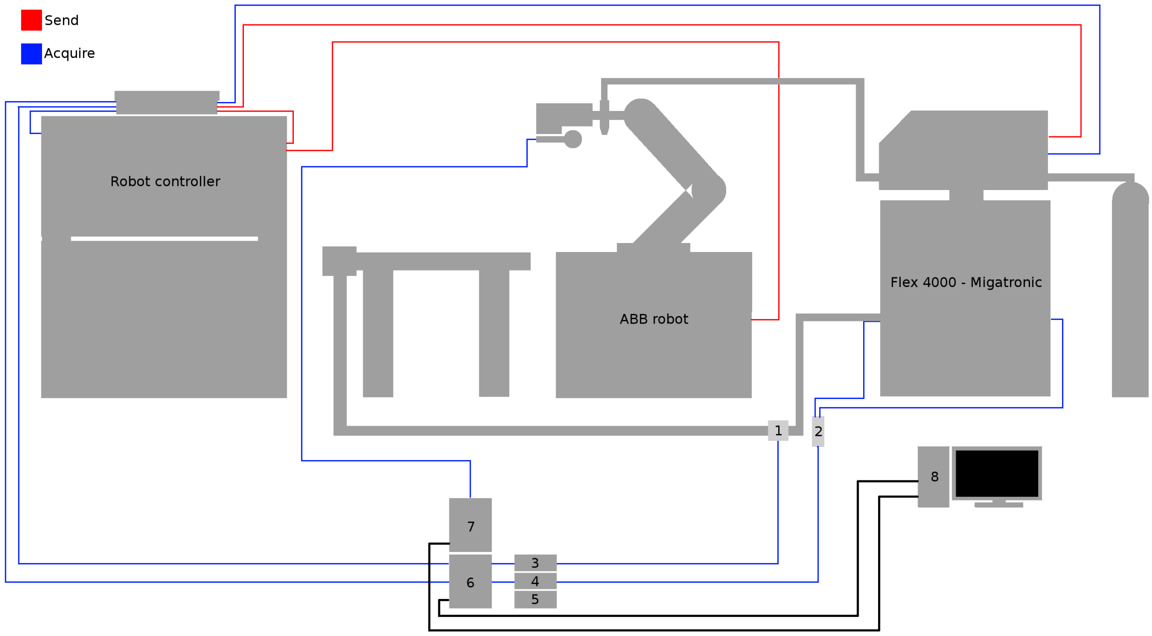

Figure 8.4: The data acquisition system at the cell at Aalborg University.

On the figure it is shown that the current sensor (1) is connected to the ground clamp cable. Furthermore the voltage probe (2) is connected to the welding equipment to capture the voltage gap. Each of the sensors' output a signal which goes through an optocoupler (3) and (4) powered by a power supply (5) to provide galvanic separation between the data acquisition system and the sensor. Wires from the two sensors along with the measured voltage and current from the Migatronic control box are all connected to a data acquisition card (6) which sends the signals to a computer (8). Lastly the microphone is connected to a sound card (7) which also sends the signal to the computer after which a program reads the data and saves it in files so it can be processed externally.

To gain a greater understanding of the equipment each module is described in detail.

Current sensor

The sensor used to acquire the current is a Hal 400-S sensor from LEM [LEM, 2015]. It requires a supply voltage of -15 V to 15 V, has a measuring range of ± 1000 A and outputs a voltage of ± 4 V. The signal can be amplified and an offset can be set directly on the sensor. The sensor is implemented in the system as shown on figure 8.5.

Figure 8.5: The Hal sensor set to measure the current through a wire connected to the work table and the ground clamp.

As indicated on the figure, the ground clamp is mounted to a piece of wire mounted to the work table. The Hal sensor is mounted on the piece of wire to measure the current running through the system.

Voltage probe

The voltage probe was included in the purchase of the setup and of an unspecified producer. It takes an input of 0 - 100 V and converts it to a 0 - 10 V signal.

Optocoupler system

The two optocouplers are of type PR 2284 [electronics, 2017a]. Although they have other functions, the function used in this report is to obtain galvanic separation between the sensors and the data acquisition system. Depending on type they take a different input and provide different outputs. The ones chosen in this project are type E6 which takes an input of 0 - 10 V and outputs 0 - 10 V. They require a power supply of 24 VDC which is provided by a PR 2220 [electronics, 2017b]. It is a switch mode power supply and enables the use of the two optocouplers.

Data acquisition card

The data acquisition card is from National Instruments and is called NI USB-6216 M series [NationalInstruments, 2009]. It is a 64 screw terminal card with the possibility to both input and output analogue signals and transfers data through a USB connection to a computer which also acts as its power supply. For inputs it has an aggregate or single channel sample frequency of 400 $\frac{kS}{s}$, an ADC resolution of 16 bit and take inputs ranging from ± 10 V. For outputs it has an update rate of 250 $\frac{kS}{s}$, a DAC resolution of 16 bit and outputs signals of ± 10 V.

Sound card

The sound card used is Edirol UA-25 [RolandCorporation, 2004]. It connects to a microphone through XLR connection, has two channels, a 24 bit resolution and a sample rate of 96 kHz. It communicates with the computer through USB connection from which it is also powered.

Software

The data from the data acquisition card and sound card is sent to the computer through USB. Since National Instruments has their own data acquisition program, LabView, it is decided to use this for data acquisition.

The developed LabView program alongside a description of its structure and functionality is found in appendix F.

Experiment design and execution 9

In this chapter the experiments to perform are designed and executed. Initially an introduction to good practice in experiments is given followed by a specification and result presentation for each performed experiment.

9.1 Experiment design

To ensure the quality of the performed experiments one must be methodical and consistent. This section aims to highlight how to perform and which factors affect the quality of experiments using the work of Douglas C. Montgomery [Montgomery, 2012].

9.1.1 A good experiment

Any designed experiment should follow the principle of KISS, i.e. *Keep it small and sequential*. This means that presented with a complex task it should be broken down into smaller experiments performed sequentially. In the case of this report it is necessary to map a feature space based on sound to a the penetration state of GMAW and its metal transfer modes. To do so it is chosen to work with supervised learning which in turn means that the need for labelling the data is present. To gain sufficient knowledge about the feature space the individual penetration states and metal transfer modes must be provoked so their respective data can be logged and used for training the model. However, being a complex process it is unclear in which ranges of the input values the desired penetration states and transfer modes are provoked. In this case using the KISS principle would be beneficial to separate the identification of the required values and the actual classification data acquisition.

Besides using the KISS model it is important to know the difference between controllable variables and uncontrollable variables. Controllable variables are process parameters such as voltage, current and WFS which can be changed on demand. In contrast uncontrollable variables can not be easily changed such as work piece thickness and environmental factors. For a good experiment it is important to minimise the effect of uncontrollable variables and to have control over the controllable variables' variance, i.e. having variable control.

9.1.2 Discussion

Seeing as the goal of the experiments in this report is complex, it is decided to use the KISS principle. Doing so has lead to a composition of four experiments:

- Identifying conversion rates
- Identifying penetration state and transfer mode settings
- Classification data acquisition for penetration states
- Classification data acquisition for transfer modes

In the composition the initial experiment involves determining the correct conversion rates for the implemented sensors. In the second experiment settings for provoking penetration states and transfer modes are found so that the classification data for the case of identifying penetration states and transfer modes can be performed.

9.2 Procedure and settings

A range of variables are held constant during the experiments and are therefore out of consideration in the experiments. These parameters and the basic procedure of the experiments are explained in this section.

9.2.1 Settings

The input parameters are voltage, WFS and travel speed. However, as presented in chapter 1, the welding process is affected by a range of other parameters. The settings used for these experiments are presented in table 9.1.

Parameters/variables	Value
Work piece parameters	
Material plate 1	S235JR
Material plate 2	S235JR
Start temperature	22^{o}C
Equipment parameters	
Gas mixture	Mison 18
Gas flow rate	14 $\frac{L}{min}$
Gas nozzle diameter	20 mm
Wire type	Flux-cored
Wire diameter	1.2 mm
Work piece variables	
Root gap	2 mm
thickness plate 1	3 mm
thickness plate 2	3 mm
surface plate 1	Unknown
surface plate 2	Unknown
Groove horizontal angle	0
Groove vertical angle	0
Welding control variables	
Work angle	8
Travel angle	22
Rotational angle	0
CTWD	5 mm
Travel speed	Input
Voltage	Input
WFS	Input
Oscillation on	No

Table 9.1: The settings used for the welding experiments.

To clarify how these parameters were chosen an explanation of the work piece parameters and variables, the equipment parameters and welding control variables is given.

Work piece parameters and variables

The work pieces used for the experiments are 150 mm long sections of 3 mm x 75 mm S235JR metal bars from Sanistål [Sanistaal, 2017] stored at room temperature, i.e. approximately 22^{o}C. The root gap of 2 mm is chosen on the basis of the rule of thumb in ISO 9692 [DanskStandard] stating that for square butt welds of plates with a thickness below 4 mm a root gap of approximately the thickness of the plate should be used. Following this rule the root gap should be 3 mm. However, using 1.2 mm diameter wire sets a relatively high requirement for the energy level in the weld. Consequently the decrease of 1 mm in the root gap is chosen to lower the probability of burn through. Lastly the surface of the work pieces are not considered in this project and since the work pieces are parallel to the ground the groove angles are both 0.

Equipment parameters

In regards to the equipment parameters no changes have been made to the current setup. Consequently the gas mixture is Mison 18, the flow rate is 14 $\frac{L}{min}$, the nozzle diameter is 20 mm and the wire is 1.2 mm rutile flux-cored wire as specified in chapter 8.

Welding control variables

Initially, since the travel speed, WFS and voltage are input variables, no value is given in table 9.1. In regards to the rotational and work angles these should be zero since the weld is a flat square butt weld. However, due to limitations of the setup, having a work angle of 0 is impractical. As a consequence of this the work angle is 8 degrees. The travel angle and CTWD are determined through initial experiments and set to 22 degrees and 5 mm respectively. Lastly the binary value for whether the oscillation is on is set to 0 since it is decided in the problem specification not to investigate the effect of oscillation patterns, see chapter 5.

9.2.2 The experiment procedure

Before the robot performs the full weld, it is decided to tack weld the work pieces. Doing so reduces the warpage of the plates during the full weld and provides the robot with a spot to strike the arc in the beginning of the process. The tack welding is done manually using the fixture presented in section 8.1. Once the work pieces are tack welded, the fixture is mounted on the work table of the robot cell.

After mounting the fixture the RAPID program for the weld is run without striking an arc so the path can be checked. Once the path is assessed to be of suitable precision the settings for the weld is input, the data acquisition program is started and the weld is performed. Once finished, the data acquisition is stopped, the work piece is dismounted from the fixture and numbered according to the name of respective data files.

9.3 Sources of variance

During the experiments variance is expected in regards to a range of controllable and uncontrollable variables. These and the preventive actions to minimise their impact is presented in this section.

9.3.1 Controllable variables

The controllable variables, the cause of their variance and the preventive action to minimise their variances' effect is shown in table 9.2.

Variable	**Cause of variance**	**Preventive action**
Welding control parameters Equipment parameters	Internal equipment variance	None
Work piece temperature	Storage temperature Heat transfer	Work pieces stored at same temperature
Root gap	Work piece geometry Fixture geometry Tack welding	Tack welded in sequence by same person Visual comparison to template gap
Groove horizontal angle Groove vertical angle	Geometry and parallelity of work table Geometry and parallelity of fixture	None

Table 9.2: Controllable variables, their cause of variance and the preventive action to minimise their effect.

As indicated by table 9.2 no preventive action is taken for the welding control parameters, equipment parameters or groove angles. In regards to the welding control parameters the decision to not perform a preventive action lies in the fact that it would require online correction of the parameters or improvement of the equipment which is out of the scope for this project to develop. For the equipment parameters, preventive actions are not taken since the variance in gas mixture, wire diameter, nozzle diameter and wire type is assessed to be of less effect relative to the other sources. Lastly no preventive action is taken to minimise variance of the groove horisontal and vertical angles since they are assessed to be subject to less variation relative to the other sources.

In regards to the work piece temperature, the problem lies in the fact that the material properties of the metal changes with temperature. It is assessed that storing the work pieces in the same room and letting them cool down after tack welding is a sufficient action to minimise the variance caused by the initial temperature. In regards to the heat transfer of the process no preventive action is taken.

The last source of variance for the controllable parameters is the root gap. This is categorised as a controllable variable since manual tack welding is performed. In an attempt to minimise the effect of performing the process manually it is performed in sequence by the same person. Furthermore, a visual comparison to a template gap size determines the usability of the work pieces to eliminate outliers.

9.3.2 Uncontrollable variables

Similarly to the controllable variables the name of the variable, the source of its variance and the preventive action to reduce its effect is presented for each uncontrollable variable in table 9.3.

Variable	Cause of variance	Preventive action
Work piece material	Material property variation	None
Work piece surface	Oxidation, oils, geometry, coating	None
Work piece thickness	Production method Cutting method	Cut using saw Deburring of non-welded edges Allignment of burrs on welded edge
Environment	Noise Temperature changes	Data acquired past regular work hours

Table 9.3: Uncontrollable variables, their cause of variance and the preventive action to minimise their effect.

As shown in table 9.3 no preventive action is taken in regards to work piece material and surface variance. This decision is made based on the assesment that the materials bought from Sanistål did not require special attention to reduce these parameters' variance.

Although the work piece thickness mostly refers to the tolerance of the thickness of the plates the presence of burrs is included in this consideration. Although no preventive action is taken to reduce the variance of the work piece thickness, several actions are taken to remove burrs. The burrs come from a combination of cutting by blade and saw. The steel bars are previously cut into 6 000 mm x 75 mm bands by blade causing the edges to suffer from a burr on the longitudinal edges, see figure 9.1 (A).

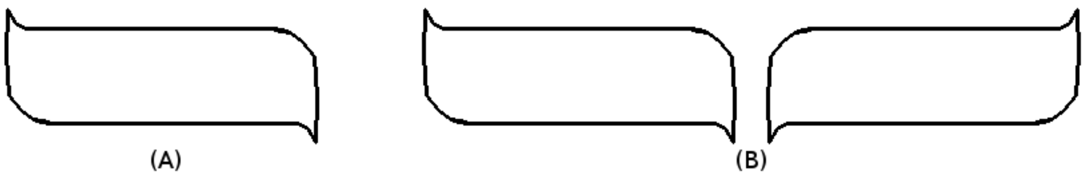

Figure 9.1: Sketched cross-sectional view of a plate post cutting.

To reduce the variance in the welds caused by this, the plates are placed with the burr facing downwards for every weld as indicated by figure 9.1 (B). The process of cutting metal with a blade also has the disadvantage of causing the material to warp. However, it is assessed not to be necessary to take preventive action to minimise this variance. To prevent further warpage it is decided to cut the steel bars using a saw when sectioning the 6 000 mm steel bar into 150 mm sections. Furthermore the burrs caused by the saw is removed after sectioning.

In regards to the environment, variance is caused by noise and temperature changes. These effects are mainly present when the area around the robot cell is subject to people working or passing through. To reduce the effect of these sources all data was acquired outside regular work hours under quiet, stable conditions.

9.4 Identifying conversion rates

An experiment is performed to determine the conversion rates from the voltage probe and current sensor. The experiments are specified and documented in appendix G. Based on the results from the experiments, conversion rates were implemented in the data acquisition system in order to acquire the actual voltage and current of the process.

9.5 Identifying penetration state and mode settings

In this section a range of experiments are performed to identify settings at which the different transfer modes and penetration states occur.

9.5.1 Specification

In regards to provoking the different metal transfer modes it is known from the theory presented in section 1.1.5 that the limit between short-circuit transfer and globular/spray transfer lies at 22 V. The transfer mode should not be affected by the travel speed which is why it is held constant through the experiments. Although the high argon gas of Mison 18 is suitable for provoking spray transfer it is assessed that an investigation of spray transfer is out of consideration. The decision is based on the fact that the work pieces used are 3 mm thick steel with a root gap of 2 mm which puts a limitation in the amount of heat put into the weld and therefore cant exceed the transition current as explained in section 1.1.5. Since the original setting of the welding equipment is approximately 22 V the settings used in the experiments are as shown in table 9.4.

Travel speed	Voltage	WFS
1	0	0
1	2	-2
1	4	-4
1	-2	2
1	-4	4

Table 9.4: The settings used to provoke short-circuit and globular transfer.

It should be noted that the settings are the adjustments made to the default settings of the welding equipment. By using the settings displayed in table 9.4 a coarse breaking point for the transfer mode can be found after which tweaking of parameters can be used to identify a finer breaking point. The adjustment of the WFS for each level of voltage is made to counteract the increase or decrease in power caused by the change in voltage from the default. Furthermore it enables the data to be used in the determination of the conversion rates in appendix G. To identify which transfer mode is active, a camera films the weld through a piece of welding glass.

In regards to provoking penetration states the range of possible states are limited to three - lack of penetration, full penetration and excessive penetration. To further narrow the problem it is decided to only investigate the welding defects for short-circuit transfer mode. Considering this, only voltages below 22 V are used and varied alongside the WFS and travel speed to identify the settings at which the different penetration states occur. Determination of the states is done visually based on the cases shown in figure 9.2.

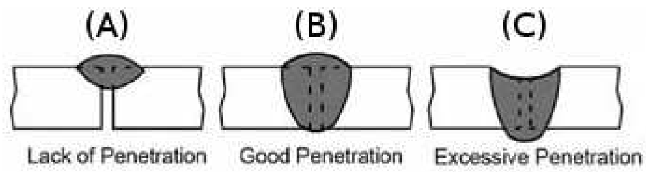

Figure 9.2: Example of (A) lack of penetration, (B) full penetration and (C) excessive penetration [Bernard, 2017].

Furthermore ISO-5817 provide the specifications listed in table 9.5 which is used to verify the presence of each negative penetration state.

Lack of penetration				**Excessive penetration**		
D	C	B		D	C	B
h $\leq$ 0.2 t (max 2mm)	Not allowed	Not allowed		h $\leq$ 1mm + 0.6 b	h $\leq$ 1mm + 0.3 b	h $\leq$ 1mm + 0.1 b

Table 9.5: Specifications for quality class B, C and D of a weld based on values t, h and b for lack of penetration and excessive penetration - h being the depth of the gap on the bottom of the weld or the bead stick-out, t being the thickness of the work pieces and b being bead width [DanskStandard, 2014].

9.5.2 Results

The result of the investigation of transfer modes is presented in table 9.6.

Travel speed	Voltage [V]	WFS [$\frac{m}{min}$]	Transfer mode
1	0	0	Globular
1	2	-2	Globular
1	4	-4	Globular
1	-2	2	Short-circuit
1	-4	4	Short-circuit

Table 9.6: The result of the investigation of settings for globular and short-circuit transfer mode

As indicated on table 9.6 the shift in transfer mode occurs between a voltage adjustment of 0 V and -2 V as illustrated on figure 9.3.

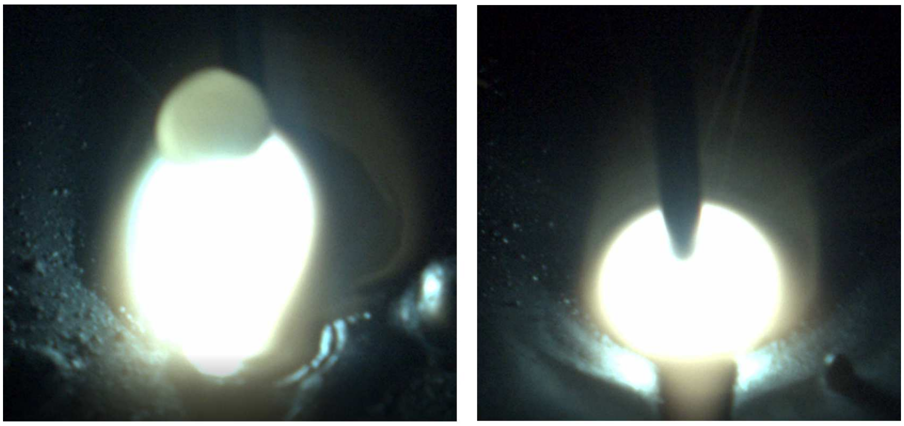

(A) (B)

Figure 9.3: (A) Globular transfer mode using the default settings of the equipment and (B) short-circuit transfer mode where voltage is adjusted by -2 V and WFS is increased by 2 $\frac{m}{min}$.

As indicated on figure 9.3 (A) a glob is clearly formed at the tip of the electrode and is about to be transferred to the material. In contrast the electrode continuously comes in contact with the molten pool of material without forming a glob in the video from where the snapshot on figure 9.3 (B) is taken. To further specify the breaking point experiments using a voltage adjustment of -1.5 V, -1.0 V and -0.5 V was performed. From these experiments it is determined that as the voltage adjustment moves towards -1.5 V the occurrence of globs is decreased. At -1.5 V occasional globs are formed when using a WFS adjustment of 0 $\frac{m}{min}$ which is why the transfer mode is classified as short-circuit. However, being on the breaking point, a voltage adjustment of above -1.5 V should not be considered if short-circuit transfer is wanted.

During the experiments to determine at which settings the different penetration states occur it became clear that provoking penetration states at low travel speeds was more reliable than at higher speeds. Therefore the travel speed was held constant at 2 $\frac{mm}{s}$ in the remaining experiments to determine at which settings lack of penetration, full penetration and excessive penetration could be provoked. The most promising results of this investigation is presented in table 9.7.

Travel speed [$\frac{mm}{s}$]	Voltage [V]	Wire feed speed [$\frac{m}{min}$]	State
2	3.5	7.0	Lack of penetration
2	2.8	5.5	Full penetration
2	3.5	7.0	Excessive penetration

Table 9.7: The settings of travel speed, voltage and wire feed speed at which the welding states of *Lack of penetration*, *Full penetration* and *Excessive penetration* occurs the most.

As shown in table 9.7 the most promising settings for provoking a lack of penetration is the same as the settings for provoking excessive penetration. During the experiments the settings of 2 $\frac{mm}{s}$, +3.5 V and +7.0 $\frac{m}{min}$ showed a tendency of welding with insufficient penetration for the first part of the work piece and suddenly shifting to excessive penetration. The phenomenon is shown on figure 9.4.

Figure 9.4: A weld during which both lack of penetration and excessive penetration occurs.

In the case of full penetration, the results were stable around a voltage of 2.8 - 3.0 V and a WFS of 5.5 $\frac{m}{min}$.

9.5.3 Comments

Overall a high sensitivity to variance was highlighted during the experiments and leads to the conclusion that adaptation to the current performance of the equipment is needed during a set of experiments. Based on this conclusion, the classification data acquisition experiments should be initially performed with the most promising settings found in this set of experiments. However, should the result start to differ from the expected, tweaking of the input parameters should be considered.

9.6 Classification data acquisition for penetration states

The purpose of these experiments is to obtain data to be used in the classification of the penetration states. To do so, experiments are performed at the most promising settings to provoke lack of penetration, full penetration and excessive penetration found in section 9.5.

9.6.1 Specification

Through the experiments presented in section 9.5 the considered settings are as shown in table 9.7. Due to the equipment's sensitivity to variance the parameters are tweaked to accommodate for unexpected results.

Each weld is 150 mm if burn through does not occur. Using a constant travel speed of 2 $\frac{mm}{s}$ enables the acquisition of 75 seconds of sound, voltage and current for each full weld. The amount of data points obtained by these 75 seconds depends on the window size and overlap used in the windowing in chapter 11. Since no rule is present as to how large a window should be and how much overlap is best, the aim of these experiments are to acquire an equal amount of data for each state, aiming for approximately 750 seconds for each state, i.e. 10 welds of 150 mm.

9.6.2 Results

The results of the experiments are shown in table 9.8 with lack of penetration, full penetration and excessive penetration denoted as (1), (2) and (3) respectively.

	Voltage [V]	WFS $[\frac{mm}{s}]$	Repetitions	Expected state	Experienced state (1)	(2)	(3)
Pre-determined	-2.8	5.5	10	(2)	17 %	83 %	0 %
	-3.5	7.0	10	(1),(3)	11 %	3 %	86 %
Tweak - state (1)	-1.5	7.0	4	(1)	8 %	0 %	92 %
	-2.5	7.0	1	(1)	0 %	0 %	100 %
	-4.5	7.0	1	(1)	0 %	0 %	100 %
	-2.5	4.5	1	(1)	0 %	100 %	0 %
	-2.8	4.5	2	(1)	29 %	71 %	0 %
	-3.0	4.5	2	(1)	50 %	50 %	0 %
	-3.0	5.0	1	(1)	20 %	80 %	0 %
	-3.0	6.0	1	(1)	0 %	100 %	0 %
	-3.0	7.5	5	(1)	24 %	0 %	76 %
	-3.2	5.5	5	(1)	29 %	71 %	0 %
	-3.3	5.5	1	(1)	36 %	64 %	0 %
	-3.5	5.0	4	(1)	25 %	75 %	0 %
	-3.5	6.0	4	(1)	13 %	12 %	75 %
	-3.5	6.5	1	(1)	13 %	9 %	78 %

Table 9.8: A list of welds performed with pre-determined and tweaked settings including the expected and experienced penetration state using (1), (2) and (3) to denote lack of penetration, full penetration and excessive penetration respectively.

As indicated on table 9.8, the pre-determined settings for full penetration derived in section 9.5 was able to provide full penetration in 83 % of the 10 welds performed. However, despite being a promising candidate, the settings for a mix of lack of penetration and excessive penetration was not able to provoke an equal amount of weld with the two states. Instead it provoked mainly excessive penetration which led to early termination of the experiments with that setting and the initiation of tweaking.

In an attempt to provoke more welds with lack of penetration a variety of settings were used and displayed in the rows of table 9.8 denoted *Tweak - state (1)*. Using these settings it was not possible to identify a setting to consistently provoke lack of penetration. Despite imbalance in the amount of data acquired for each penetration state the experiments were terminated after the 33 welds performed in this section because of a limited supply of work pieces.

9.6.3 Comments

As a combination of the fact that the amount of work pieces were limited and that welds with a lack of penetration was challenging to provoke for a full weld of 150 mm, the result of the experiments is an imbalanced amount of data for welds with a lack of penetration and welds with full or excessive penetration. However, data is collected from all of the three penetration states enabling the possibility of training a neural network.

9.7 Classification data acquisition for transfer modes

The purpose of these experiments is to obtain data to be used in the classification of the transfer modes. Since a range of data for short-circuit transfer mode is obtained in the classification data acquisition for welding defects, see section 9.6, only data for globular transfer is to be obtained in this range of experiments.

9.7.1 Specification

For the simplest case of classifying the transfer modes only data from stable welds should be used to provide a general guideline for the type of data the individual modes produce. In the case of short-circuit transfer a stable setting turned out to be with a travel speed of 2 $\frac{mm}{s}$, a voltage adjustment of -2.8 V and a WFS adjustment of 5.5 $\frac{m}{min}$, see section 9.5 and section 9.6. In the identification of penetration state and transfer mode settings, see section 9.5, a stable weld for globular transfer was found when using a travel speed of 1 $\frac{mm}{s}$, a voltage adjustment of 2 V and a WFS adjustment of -2 $\frac{m}{min}$. To obtain a suitable amount of data for classification, repetitive experiments using these settings should be performed until the amount of data from the case of globular transfer roughly matches the amount of data for short-circuit transfer, i.e. $\approx$ 10 repetitions of a 150 mm weld.

9.7.2 Results

Due to a machine breakdown the ABB robot was incapacitated and therefore did not allow for the execution of further experiments.

9.7.3 Comments

Due to the machine breakdown of the ABB robot it was not possible to perform further experiments. However, from the experiments of section 9.5 a small amount of data can be extracted to use in the classification. Although the data is sparse it could provide knowledge as to whether classifying globular transfer and short-circuit transfer using sound is feasible.

10 Data analysis

As mentioned in chapter 6 the data acquired from the experiments in chapter 9 needs to be preprocessed through labelling, removal of improper classification data and filtering. In this chapter these steps are presented.

10.1 Data labelling

The labelling process is performed in two rounds - one for each hypothesis to test. Generally one-hot encoding is used as specified in appendix E to enable the use of cross-entropy.

10.1.1 Labelling of penetration states

As explained in section 9.5, three penetration states states exist:

[1 0 0] Lack of penetration

[0 1 0] Full penetration

[0 0 1] Excessive penetration

The labelling is done using Matlab. Initially the sound file is imported and cut to only include sound between the initial pulse of the weld to the final extinguishing pulse of the weld. By doing so, a sound file containing n amount of samples, equivalent to $\frac{n}{Fs}$ seconds, can be compared to the length of the weld in question. Afterwards it is determined how much of the start and finish of the weld should not be included due to the effect of the tack weld. Through visual inspection and random sample comparison to ISO-5817, the weld is then classified in segments of constant penetration state after which each segment is cut from the sound file and given a label as indicated on figure 10.1.

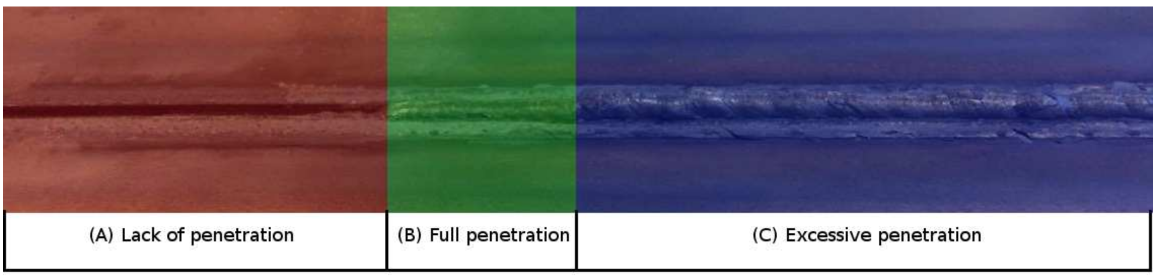

Figure 10.1: A weld segmented into three sections based on the penetration state.

Once this process is performed for all welds presented in section 9.6, merged sound files for each penetration state is made.

10.1.2 Labelling of transfer modes

As explained in section 9.7, two transfer modes are investigated:

[1 0 0] Globular transfer

[0 1 0] Short-circuit transfer

Due to the mechanical breakdown of the ABB robot, see section 9.7, a limited set of data is used for globular transfer. Specifically only segments of two welds from the experiments for identification of penetration state and mode settings are assessed useful. In case of the data for short-circuit transfer, the sound file for full penetration extracted in the labelling of the penetration states is used.

Since the transfer mode is constant for each full weld the labels are assigned to the full sound file. In the case for globular transfer, initially the sound file is cut to include only the sound of the weld excluding the start and finish. Once this process is performed for the two considered welds they are merged to one sound file. In the case of short-circuit transfer, the sound file is simply relabelled.

10.2 Removal of improper classification data

Since the merged sound files consist of segments from welds performed at different settings, an amount of variance is expected in the data. Using this data trains the ANN to classify despite of the variance which in turn makes it more flexible. However, the variance of the data can be too excessive for the ANN to distinguish between the classes. Therefore the merged sound files are plotted and visually inspected for noticeable difference between the segments from which they are merged. Should the data be assessed to cause more confusion between classes than flexibility for the given class, the segment is removed from the file.

The amount of data removed due to the inspection results is shown in table 10.1.

Class	Reduction of data [%]
Lack of penetration	39
Full penetration	2
Globular transfer	0

Table 10.1: The reduction of data after removal of bad data from each penetration state and globular transfer.

As specified in table 10.1, the data from welds with lack of penetration had the largest reduction of data with 39 %, whereas the data for the full penetration and globular transfer suffered a reduction of 2 % and 0 % respectively.

10.3 Filtering

Since a noisy signal may cause certain features to be hidden, generally it is beneficial to filter the signal. In order to do so, a noise profile is made.

10.3.1 Noise profile

In order to potentially design a filter it is required to have an idea of which frequencies are dominant in the noise. A segment of noise is therefore extracted from one of the sound files acquired during the performed experiments. On figure 10.2 (A) the segment of sound is presented and the corresponding spectrum is seen on figure 10.2 (B).

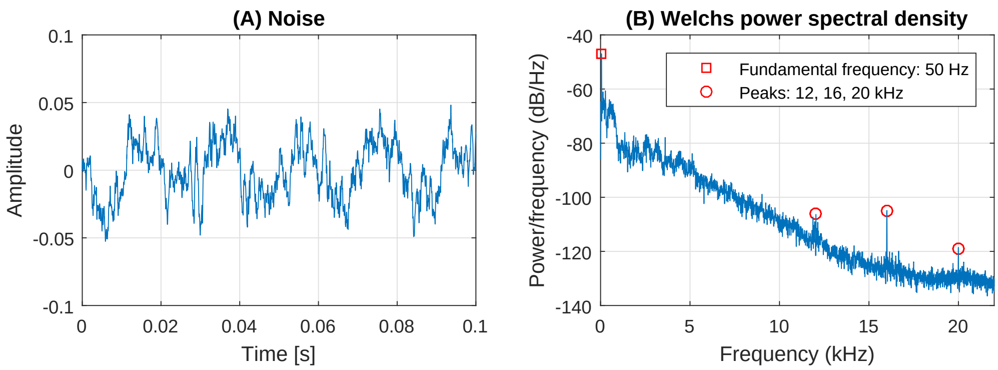

Figure 10.2: (A) a segment of noise and (B) its corresponding spectrum.

As indicated on figure 10.2 (B) the fundamental frequency of noise is found at 50 Hz which is also reflected in the 0.1 s of noise shown on figure 10.2 (A). Besides the fundamental frequency three dominant frequencies are spotted at 12, 16 and 20 kHz. However, the primary frequencies to remove lie in the range of 0 - 900 Hz.

10.3.2 Filter design

Based on the noise profile it is determined that the use a high-pass filter with a cut-off frequency at $\approx$ 900 Hz would remove the primary effect of the noise. An example of the implementation of a 4^{th} order butterworth high-pass filter is shown on figure 10.3 (A) and (B).

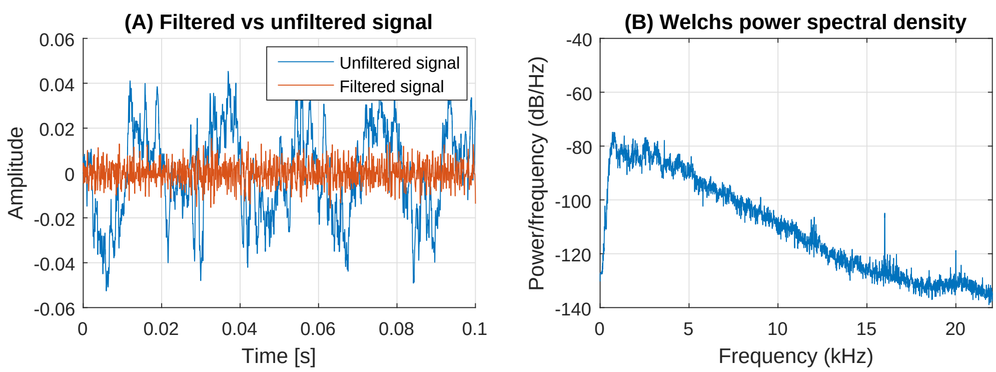

Figure 10.3: (A) The filtered and unfiltered noise as well as (B) its corresponding spectrum.

As shown on figure 10.3 (A) the primary influence of the noise is eliminated. The spectrum on figure 10.3 (B) illustrates the consequence of the filtering - frequencies below 900 Hz are filtered from the signal while the remaining spectrum is maintained.

10.3.3 Discussion

Applying a high-pass filter with a cut-off frequency of $\approx$ 900 Hz, e.g. a butterworth filter, eliminates the primary influence of the noise. However, since filtering involves a loss of information it is not necessarily beneficial to perform. It is assessed that filtering should be avoided if possible but may be applied in an attempt to increase performance of the ANN.

10.4 Feature extraction

In this section the discussion of which features to extract from the preprocessed data from chapter 10 is presented alongside the complete list of features.

10.4.1 Feature choice discussion

As introduced in chapter 2 a range of temporal, spectral shape, harmonic and perceptual features can be used to describe a signal. Especially the extraction of MFCCs as perceptual features includes the interesting aspect of being well-known for its use in speech recognition, which has been used for penetration state classification in other reports, see chapter 4. Furthermore, chapter 4 showed that using a wavelet packet decomposition, henceforth WPD, made it possible to classify penetration state for GTAW based on acoustic emission. Based on the two mentioned chapters it is decided to combine the methods to obtain a rich feature space with features known to be useful in the classification based on acoustic signals.

10.4.2 List of features

The feature extraction is done in Matlab using primarily built-in functions. Should a function for a given feature not be available, it will be manually coded or found from an external source. The set of temporal, spectral shape, harmonic and perceptual features alongside the code used to to extract them is shown in table 10.2.

Feature name	Symbol	Matlab code:
Temporal:		
Root amplitude	y_r	$\left(\frac{1}{N}\sum_{i=0}^{N-1}\sqrt{\lvert y_i\rvert}\right)^2$
Root mean square	y_{rms}	$rms(y)$
Mean	$\bar{y}$	$mean(y)$
Peak	$\hat{y}$	$max(\lvert\mathbf{y}\rvert)$
Shape factor	y_s	$\frac{y_{rms}}{\bar{y}}$
Crest factor	y_c	$\frac{\hat{y}}{y_{rms}}$
Clearance factor	y_L	$\frac{\hat{y}}{y_r}$
Impulse factor	y_I	$\frac{\hat{y}}{\bar{y}}$
Median	y_{med}	$median(y)$
Minimum	y_{min}	$min(y)$
Mode	y_{mod}	$mode(y)$
Variance	y_{σ^2}	$var(y)$
Kurtosis	y_K	$kurtosis(y)$
Skewness	y_S	$skewness(y)$
Zero crossing rate	y_{ZCR}	$\frac{\sum_{i=1}^{N}\lvert diff(y_i>0)\rvert}{N}$
Peak to peak value	y_{p2p}	$peak2peak(y)$
Peak to root mean square value	y_{p2rms}	$peak2rms(y)$
Root sum squared	y_{rssq}	$rssq(y)$
Spectral shape:		
Spectral centroid	S_{sc}	$meanfreq(Pxx, F)$
Spectral spread	S_{sp}	$\frac{\sum_{i=0}^{N-1}(F_i-S_{sc})^2 Pxx_i}{\sum_{n=0}^{N-1} Pxx_i}$
Spectral skewness	S_S	$\frac{\frac{\sum_{i=0}^{N-1}(F_i-S_{sc})^3 Pxx_i}{\sum_{n=0}^{N-1} Pxx_i}}{(S_{sc})^3}$
Spectral kurtosis	S_K	$\frac{\frac{\sum_{i=0}^{N-1}(F_i-S_{sc})^4 Pxx_i}{\sum_{n=0}^{N-1} Pxx_i}}{(S_{sc})^4}$
Median frequency	S_{med}	$medfreq(Pxx, F)$
Average power	S_{bw}	$bandpower(Pxx, F,' psd')$
Two-sided equivalent noise bandwidth	S_{enbw}	$enbw(y, Fs)$
Occupied bandwidth	S_{obw}	$obw(Pxx, F)$
3 dB bandwidth	S_{pbw}	$powerbw(Pxx, f)$
Harmonic:		
Total harmonic distortion	H_{thd}	$thd(Pxx, F,' psd')$
Signal to noise ratio	H_{snr}	$snr(Pxx, F,' psd')$
Signal to noise and distortion ratio	H_{sinad}	$sinad(Pxx, F,' psd')$
Perceptual:		
20 MFCC	P_{mfcc}	$melfcc(y, Fs, varargin)$(External script) [Ellis, 2012]

Table 10.2: The complete set of temporal-, spectral shape-, harmonic- and perceptual features extracted from each window of sound.

As shown in table 10.2 18 temporal features, 9 spectral shape features, 3 harmonic features and 20 perceptual features are extracted. This sums up to a total of 50 features covering both the time- and frequency domain. In addition to these, a WPD is made using Matlab's built-in function *wpdec()*, which is explained in the user guide [Misiti et al., 1996]. Doing so creates a WPD tree as shown in figure 10.4.

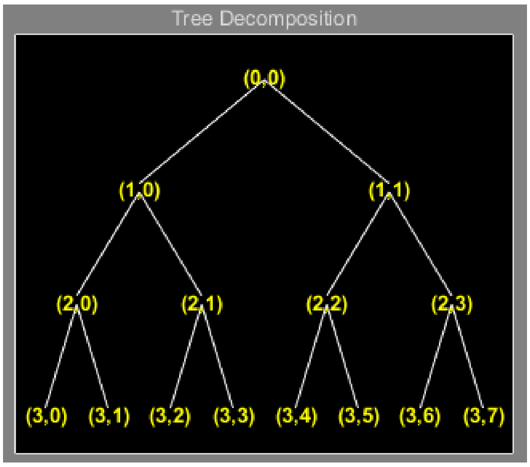

Figure 10.4: A wavelet packet decomposition tree of depth = 3.

Illustrated on figure 10.4 is a full WPD tree of depth three. It is naturally a binary tree due to the nature of the decomposition. It starts at the root with the original signal consisting of N samples. This is passed through two wavelet filters consisting of a low-pass filter going to node (1,0) and high-pass filter going to node (1,1). After downscaling the output, the result is $\frac{N}{2}$ discrete wavelet transform coefficients for both the low-frequency information, known as the *approximation coefficients*, and high-frequency information, known as the *detail coefficients*. The process is then repeated for the new nodes and continued until a desired depth is reached.

Since each node of the WPD tree is a set of coefficients, their nature can be described through descriptive statistics. Seeing as the temporal features in table 10.2 are mainly features from descriptive statistics, it is decided to extract the same features from each node of the WPD tree resulting in $18 \cdot (2 \cdot 2^{depth} - 1)$ features. Furthermore it is assessed that a depth of five is suitable for analysis of the signals in this report.

Seeing as the root of the wavelet packet decomposition tree is the original signal, the total amount of features to extract is given by:

$$\begin{aligned}
No.features &= No.\ of\ WPD\ features\ +\ No.\ of\ spectral\ shape\ features\ ...\\
&\quad +\ No.\ of\ harmonic\ features\ +\ No.\ of\ perceptual\ features\\
No.features &= (18 \cdot (2 \cdot 2^5 - 1)) + (9) + (3) + (20)\\
No.features &= 1166
\end{aligned}$$

11 Model training and performance evaluation

In this chapter a range of neural networks are trained with the aim of providing evidence to either accept or reject the hypotheses listed in chapter 5. Initially the challenges of designing the network and handling the data is discussed along with a description of the program used to execute the procedure. The results are then presented and commented on individually for the two sub-hypotheses.

11.1 Procedure

Before training a neural network, a range of decisions must be made:

- Should the signal be filtered?
- What window type, window size and overlap should be used?
- Should feature scaling be performed?
- Should dimensionality reduction be performed?
- What should the configuration of the network be?
- What optimisation method should be used?

The grounds for each decision is presented individually including an explanation of the final program made to execute the developed procedure.

11.1.1 Filtering

Based on the information presented in section 10.3, it is decided not to filter the signal to preserve as much information about the signal as possible. To obtain an idea of the impact of this decision initial experiments were made with various high-pass filters which showed little to no change in the accuracy of the trained models.

11.1.2 Window type, window size and overlap

The window size and overlap play an important role in the balancing of *data set size* and *information per segment* when working with limited data, see chapter 2. Furthermore the type of window determines where the weight of the window should be, see chapter 2. The effect of each and the decision made is presented individually.

Window type

Using a non-constant window such as the Hamming window, see chapter 2, subjects the values in the window to a variable gain, hereby putting more or less focus on parts of the window. While this can cause a potential benefit, it is decided to use of a rectangular, i.e. constant, window for the testing of the hypotheses in this report.

Window size

When determining the size of the window to use, one should analyse the signal to ensure that at least one repetition of the expected behaviour is performed. However, under the assumption that a state is constant for the duration of the window, an increased windows size causes an averaging effect over multiple repetitions which counteracts the variance between individual repetitions. Although providing a possible benefit in terms of averaging, doing so results in fewer windows for a given length of signal which potentially has a negative effect on the performance of the trained model by not capturing enough variance to properly classify the data.

Based on the uncertainty of the choice, it is determined to investigate the cases of using a window size of either 0.25 s, 0.50 s, 1.00 s, 2.00 s and 4.00 s. Using this range of window sizes is assessed to produce indications of the effect of increasing and decreasing window size and provide a guideline for future projects.

Overlap

As explained in chapter 2, using an overlap also creates an averaging effect on the features extracted from the signal. Furthermore, when using a limited data set, more windows can be extracted from the signal depending on the length of the signal and the size of the overlap. However, since the averaging effect is in the transition from a previous window to the current, it is unclear whether the use of the overlap has a beneficial effect on the performance of the ANN or if the repetition of the same data yields no improvement.

Based on the uncertainty of the choice, it is determined to investigate the cases of using an overlap of either 0 %, 25 % or 50 % on each case of window size.

11.1.3 Feature scaling

As presented in chapter 3, feature scaling can yield a beneficial effect on the performance of the ANN. It is therefore decided to include feature scaling.

11.1.4 Dimensionality reduction

Having 1166 features in total, see chapter 10, the use of dimensionality reduction might prove to be beneficial for the performance of the algorithm. However, before investigating the effect of dimensionality reduction, it is decided to train the ANNs on the full set of features.

11.1.5 Network configuration

The term *Network configuration* is in this report used to denote the structure of the ANN, i.e. the amount of hidden layers and neurons in each layer. Since the best network configuration is unknown it is decided to investigate a range of possibilities, see chapter 7. Specifically it is decided to consider the network having either one or two layers each consisting of 5-15 neurons. It is assessed that using this range of neurons and layers gives general insight as to which configuration is desired in the classification cases of this project.

11.1.6 Optimisation method

Based on the information presented in chapter 3 and chapter 7, it is decided to investigate the use of both GDA and SCG. The decision of using GDA lies in the use of adaptive learning rate, which improves the convergence rate of the optimisation compared to GD. In addition to this characteristic, the SCG is supposedly better at handling non-convex problems and allows faster convergence based on non-orthogonal steps and use of second-order information.

11.1.7 Program

To analyse the performance of the ANN model based on the decisions made in section 11.1, a Matlab program is made to cycle through all combinations. The general procedure is shown in a tree representation on figure 11.1.

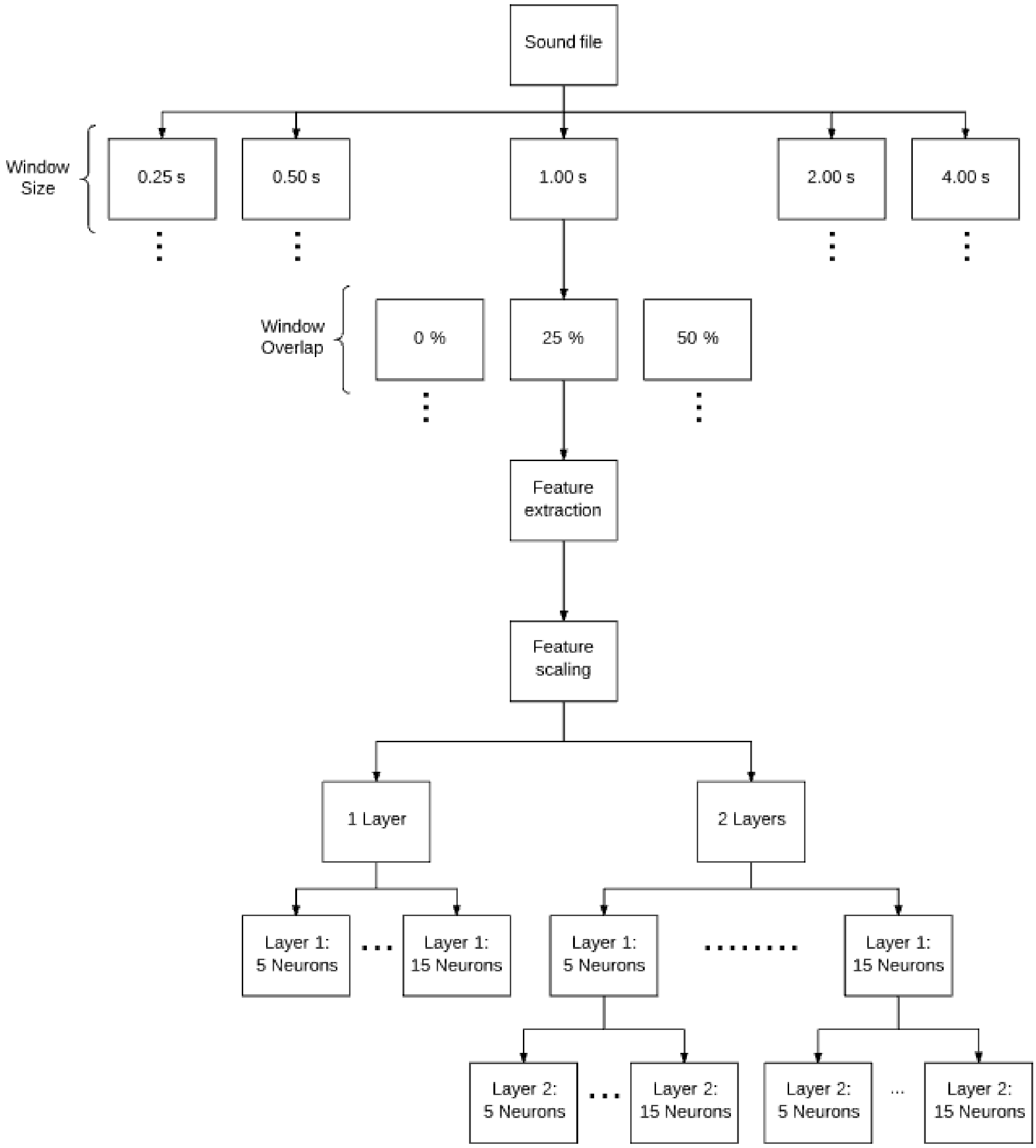

Figure 11.1: A tree representation of the program used to window a signal, extract features from the windows and train a range of ANNs.

To ease the explanation of the procedure only one branch of the tree is shown on figure 11.1. As shown, the *sound file*, is initially windowed using a window size of either 0.25 s, 0.50 s, 1.00 s, 2.00 s or 4.00 s and an overlap of either 0 %, 25 % or 50 %. Once the windowing is done, the features are extracted, feature scaled and sent to loop through ANN training with the specified network configuration.

For the network generation and training the *Neural Network Toolbox* of Matlab is used. The following settings are set for GDA:

- Initial learning rate: 0.5
- Maximum cost increase: 1.04
- Ratio to increase learning rate: 1.05

- Ratio to decrease learning rate: 0.7

For SCG two constants need to be defined:

- Change in weight for second derivative approximation: $5.0 \cdot 10^{-5}$
- Parameter for regulating the indefiniteness of the Hessian: $5.0 \cdot 10^{-7}$

Lastly training termination occurs if:

- ... 1000 iterations is reached
- ... the gradient reaches $1 \cdot 10^{-5}$
- ... 6 consecutive cost increases is experienced
- ... the performance goal of 0 is reached.

For a commented version of the entire Matlab program and used functions, see enclosure B.

11.2 Results

After running the program for both the penetration state classification and transfer mode classification, information about the network configuration with the best test set performance is extracted and presented individually. Throughout this section the terminology presented in table 11.1 is used.

Abbreviation	Full name
w_{size}	Window size
w_o	Overlap
N_1	No. of data points for class 1
N_2	No. of data points for class 2
N_3	No. of data points for class 3
N_{all}	No. of data points in total
GDA	Gradient descent with adaptive learning rate
SCG	Scaled conjugate gradient descent
FS	Feature scaling
PCA	Principle component analysis
BC	Best configuration
ACC	Accuracy

Table 11.1: A list of abbreviations and their full names.

11.2.1 Penetration state classification

In order to gather evidence to either accept or reject $\mathbf{h}_{1.1}$ from chapter 5, the program presented in section 11.1 is run on the data collected in the classification data acquisition for penetration states, see section 9.6, after performing the preprocessing described in chapter 10. The result is shown in table 11.2.

						GDA		SCG	
w_{size} [s]	w_o [%]	N_1	N_2	N_3	N_{all}	BC	ACC [%]	BC	ACC [%]
0.25	0	1291	5571	4560	11422	[8 0]	65.3	[13 5]	80.2
0.25	25	1721	7429	6080	15230	[13 6]	65.4	[15 10]	81.8
0.25	50	2583	11145	9121	22849	[9 0]	64.5	[11 9]	82.4
0.50	0	645	2785	2279	5709	[12 6]	70.4	[15 12]	83.7
0.50	25	860	3714	3039	7613	[12 10]	70.5	[6 15]	84.6
0.50	50	1291	5571	4560	11422	[8 5]	68.9	[10 6]	84.2
1.00	0	322	1392	1139	2853	[15 5]	74.4	[13 11]	84.1
1.00	25	429	1856	1519	3804	[12 10]	73.9	[12 0]	87.0
1.00	50	645	2785	2279	5709	[7 7]	72.5	[15 14]	86.3
2.00	0	160	695	569	1424	[13 9]	76.8	[12 0]	86.7
2.00	25	214	927	759	1900	[9 0]	77.4	[11 12]	87.1
2.00	50	322	1392	1139	2853	[14 5]	77.8	[14 13]	87.9
4.00	0	79	347	284	710	[5 0]	83.8	[13 5]	86.6
4.00	25	106	463	379	948	[14 0]	82.1	[14 8]	89.0
4.00	50	160	695	569	1424	[9 12]	80.7	[11 14]	90.2

Table 11.2: The test set accuracy of an ANN of the specified configuration with varying window size and overlap optimised by gradient descent with adaptive learning rate, GDA, and scaled conjugate gradient, SCG, descent.

Based on the results presented in table 11.2 initially an evaluation of the two optimisation methods and the general performance is presented. Afterwards an evaluation of the choice of windows size's effect on the credibility of the model is given followed by an investigation of the tendencies in regards to the network configurations. Lastly an assessment is made as to which ANN performs the best.

Optimisation method and general performance evaluation

A comparison of the results from using GDA and SCG is shown on figure 11.2.

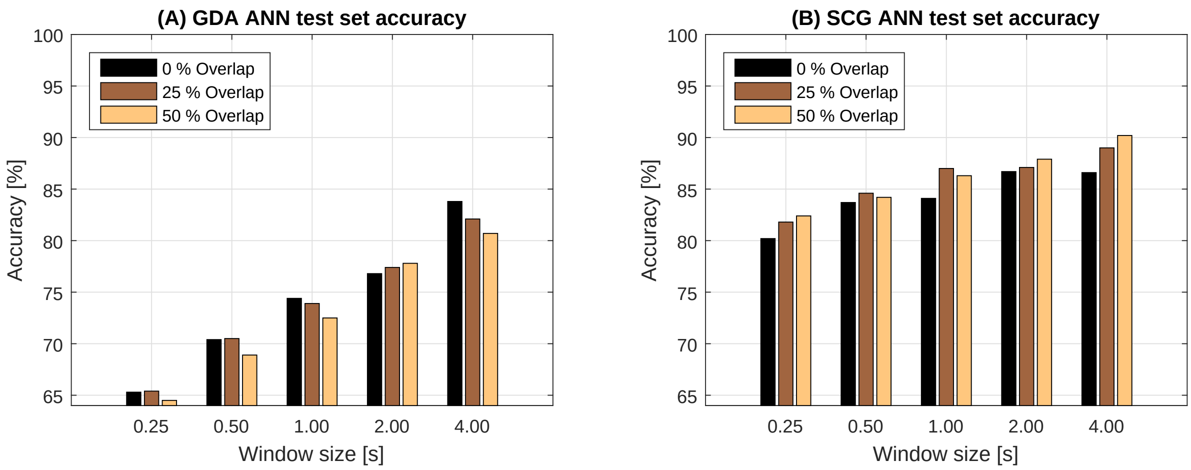

Figure 11.2: The ANN test set accuracy at different window sizes and overlap percentages using both (A) gradient descent with adaptive learning rate, GDA, and (B) scaled conjugate gradient, SCG, descent.

The result of using GDA is shown on figure 11.2 (A). It shows an increasing tendency with an increase in window size while showing a general tendency to obtain lower accuracy with an increase of overlap. The accuracy ranges from 64.5 % using a window size of 0.25 s and overlap of 50 % to 83.8 % using a window size of 4.00 s and an overlap of 0 %.

On figure 11.2 (B) the result of using SCG is shown. Similar to the case of GDA optimisation, the accuracy of the trained networks rises when the window size is increased. However, in contrast to the use of GDA optimisation, a tendency to increase with additional overlap is present for SCG. The accuracy ranges from 80.2 % with a window size of 0.25 s and an overlap of 0 % to 90.2 % with a window size of 4.00 s and an overlap of 50 %.

Comparing the two optimisation methods they both have a tendency to provide better test set accuracy when increasing the window size. However, comparing the results obtained at the same window size and overlap entails that the use of SCG generally provides better results. To obtain a deeper understanding of the trained ANNs, the individual target and class accuracy is presented in table 11.3.

		GDA			SCG		
		Target ACC/Output ACC [%]			Target ACC/Output ACC [%]		
w_{size}	w_o	(1)	(2)	(3)	(1)	(2)	(3)
0.25	0	24.9 / 59.8	78.9 / 68.9	59.0 / 60.7	56.6 / 68.4	84.5 / 81.0	81.4 / 81.8
0.25	25	20.1 / 62.3	75.0 / 69.8	65.6 / 60.2	61.1 / 70.1	86.7 / 82.7	81.7 / 83.5
0.25	50	12.8 / 82.1	78.0 / 66.7	62.2 / 60.8	59.2 / 73.5	87.7 / 82.6	82.4 / 84.1
0.50	0	36.6 / 75.4	75.1 / 74.7	74.7 / 65.3	53.8 / 71.1	90.4 / 83.6	83.3 / 86.5
0.50	25	39.9 / 57.8	73.9 / 73.6	74.6 / 69.4	65.3 / 78.8	89.4 / 84.2	84.4 / 86.5
0.50	50	33.8 / 76.4	78.9 / 71.2	65.5 / 64.7	59.8 / 76.5	89.5 / 83.1	84.7 / 87.3
1.00	0	49.1 / 84.4	75.6 / 79.5	79.0 / 68.0	59.7 / 72.9	86.2 / 86.5	89.2 / 84.1
1.00	25	44.7 / 70.4	80.0 / 77.9	74.4 / 69.6	59.0 / 82.1	91.3 / 86.7	88.7 / 88.4
1.00	50	44.2 / 73.5	77.7 / 74.3	74.9 / 70.3	64.9 / 72.5	89.7 / 87.4	87.3 / 87.9
2.00	0	48.6 / 100	85.5 / 77.1	75.5 / 72.8	45.5 / 66.7	90.3 / 87.3	89.8 / 88.3
2.00	25	40.0 / 84.2	84.2 / 78.9	78.5 / 74.3	63.4 / 68.4	89.6 / 90.6	90.4 / 87.6
2.00	50	49.1 / 75.0	78.7 / 83.4	83.4 / 72.3	63.5 / 73.3	90.4 / 88.2	90.4 / 90.4
4.00	0	76.9 / 90.9	90.8 / 79.7	78.1 / 87.7	76.9 / 90.9	82.7 / 93.9	94.4 / 78.5
4.00	25	46.7 / 87.5	90.5 / 83.3	77.1 / 79.4	88.9 / 80.0	89.0 / 89.0	88.9 / 92.3
4.00	50	42.9 / 100	84.1 / 84.1	85.8 / 74.6	73.5 / 78.1	92.8 / 91.5	92.0 / 92.0

Table 11.3: Breakdown of the test set accuracy through the individual target and output class accuracy of the trained ANNs with varying window size and overlap optimised by gradient descent with adaptive learning rate, GDA, and scaled conjugate gradient, SCG, descent.

In table 11.3 the *target accuracy* refers to how many of the the data points introduced for a certain class were predicted correctly. In contrast the *output accuracy* refers to how many times the model's prediction for a certain class was correct.

A tendency to be noted is the difference between target class and output class accuracy for lack of penetration when using GDA. Generally it performs poorly and only reaches beyond 50 % accuracy in one of the shown ANNs. Furthermore it goes as low as 12.8 %. However, the output class accuracy shows a mean accuracy of 78.6 %. This means that the ANN is not prone to predict that a given input is class 1 and therefore wrongly classifies the majority of class 1 inputs. However, when it does predict class 1, it is more accurate.

Considering the target class and output class accuracy of the remaining two classes, the model performs better than for class 1 with higher target class accuracy and a smaller gap between target class accuracy and output class accuracy.

In the case of the ANNs trained with SCG, the results are generally better. The same tendency of having a lower target class and output class accuracy for class 1 compared to class 2 and 3 is also found for these ANNs. However, the gap between the target class accuracy and output accuracy for class 1 is smaller than for the ANNs trained using GDA. Furthermore, the general accuracy for the ANNs trained using SCG is better than for those trained using GDA.

Window size and overlap evaluation

Based on the data presented in table 11.2 the effect of averaging with increased window size explained in section 11.1 seems to yield an improvement of the performance of the networks. In the case of increasing overlap only the ANNs trained on SCG seem to experience a stable improvement, while cases of increases and decreases in the accuracy of the ANN is experienced using GDA. In regards to the window size, it should be noted that the effect on the size of the data set lowers the credibility of the result. To illustrate the reduction, figure 11.3 shows the total amount of data points extracted from the signal based on the window size and overlap.

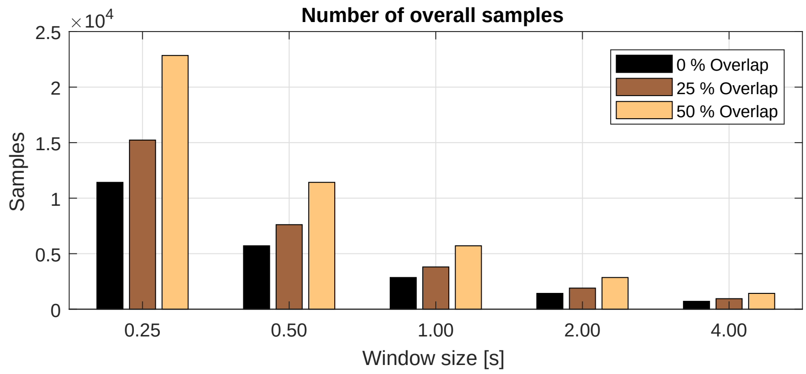

Figure 11.3: The number of samples as a function of the window size and overlap percentage.

As seen on figure 11.3 the amount of data points is halved with a doubling of the window size. With the limited data set used in this project this decrease can result in insufficient training data and in turn poor flexibility when introduced to new data, i.e. being overfitted. With an increase of overlap it is possible to obtain more windows per data set which could explain the increase in test set accuracy due to overlap experienced for the ANNs trained using SCG.

Network configuration tendency evaluation

As indicated in table 11.2 the best network configuration for the majority of the combinations consists of two layers. To obtain a general idea of how many neurons to place in each layer in this case, the distribution of neurons in the two layers for the best configurations is shown on figure 11.4.

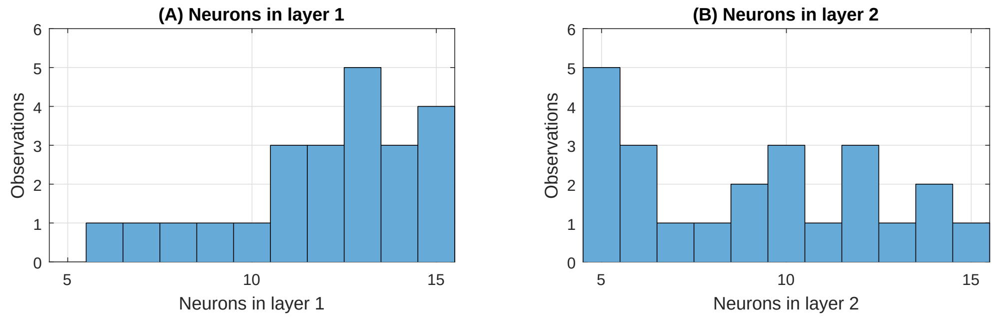

Figure 11.4: The distribution of neurons in the cases where two layers are used.

As indicated by figure 11.4 (A), the distribution of neurons in the first layer shows a mode of 13 neurons and a mean of 12.0 neurons. In relation to the second layer, the distribution on figure 11.4 (B) shows a mode of 5 neurons with a mean of 9.1 neurons. Furthermore the difference in neurons from the first to the second layer yields a tendency to have fewer neurons in the second layer. The mean difference is calculated to 2.9 neurons with a mode of 2 neurons.

In the case of having one layer the mode is 9 neurons and shows a mean of 9.9 neurons.

Best performance evaluation

Determining the overall best ANN based on the overall accuracy of the network as presented in table 11.2 may result in a network with poor performance when classifying class 1. Therefore the decision is also based on the target class and output class accuracy measures leading to the conclusion that the ANN trained using SCG based on features from windows of 4.00 s with an overlap of 25 % is the best of the trained ANNs. This network shows target class accuracy measures of 88.9 %, 89.0 % and 88.9 % and corresponding output class accuracy measures of 80.0 %, 89.0 % and 92.3 % for class 1, class 2 and class 3 respectively resulting in an overall accuracy of 89.0 %.

11.2.2 Transfer mode classification

In order to gather evidence to either accept or reject $\mathbf{h}_{1.2}$ from chapter 5, the program presented in section 11.1 is run on the acquired data for globular transfer and an equal amount of data for short-circuit transfer from the classification data acquisition for penetration state, see section 9.7, after performing the preprocessing described in chapter 10. A tendency to have an accuracy of 100 % regardless of network configuration was discovered during initial experiments. Based on this the program was simplified to only train networks of one layer with 10 neurons. The results are shown in table 11.4.

Window size [s]	Overlap [%]	N_{Glob}	N_{SC}	Accuracy (GDA) [%]	Accuracy (SCG) [%]
0.25	0	153	247	100	100
0.25	25	204	330	100	100
0.25	50	307	496	100	100
0.50	0	76	123	100	100
0.50	25	101	164	100	100
0.50	50	153	247	100	100
1.00	0	37	61	100	100
1.00	25	50	81	100	100
1.00	50	76	123	100	100
2.00	0	18	30	100	100
2.00	25	24	40	100	100
2.00	50	37	61	100	100
4.00	0	8	14	100	100
4.00	25	11	19	100	100
4.00	50	18	30	100	100

Table 11.4: The test set accuracy of an ANN with on hidden layer of 10 neurons with varying window size and overlap using both gradient descent with adaptive learning rate, GDA, and scaled conjugate gradient, SCG, descent optimisation.

As indicated on table 11.4, all of the trained networks has an accuracy of 100 %. It should be noted that the amount of data is limited as indicated by table 11.4 with the worst case being the use of a window of 4.00 s and no overlap, which causes the amount of samples for globular transfer and short-circuit transfer to drop to 8 and 14 respectively. Since no additional data can be added for globular transfer, an investigation is made where an increasing amount of data for short-circuit transfer mode is introduced in the learning algorithm. To gain the largest amount of data for globular transfer, the investigation was performed using only a window size of 0.25 s and 50 % overlap. The investigation is performed by gradually adding more short-circuit transfer data and training a network. The result is presented in table 11.5.

n_{Glob}	n_{SC}	Accuracy (GD) [%]	Accuracy (SCG) [%]
307	496	100	100
307	709	100	100
307	1936	100	100
307	3682	100	100
307	5858	100	100

Table 11.5: The test set accuracy of an ANN with 1 hidden layer of 10 neurons with a constant number of data points for globular transfer and a gradually increased number of data points for short-circuit transfer using both gradient descent with adaptive learning rate, GDA, and scaled conjugate gradient, SCG, descent optimisation.

As indicated in table 11.5, the addition of more short-circuit transfer data does not have an effect on the accuracy of neither of the networks.

Discussion 12

Based on the results from the classification of penetration state and transfer mode a discussion is made to argue whether sufficient evidence is present to accept the hypotheses presented in chapter 5. An individual discussion for each sub-hypothesis is presented in this section.

> $\mathbf{h}_{1.1}$: *It is possible to identify the penetration state of GMAW through its acoustic emission using an artificial neural network*

A range of networks was trained through both gradient descent with adaptive learning rate, GDA, and scaled conjugate gradient, SCG, descent using a total of 1166 features from rectangular windows of 0.25 s, 0.50 s, 1.00 s, 2.00 or 4.00 s with an overlap of 0 %, 25 % or 50 %. The results showed a tendency for increased accuracy for ANNs trained through GDA and SCG with increased window size as expected from the averaging effect it has. Furthermore the use of overlapping yielded beneficial results in terms of accuracy for ANNs traing through SCG while both increases and decreases are experienced for ANNs trained through GDA. The accuracy is expected to increase based on the averaging effect of larger windows as well as overlapping which is true for the case of ANNs trained through SCG. Since a contradictory result is found for the ANNs trained through GDA, it is plausible that the choice of optimisation method is to blame. From the investigation of the target class and output class accuracy measures it is derived that the target accuracy for the ANNs trained through GDA primarily lies below 50 %. This suggests the model being biased towards class 2 and 3, possibly due to the imbalance of data or wrong choice of features. However, based on the fact that ANNs trained through SCG do not have this problem and are able to produce target class and output class accuracy measures of 80 % and above, it is assessed that the problem lies with the optimisation method. A reason for this may be GDA's challenge of handling non-convexity.

Since target class and output class accuracy measures for class 2 and 3 for the ANNs trained through GDA are consistently greater than 70 % when using a window size of 2.00 s or 4.00 s regardless of overlap it is assessed that there is not enough evidence to reject $h_{1.1}$ for these cases. However, based on the consistently low target class accuracy for class 1, it is assessed that there is enough evidence to reject the hypothesis for these cases.

In regards to the ANNs trained through SCG it is assessed that there is not enough evidence to reject $h_{1.1}$ for any of the classes when using either a window size of 2.00 s with an overlap of 25 % or 50 % or a window size of 4.00 s regardless of overlap.

> $\mathbf{h}_{1.2}$: *It is possible to identify the metal transfer mode of GMAW through its acoustic emission using an artificial neural network*

In the case of classification of transfer mode, the same program as for the classification of penetration state was used. However, in this case the trained ANNs all consist of one hidden layer with 10 neurons based on early indications of producing models with 100 % overall accuracy regardless of network configuration. The results show that the trained ANNs all have 100 % accuracy regardless of window size, overlap and optimisation method. This is possibly the result of the lack of data present in the classification. The lack of data is illustrated in the data sets reaching a total of 22 data points for the worst case. However, the lack of data is also caused by the total data set for globular transfer only being based on two separate welds. Because of this only a small amount of variance is experienced which causes the model to be overfitted to the presented data and a poor performance on newly introduced data is expected. However, based on the fact that all the trained ANNs has an accuracy of 100 % it is assessed that there is not enough evidence to reject $h_{1.2}$.

Conclusion 13

The purpose of this report was to investigate the acoustic response of GMAW's capabilities in machine learning-based weld quality monitoring. To do so, an understanding of welding theory, signal theory and machine learning was built. In combination with a study of related work, a research area was specified through the following hypothesis and sub-hypotheses:

> $\mathbf{h}_1$: It is possible to monitor GMAW using an artificial neural network trained on labelled acoustic data
>
> > $\mathbf{h}_{1.1}$: *It is possible to identify the penetration state of GMAW through its acoustic emission using an artificial neural network*
> >
> > $\mathbf{h}_{1.2}$: *It is possible to identify the metal transfer mode of GMAW through its acoustic emission using an artificial neural network*

In order to test the hypotheses a robot cell capable of performing GMAW was modified so that voltage, current and sound from the process could be acquired. Experiments were performed to acquire data from three penetration states - lack of penetration, full penetration and excessive penetration - and two transfer modes - globular transfer and short-circuit transfer. The sound files were then windowed and labelled according to penetration state and transfer mode using one-hot encoding. In order to investigate the effect of window size, overlap, optimisation method and network configuration, a Matlab program was developed to run through every combination of a range of a range of window sizes and overlaps as well as 110 different ANN configurations. Furthermore the ANNs were trained through gradient descent with adaptive learning rate, GDA, and scaled conjugate gradient, SCG, descent. For each combination of window size and overlap, 1166 features were extracted consisting of 18 temporal features, 9 spectral shape features, 3 harmonic features, 20 perceptual features and 18 features from descriptive statistics for each node of a 5-level wavelet packet decomposition with a db4 mother wavelet.

Using the described method it was possible to train an ANN with target class accuracy of 88.9 %, 89.0 % and 88.9 % and corresponding output class accuracy of 80.0 %, 89 % and 92.3 % for the three penetration states respectively resulting in an overall accuracy of 89.0 %. Furthermore it was possible to train ANNs of 100 % overall accuracy in the classification of transfer mode.

Based on the findings of this project it is assessed that there is not enough evidence to reject the hypothesis, $\mathbf{h}_1$, based on the following assessments for hypothesis $h_{1.1}$ and $h_{1.2}$.

> $\mathbf{h}_{1.1}$: *It is possible to identify the penetration state of GMAW through its acoustic emission using an artificial neural network*

Based on the results of the classification of penetration states it is assessed that not enough evidence is present to reject the hypothesis for ANNs trained through SCG using features from windows of 2.00 s with an overlap of 25 % or 50 % or windows of 4.00 s using an overlap of either 0 %, 25 % or 50 %. Furthermore, it is assessed that there is not enough evidence present to reject the hypothesis for classification of full penetration and excessive penetration for ANNs trained through GDA using features from windows of 2.00 s or 4.00 s regardless of having an overlap of 0 %, 25 % or 50 %. Lastly it is assessed that enough evidence is present to reject the hypothesis for classifying lack of penetration in the case investigated in this project for ANNs trained through GDA regardless of using a window size of 0.25 s, 0.50 s, 1.00 s, 2.00 s, 4.00 s with an overlap of 0 %, 25 % or 50 %.

> $\mathbf{h}_{1.2}$: *It is possible to identify the metal transfer mode of GMAW through its acoustic emission using an artificial neural network*

Based on the results of the classification of transfer mode it is assessed that not enough evidence is present to reject the hypothesis for any combination of window size, overlap and optimisation method investigated in this project.

Perspectives 14

Based on the decisions made and consequent findings of this report, a range of perspectives and ideas for future work is derived and presented in this chapter.

14.1 Perspectives

The following perspectives are presented:

- Reduction of process variance
- Acquisition of more data
- Investigation general performance
- Noise reduction
- Reduction of feature space
- Expansion of feature space
- Inclusion of voltage and current features
- Inclusion of seam geometry features
- Inclusion of molten pool monitoring
- Inclusion of more transfer mode classes
- Alternative optimisation methods
- Alternative supervised classifiers
- Use of regression
- Use of reinforcement learning
- Implement online monitoring
- Implement control

To specify, each of the listed perspectives are discussed individually.

Reduction of process variance

The experienced variance due to the process nature and setup limitations in this project caused problems in consistent penetration state provoking. By reducing the variance the quality of the acquired data could be improved and potentially improve the accuracy of the trained classifier.

Acquisition of more data

To increase the credibility of the trained models, more data for the cases of short-circuit lack of penetration and globular transfer mode could be collected.

Investigation of general performance

Since the classifiers of this report was trained on data for a specific case of short-circuit GMAW of flat square grooved butt welds in steel with a 2 mm gap using a 1.2 mm rutile flux-cored wire using constant control variables, it could be interesting to investigate the trained ANNs' accuracy when introduced to new cases or train new models to accommodate for the introduced changes.

Noise reduction

The acquired sound showed a significant amount of sound which was only briefly investigated. A thorough investigation of the noise profile and the use of filtering could be done to reduce its potential effect on the model. Furthermore, to make the model suitable for implementation in industry, a study on the sensitivity of the method could be performed possibly involving the implementation of more microphones and use of the *Cocktail-party algorithm*.

Reduction of feature space

Through this project it was not attempted to reduce the feature space. As a consequence of this, no insight as to which features are dominating is derived and the feature space may include redundancies. To keep simple feature interpretation methods such as *forward feature construction* or *backwards feature elimination* could be used. If feature interpretability is less important, the use *principle component analysis* could be used.

Expansion of feature space

Although 1166 features were extracted from every window in case of this report, the list of possible features is endless. Including more features may improve the accuracy of the models if the new features are better at discriminating between the investigated classes.

Inclusion of voltage and current features

Since it was concluded in chapter 4 that the sound is highly related to the arc stability, using information from the current and voltage measurements may prove beneficial for the accuracy of the model.

Inclusion of seam geometry features

Although the goal of this project was to investigate the acoustic response of GMAW's capability within machine learning-based quality monitoring, it may increase general performance of the model to be trained on features describing the seam geometry.

Inclusion of molten pool monitoring

Including monitoring of the molten weld pool may provide information relevant for the penetration status and transfer mode of the process.

Inclusion of more transfer mode classes

In the case of this report, only globular transfer and short-circuit transfer was investigated. However, more metal transfer modes could be included in the classification such as spray transfer and pulsed spray transfer, which would further generalise the model.

Alternative optimisation methods

Only gradient descent with adaptive learning rate and scaled conjugate gradient descent was investigated in this report. However, the use of other optimisation methods may prove to have a positive effect on the accuracy of the ANNs and their training convergence rate.

Alternative supervised classifiers

In this report it was decided to investigate ANNs. However, a wide range of other supervised classifiers exist which may improve the accuracy of the prediction. Examples could be the use of decision trees as introduced in chapter 4 or instance-based algorithms.

Use of regression

Besides alternative supervised classifiers, the use of regression could be investigated. Mapping a continuous function to the sound features would ease the process of developing a closed loop system able of e.g. securing the correct penetration state.

Use of reinforcement learning

Another interesting direction is investigating the use of reinforcement learning. When introduced to a new material or joint design it is possibly required to determine new settings for the process. Reinforcement learning could be applied to develop a versatile, automated process to handle this aspect through a fitness function based on e.g. the seam geometry.

Implement online monitoring

Since the current models are performed post-weld, it could be beneficial to implement the model for online monitoring. Doing this also opens up for the possibility of implementing a control system.

Implement control

With the current model, it could be interesting to develop a closed loop control system which actions are based on the output of the trained model. Doing this also highlights the practical usage of the solution and the profitability of including this in production systems may be studied.

List of Figures

List of Tables

Bibliography

Aasvik, 2016. Mads Aasvik. *Arduino Tutorial: Simple High-pass, Band-pass and Band-stop Filtering*. https://www.norwegiancreations.com/2016/03/arduino-tutorial-simple-high-pass-band-pass-and-band-stop-filtering/, 2016.

ABB, 2017. ABB. *IRB 140*. http://www02.abb.com/global/inabb/inabb509.nsf/0/69745070bea1bbde6525703b00302f57/$file/Robotics+IRB140.pdf, 2017.

AGA, 2015. AGA. *Sikkerhedsblad - MISON 2, 8, 16, 18, 25*. http://www.aga.dk/internet.lg.lg.dnk/da/images/MISON_2%2C8%2C16%2C18%2C25_DK575_123025.pdf?v=2.0, 2015.

Alcotec, 2017. Alcotec. *Destructive Testing of Welds*. http://www.alcotec.com/us/en/education/knowledge/weldinginspection/Destructive-Testing-of-Welds.cfm, 2017.

ASNT, March 2017. ASNT. *Introduction to Nondestructive Testing*. https://asnt.org/MinorSiteSections/AboutASNT/Intro-to-NDT, 2017.

A.Sumesh et al., 2015. A.Sumesh, K.Rameshkumar, K.Mohandas and R. Shyam Babu. *Use of Machine Learning Algorithms for Weld Quality Monitoring using Acoustic Signature*. ScienceDirect, 2015.

Baskoro et al., 2011. Ario Sunar Baskoro, Erwanto and Winarto. *Monitoring of Molten Pool Image during Pipe Welding in Gas Metal Arc Welding (GMAW) Using Machine Vision*. 2011.

BBC, 2014. BBC. *Ultrasound and infrasound*. http://www.bbc.co.uk/schools/gcsebitesize/science/edexcel/waves_earth/ultrasound_infrasoundrev1.shtml, 2014.

Bernard, 2017. Bernard. *The Basics: MIG Troubleshootin*. http://www.bernardwelds.com/the-basics-mig--p152389, 2017.

Bi et al., 2010. Shujuan Bi, Hu Lan, Hongyan Zheng and Lijun Liu. *Characteristic Analysis and Pattern Recognition of Arc Sound under Typical Penetration Status in MIG Welding*. 2010.

Brownlee, 2013. Jason Brownlee. *A Tour of Machine Learning Algorithms*. http://machinelearningmastery.com/a-tour-of-machine-learning-algorithms/, 2013.

Cayo and Alfaro, 2008. E. H. Cayo and S. C. Absi Alfaro. *Weld transference modes identification through sound pressure level in GMAW process*. Journal of Achievements in Materials and Manufacturing Engineering, 29, 2008.

cryptography, 2012. Practical cryptography. *Mel Frequency Cepstral Coefficient (MFCC) tutorial*. http://practicalcryptography.com/miscellaneous/machine-learning/guide-mel-frequency-cepstral-coefficients-mfccs/#eqn1, 2012.

DanskStandard, 2014. DanskStandard. *DSEN ISO 5817 - Svejsning - Smeltesvejste samlinger i staal, nikkel, titanium og legeringer heraf (undtagen straalesvejsning) - Kvalitetsniveauer for svejsefejl - 4. udgave*. Dansk Standard, 2014.

DanskStandard. DanskStandard. *DSEN ISO 9692-1:2013*. https://www.iso.org/standard/62520.html.

Di et al., 2000. Li Di, Song Yonglun and Ye Feng. *On Line Monitoring of Weld Defects for Short-circuit Gas Metal Arc Welding Based on the Self-Organize Feature Map Neural Networks*. 2000.

electronics, 2017a. PR electronics. *2284 Isolation amplifier*. http://www.prelectronics.com/filearkiv/PDF/2200%20series/2284/Manual/2284V104_UK.pdf, 2017.

electronics, 2017b. PR electronics. *Switchmode power supply*. http://www.prelectronics.com/pdf/2220-2478-US.pdf, 2017.

Ellis, 2012. Dan Ellis. *PLP and RASTA (and MFCC, and inversion) in Matlab using melfcc.m and invmelff.m*. http://www.ee.columbia.edu/ln/rosa/matlab/rastamat/, 2012.

Feng et al., 2002. Ye Feng, Song Yong Lun, Li Di and Lai Yi Zong. *Application of Support Vector Machine to Quality Monitoring in Robotized Arc Welding*. 2002.

FMA communications, 2008. Inc FMA communications. *Understanding transfer modes for GMAW*. http://www.thefabricator.com/article/consumables/understanding-transfer-modes-for-gmaw, 2008.

Grad et al., 2003. Ladislav Grad, Janez Grum, Ivan Polajnar and Janez Marko Slabe. *Feasibility study of acoustic signals for on-line monitoring in short circuit gas metal arc welding*. 2003.

Hera, March 2017. *Hera*. http://www.hera.org.nz/images/inspectionqualitycontrol/WeldingProcessGMAW.jpg, 2017.

Kristiansen, 2007. Morten Kristiansen. *Modelling of the Welding Process using Bayesian Network and Applying Data Collected from Several Sources*. 2007.

LEM, 2015. LEM. *Current Transducer HAL 50 .. 600-S*. http://www.lem.com/docs/products/hal_50_600-s.pdf, 2015.

Lv et al., 2013. Na Lv, Yanling Xu, Jiyong Zhong, Huabin Chen, Jifeng Wang and Shanben Chen. *Research on detection of welding penetration state during robotic GTAW process based on audible arc sound*. Industrial Robot: An International Journal, Vol. 40, 2013.

Marlow, 2012. Frank Marlow. *Welding Know-How*. http://www.metalartspress.com/books/chapters/chapter-3-terms-joints-edge-preparation, 2012.

Marr, 2016. Bernard Marr. *A Short History of Machine Learning – Every Manager Should Read*. https://www.forbes.com/sites/bernardmarr/2016/02/19/a-short-history-of-machine-learning-every-manager-should-read/#38befba815e7, 2016.

Migatronic, 2017. Migatronic. *Flex 4000 STB*. http://www.svejsecenteret.dk/flex/4000.pdf, 2017.

Misiti et al., 1996. Michel Misiti, Yves Misiti, Georges Oppenheim and Jen-Michel Poggi. *Wavelet Toolbox For Use with MATLAB*. http://feihu.eng.ua.edu/NSF_TUES/w7_1a.pdf, 1996.

Moeller, 1991. Martin Fodslette Moeller. *A Scaled Conjugate Gradient Algorithm for Fast Supervise Learning*. 1991.

Montgomery, 2012. Douglas C. Montgomery. *Design and Analysis of Experiments*. John Wiley and Sons, 2012.

Na et al., 2013. Lv Na, Zhong Ji-yong, Chen Hua-bin, Chen Shan-ben and Wang Ji-feng. *Penetration Feature Extraction and Modeling of Arc Sound Signal in GTAW based on Wavelet Analysis and Hidden Markov Model*. 2013.

NationalInstruments, 2009. NationalInstruments. *DAQ M Series*. http://www.ni.com/pdf/manuals/375198c.pdf, 2009.

Ng, 2017. Andrew Ng. *Machine Learning - Stanford University*. https://www.coursera.org/learn/machine-learning/home/info, 2017.

Nielsen, 2017. Michael Nielsen. *Neural Networks and Deep Learning*. http://neuralnetworksanddeeplearning.com/index.html, 2017.

Peeters, 2004. Geoffroy Peeters. *A large set of audio features for sound description (similarity and classification) in the CUIDADO project*. 2004.

Penn, 2010. Gerald Penn. *Natural Language Computing*. http://www.cs.toronto.edu/~gpenn/csc401/soundASR.pdf, 2010.

Roelants, 2017. Peter Roelants. *Peter's notes - How to implement a neural network*. http://peterroelants.github.io/posts/neural_network_implementation_part01/, 2017.

RolandCorporation, 2004. RolandCorporation. *USB Audio Capture UA-25*. https://www.google.dk/url?sa=t&rct=j&q=&esrc=s&source=web&cd=4&cad=rja&uact=8&ved=0ahUKEwip0vKtt9HTAhVn0poKHa3aAYgQFgg_MAM&url=http%3A%2F%2Fc3.zzounds.com%2Fmedia%2FUA-25_e2-a843de98731b5bbdee5a0fffa7608fe3.pdf&usg=AFQjCNEUIgfGVw1dMg3wKvA8pUdKoCSetQ&sig2=D5Q3Y-0VBkNHHfJ3cG-kqg, 2004.

Saini and Floyd, **1998**. D Saini and S Floyd. *An Investigation of Gas Metal Arc Welding Sound Signature for On-Line Quality Control*. 1998.

Sanistaal, **2017**. Sanistaal. *Baandstaal S 235 JR EN 10025:2 - 2004*. https://www.sanistaal.com/da/produkter/staal-og-metaller/staal/stangstaal/baandstaal-s235-jr/c-202801/425116/baandstaal-s-235-jr-en-100252-2004, 2017.

Tam and Huissoon, **2005**. Joseph Tam and Jan Huissoon. *Developing Psycho-Acoustic Experiments in Gas Metal Arc Welding*. 2005.

unlimited, **2006**. Projects unlimited. *AOM-6738P-R*. http://www.farnell.com/datasheets/40086.pdf?_ga=2.116958339.422264326.1493810285-1050738038.1491568322, 2006.

Wall Mountain Company, **2002**. Inc Wall Mountain Company. *GMAW (MIG) Wire Feed*. DVD, 2002.

Wang et al., **2011**. J F Wang, H D Yu, Y Z Qian, R Z Yang and S B Chen. *Feature extration in welding penetration monitoring with arc sound signals*. 2011.

Welch, **1967**. Peter D. Welch. *The Use of Fast Fourier Transform for the Estimation of Power Spectra: A Method Based on Time Averaging Over Short, Modified Periodograms*. IEEE Transactions on Audio and Electroacoustics, 15, 1967.

welding, **2013**. Bohler welding. *Bohler Ti 52 T-FD*. http://spawalnicze-online.pl/templates/images/files/19968/1454667651-bohler-ti-52-t-fd.pdf, 2013.

Wikiwand, **March 2017**. *Wikiwand*. https://upload.wikimedia.org/wikipedia/commons/6/63/Butt_Weld_Geometry.png, 2017.

World, **2012**. RF Wireless World. *FIR filter vs IIR filter*. http://www.rfwireless-world.com/Terminology/FIR-filter-vs-IIR-filter.html, 2012.

Xiuping et al., **2014**. Wang Xiuping, Bai Ruilin and Liu Ziteng. *Weld Seam Detection and Feature Extraction Based on Laser Vision*. 2014.

MONITORING AND CONTROL OF ROBOTIC GAS METAL ARC WELDING THROUGH ACOUSTIC SENSING

A study on the acoustic signal of gas metal arc welding and it's capability in monitoring and control

By

Anders Bidstrup

Master thesis
M.Sc. Manufacturing Technology
Aalborg University

AALBORG UNIVERSITY
STUDENT REPORT

APPENDIX

Table of contents

Quality inspection methods A

In this appendix a range of non-destructive tests, NDTs, and destructive tests, DTs, are presented.

A.1 Non-destructive tests

As the name suggest, non-destructive tests can be carried out without damaging the component, hereby maintaining the products functionality. Since the category covers a range of methods, it is important to evaluate which methods should be used based on the criteria put up by the developer. *The American Society for Nondestructive Testing*, henceforth ASNT, has compiled a list of commonly used NDT methods [ASNT, 2017]:

- **Magnetic Particle Testing (MT)**
  The process of using magnetic fields to detect and locate surface and near-surface discontinuities in ferromagnetic materials.

- **Liquid Penetrant Testing (PT)**
  The process of applying a low viscosity liquid to the surface of the weld, letting the liquid fill up fissures and voids open to the surface, cleaning the surface and identifying where the liquid flows out.

- **Radiographic Testing (RT)**
  The process of exposing the weld to penetrating radiation and recording the radiation in a medium on the other side of the weld.

- **Ultrasonic Testing (UT)**
  The process of introducing a high frequency sound in the weld, recording and interpreting the response.

- **Electromagnetic Testing (ET)**
  The process of recording the effects of induction of an electric current or magnetic field in a conductive part.

- **Visual Testing (VT)**
  The process of looking at the weld to detect surface defects either by direct viewing, line-of-sight vision or optical instruments.

Of the mentioned tests, the direct viewing VT is the simplest. It does not require any special tools and allows the inspector to identify most of the surface imperfections as well as the joint imperfection. To capture internal imperfection other tests are necessary. These often include either RT or UT whom both provide insight regarding the internal structure of the weld.

A.2 Destructive tests

In contrast to NDT there is DT. As the name suggests these tests require physical destruction of the component, hereby making them unfit for their intended purpose. Due to this, these tests are performed either in practice, where samples can be selected and tested to secure worker as well as procedure performance, or research where destruction of the components can be permitted. A few examples of common DT's are given by Alcotec [Alcotec, 2017]:

- **Macro Etch Testing**
  The process of cutting a weld and polishing the cross section to gain a snapshot of the internal structure.

- **Fillet Weld Break Test**
  The process of applying a load to the unwelded side of a fillet weld until it fails and studying the break along the weld.

- **Transverse Tension Test**
  The process of performing a tensile test on a welded component, i.e. pulling the two welded work pieces apart until failure.

- **Guided Bend Test**
  The process of bending the component to a specified angle and analysing the results.

The choice of destructive test depends solely on the purpose of the quality inspection.

Digital signals B

This appendix aims to clarify the distinction between the two as well as present terminology and possible pitfalls when working with digital data.

B.1 Analogue vs digital

A common feature for the acoustic, current and voltage signal is that they are analogue outputs. In theory this means that they are continuous signals, i.e. a signal with no gaps or jumps in output values, see figure B.1 (A).

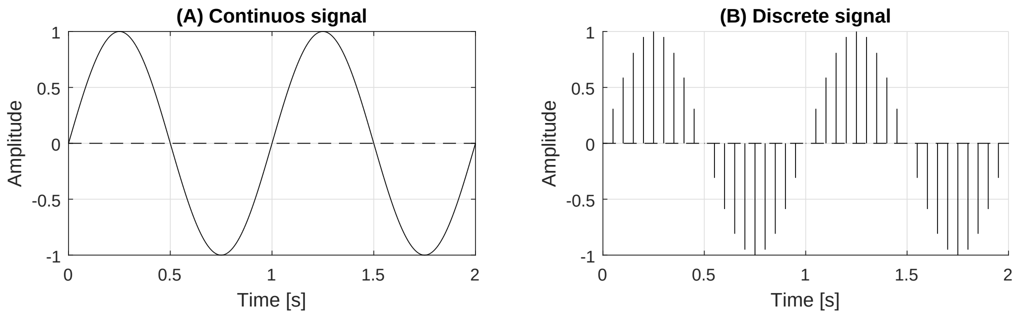

Figure B.1: (A) A continous signal and (B) its discrete equivalent.

When acquiring one of these analogue signals to a computer, the signal magnitude is measured at a certain rate per time unit denoted the sampling frequency, f_s making the signal discrete or digital. Doing this results in the computer getting a chronological range of magnitude values in which gaps in time are missing values, see figure B.1 (B). A function can be fitted to the discrete signal which can be analysed or used to replicate the original signal, i.e. synthesising the signal.

B.2 Data collection

To better understand the parameters and potential pitfalls of data collection, the concepts of sample frequency and resolution are elaborated further.

Sample frequency

The sample frequency refers to how many measurements are taken every second and thereby has the unit of hertz, Hz. Since there is a gap between samples where no data is collected, the captured signal lacks information. An example of a discrete signal and its corresponding continuous signal is presented in figure B.2.

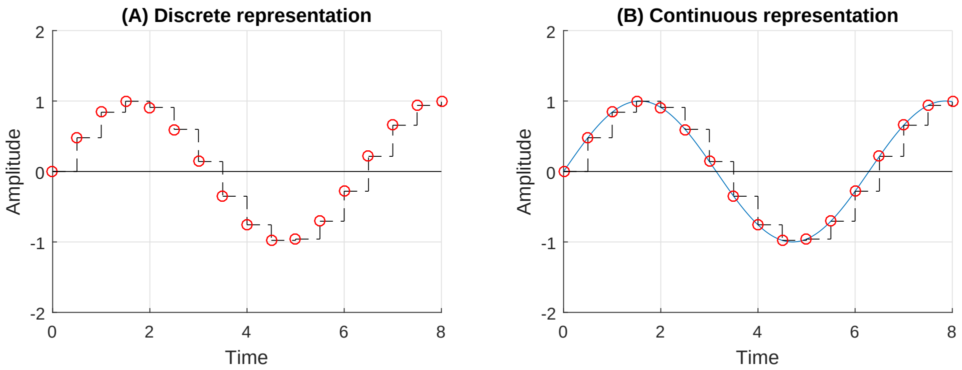

Figure B.2: The (A) discrete and (B) continuous representation of a sine function with a sampling frequency of 2 Hz.

Figure B.2 (A) is an example of a discrete signal a computer could be receiving through data acquisition hardware. From this representation it is relatively simple to fit a continuous function as shown in figure B.2 (B). However, analogue signals can have noise and not be represented as simple as the case in figure B.2. In these cases it is important to understand the effect of the sample frequency. Consider the case in figure B.3.

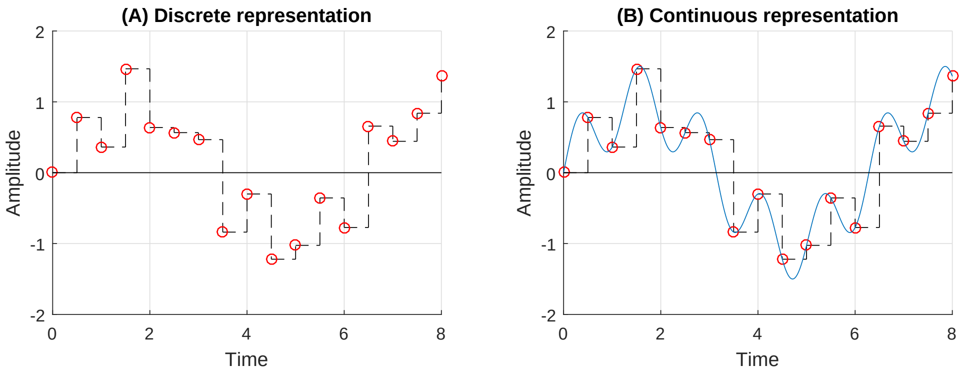

Figure B.3: The (A) discrete and (B) continuous representation of a combined sine function with a sampling frequency of 2 Hz.

In this case the discrete representation in figure B.3 (A) does not intuitively lead to the continuous function showed in figure B.3 (B) from which the discrete data is sampled. The lack of information due to the gap between samples hide crucial information about the shape which leads to the conclusion that a higher sample frequency should be used. Increasing the sample frequency to 10 Hz gives more magnitude values per second and thereby increases the amount of information about the signal and consequently the likelihood of fitting a representative continuous function, see figure B.4.

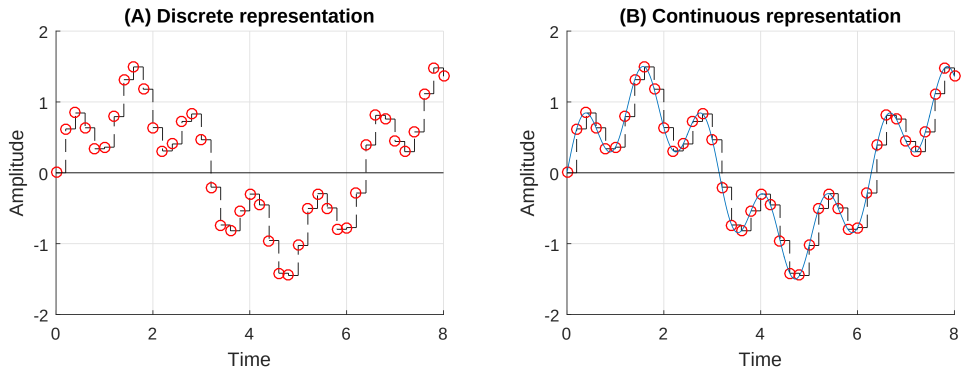

Figure B.4: The (A) discrete and (B) continuous representation of a sine function with a sampling frequency of 10 Hz.

As illustrated, the discrete representation, see figure B.4 (A), provides sufficient information to fit an accurate continuous function, see figure B.4 (B), and highlights the importance of choosing a sufficiently large sample frequency. It should be noted that in practice the shape of the analogue signal is unknown and only magnitude values are collected. It is then up to the receiver to attempt to fit a function and evaluate whether the result is reasonable.

Resolution

Besides the lack of information due to the gap between samples there is another gap depending on how many bits are used to measure the magnitude of the signal, i.e. the resolution of the signal. A bit is a unit of information which can take the value of 0 or 1, i.e. using one bit gives two possible integer values like an on/off switch. Increasing the bit precision adds more switches hereby increasing the amount of possible combinations of ones and zeros. The concept is shown in table B.1.

	1 bit	2 bit		3 bit		
Bits	b1	b1	b2	b1	b2	b3
Combinations	0	0	0	0	0	0
	1	0	1	0	0	1
		1	0	0	1	0
		1	1	0	1	1
				1	0	0
				1	0	1
				1	1	0
				1	1	1

Table B.1: The possible combinations of 1 bit, 2 bit and 3 bit precision.

In the table the possible combinations of 1 bit, 2 bit and 3 bit precision is presented. As shown the amount of combinations for 1 bit, 2 bit and 3 bit are two, four and eight respectively. In the context of signal measuring, each combination can be assigned a value hereby defining the levels at which the signal can be measured. The amount of combinations is calculated as $2^{n_{bits}}$ which means that even a slight increase of the bit precision can be advantageous if more magnitude levels are necessary.

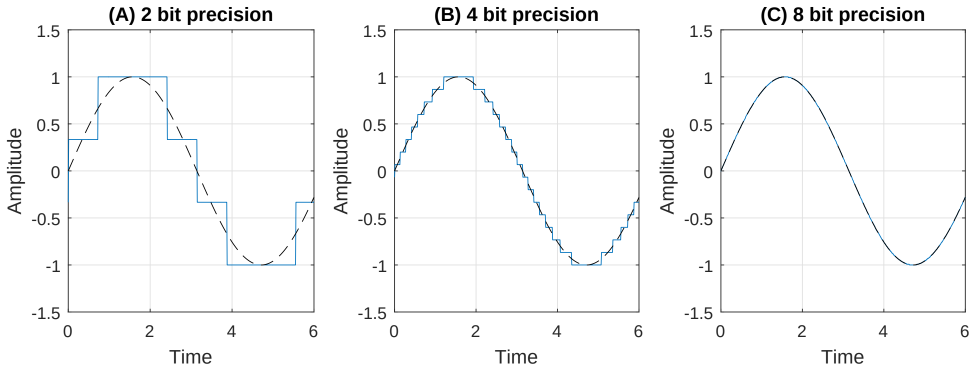

Figure B.5: A sine wave and its corresponding representation using (A) 2 bit, (B) 4 bit and (C) 8 bit precision with a sample frequency of 10 Hz.

On figure B.5 a sine wave is presented with (A) 2 bit, (B) 4 bit and (C) 8 bit precision. Note that even though the data is sampled at a rate of 10 Hz the resolution makes the signal look like its sampled at a different frequency. The choppiness of figure B.5 (A) makes the signal seem to be sampled at a significantly lower frequency as a consequence of the limited magnitude levels. This highlights the loss of data taking place which in some cases could be critical. In the case of figure B.5 (B) the increased amount of magnitude levels result in a lowered amount of data loss and thereby a better data set for fitting a continuous function. Further improvement is shown on figure B.5 (C) where the discrete and continuous sample can not be told apart.

When choosing the resolution for data acquisition it is necessary to consider the range of possible measured values. In the case of having a 3 bit precision in the range of values from -1 to 1 three situations are shown in figure B.6.

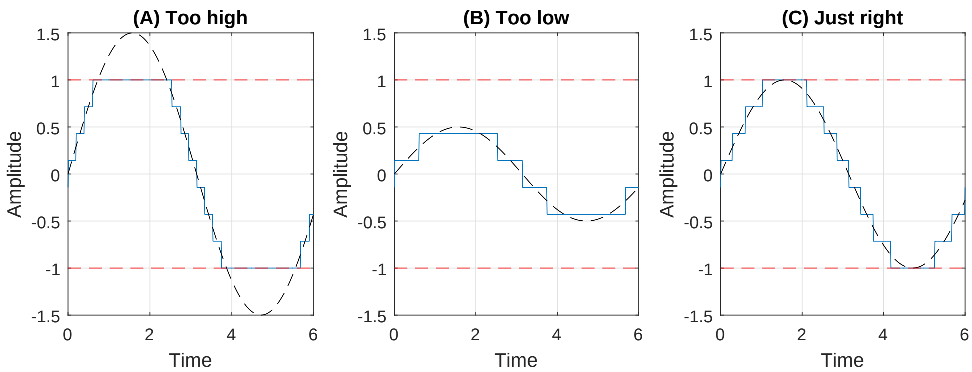

Figure B.6: Acquiring a sine wave with an amplitude of (A) 1.5, (B) 0.5 and (C) 1.0 with 3 bit precision on a range from -1 to 1.

In the case of figure B.6 (A) a sine wave with an amplitude of 1.5 is measured. As indicated on the graph the amplitude of the sine wave is too high compared to the range resulting in the measuring equipment capping at 1.0. Consequently a loss of data near the peaks occur making the situation undesirable. In contrast figure B.6 (B) shows the measured signal for a sine wave with an amplitude of 0.5. In this case the sine wave does not utilise the full range of the setup. Although the equipment is far from capping, by not using the full range of the equipment, a low resolution is achieved relative to the potential of the setup. Therefore, to reach the highest resolution possible the signal should take advantage of the whole range of the equipment whilst avoiding capping as seen on figure B.6 (C).

Digital filtering C

This appendix presents the basics of the design and effect of digital filters through an introduction to the two primary groups of filter - FIR and IIR - and the sub-groups of filters - low-pass, high-pass, band-pass and band-stop.

C.1 Finite and infinite impulse response filters

There are two overall types of filters - finite impulse response, henceforth FIR, and infinite impulse response, henceforth IIR [World, 2012]. The difference between the two lie in whether the filter requires past outputs or not. If the filter does not require past outputs but is solely dependent on present and past inputs, it is an FIR filter. Given a signal, x as a function of the sample number, n, the output after implementing a FIR filter could be as in equation (C.1).

$$y(n) = \frac{x(n) + x(n-1)}{2} \tag{C.1}$$

The filter used in this equation is a two-term average filter and, as shown, only depends on values of the input x. In contrast the IIR filters use recursion. This means that the filter uses past outputs to calculate the new output as in the case of equation (C.2).

$$y(n) = x(n) + y(n-1) \tag{C.2}$$

In this case the newest signal value is added to the previous output value to create the newest output.

C.2 Types of filters

When moving past the overall classification of FIR and IIR filters, there is a sub-classification based on the effect of the filter. In the case of applying a filter to a signal it is often desired to cut out part of the frequencies. Consequently a range of frequency-selective filters have been developed to cope with common cases. It should be noted that the possibilities are endless when it comes to the specific functionality of a filter even if they are classified as the same type. However, the four main groups are shown on figure C.1.

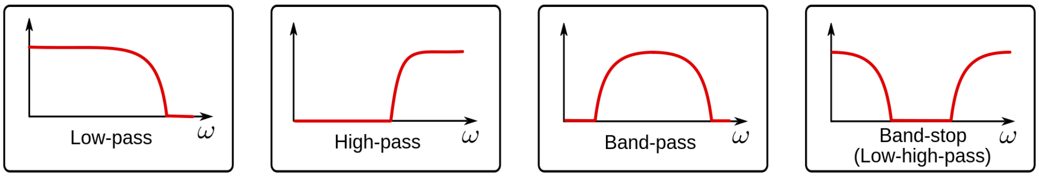

Figure C.1: Gain vs angular frequency plot of a low-pass, high-pass, band-pass and band-stop filter [Aasvik, 2016]

The first filter on the figure is a *low-pass* filter. As indicated by the gain-frequency plot the principle with the filter is to define a *cut-off frequency* at which the gain becomes zero. In this way post-filtering the signal only contains frequencies below the cut-off frequency. The inverse version of this is a *high-pass* filter as shown on figure C.1. In this case the frequencies below the cut-off frequency are removed whereas the rest is preserved. The two remaining filters are simply combinations of low-pass and high-pass filters. By having a low-pass filter remove frequencies above some value followed by a high-pass filter removing frequencies below some value, a *band-pass* filter is created. Similarly a *band-stop* filter can be made where the high-pass and low-pass filters are used on the signal in parallel and then combined to provide the final output. These are examples of some characteristics digital filters can have and are in no way an exhaustive list of the possibilities within the subject.

Algorithm overview D

In this appendix the grouping of machine learning algorithms is based on the classification proposed by Dr. Jason Brownlee [Brownlee, 2013]. In an attempt to provide a graspable overview the algorithms are grouped both by style and similarity.

D.1 Algorithm styles

The style of an algorithm refers to the way it interacts with the data or environment. In this section four style groups are presented:

- Supervised learning
- Unsupervised learning
- Semi-supervised learning
- Reinforcement learning

Supervised learning

In this group the algorithms are trained by a data set with labelled data. This means that for each set of input data the output is specified. The algorithm uses this data to make a model where new input data is provided with a suitable output based on the relations found in the training data.

Unsupervised learning

This group stands in direct contrast to supervised learning in the sense that the data for these algorithms is unlabelled. Being unaware of the output the algorithms in this group search for structure in the data with the aim of spotting redundancies or extracting rules.

Semi-supervise learning

As the name suggests this group hosts algorithms fed with a mixture of labelled and unlabelled data. The algorithms of this group combine the functionalities of the supervised and unsupervised learning groups by attempting to develop a predictive model while organising the unlabelled data.

Reinforcement learning

Lastly the group of reinforcement learning works with a changing environment. An agent is set to interact with the environment to achieve a goal and makes decisions based on a reward/punishment feedback system.

D.2 Algorithms by similarity

Knowing the basic styles of algorithms makes it easier to understand the similarity between algorithms. The grouping by similarity given by GP:

- Regression
- Instance-based algorithms
- Regularisation algorithms
- Decision tree algorithms
- Bayesian algorithms
- Clustering algorithms
- Association rule learning algorithms
- Artificial neural network algorithms
- Deep learning algorithms
- Dimensionality reduction algorithms
- Ensemble algorithms

Despite being thorough the grouping does not consider all algorithm. However, for the sake of basic understanding of the possibilities within algorithm choice, each of the proposed groups are presented in this section.

Regression

Regression models attempt to describe the trend of a training set based on an error measurement. The type of output can either be continuous or discrete. An example of regression with a continuous output is the case of linear regression where the model can predict a specific value for each input data point. In case of the discrete output an example is logistic regression which associates data regions with groups or classes, e.g. spam/not-spam classification.

Instance-based algorithms

In this group algorithms build a model which, based on a database of example data, classify new data through a similarity measure.

Regularisation algorithms

Regularisation algorithms work as an extension to another method where they are used to secure a simple model. They do this by penalising complexity and favouring simplicity of the model to which it is an extension to.

Decision tree algorithms

As the name suggests the algorithms within this group consist of decision trees. A decision tree is a tool that structures a range of decisions in a flow chart manner. Starting from the root decision it forks via branches to either zero nodes, meaning the outcome of the branch, or n new decision nodes. Each of these decision nodes fork to extra decision nodes until only outcomes remain. Once constructed, the tree consists of a range of decision rules which can be used to predict the output or determine an action based on the input.

Bayesian algorithms

The group of bayesian algorithms consist solely of algorithms which apply Bayes' Theorem.

Clustering algorithms

The algorithms in this group use unlabelled data and attempt to find structure so that it can be organised in groups, i.e. clusters.

Association rule learning algorithms

The algorithms contained in this group derive rules to explain relationships between features.

Artificial neural network algorithms

Artificial neural networks are algorithms made to mimic the way the human brain works. It consists of neurons which, based on an activation function, either take the value of one or zero. The configuration of ones and zeros are then used to determine the output based on a set of input data.

Deep learning algorithms

Deep learning algorithms are neural networks which, as a consequence of technological advances, are bigger and more complex than traditional artificial neural networks.

Dimensionality reduction algorithms

The algorithms in this group are used to highlight features which contribute the least to a potential discrimination case. In this way the feature space can be reduced hereby freeing computational power and making the training as well as usage of the algorithm faster.

Ensemble algorithms

This group refers to algorithms which produce a model using multiple independently trained models to predict the output.

ANN structure and functionality E

In this appendix an introduction to the structure and functionality of the chosen ANN is presented. The introduction includes descriptions of the visual representation of the ANN, the used activation functions, the cost function, forward propagation, backpropagation and how to calculate the derivative of the cost function. The chapter is primarily based on the work of Michael Nielsen [Nielsen, 2017] but inspiration was drawn from Andrew Ng of Stanford University [Ng, 2017] and Peter Roelants [Roelants, 2017].

E.1 Visual representation

To understand the structure of an ANN an example is shown on figure E.1.

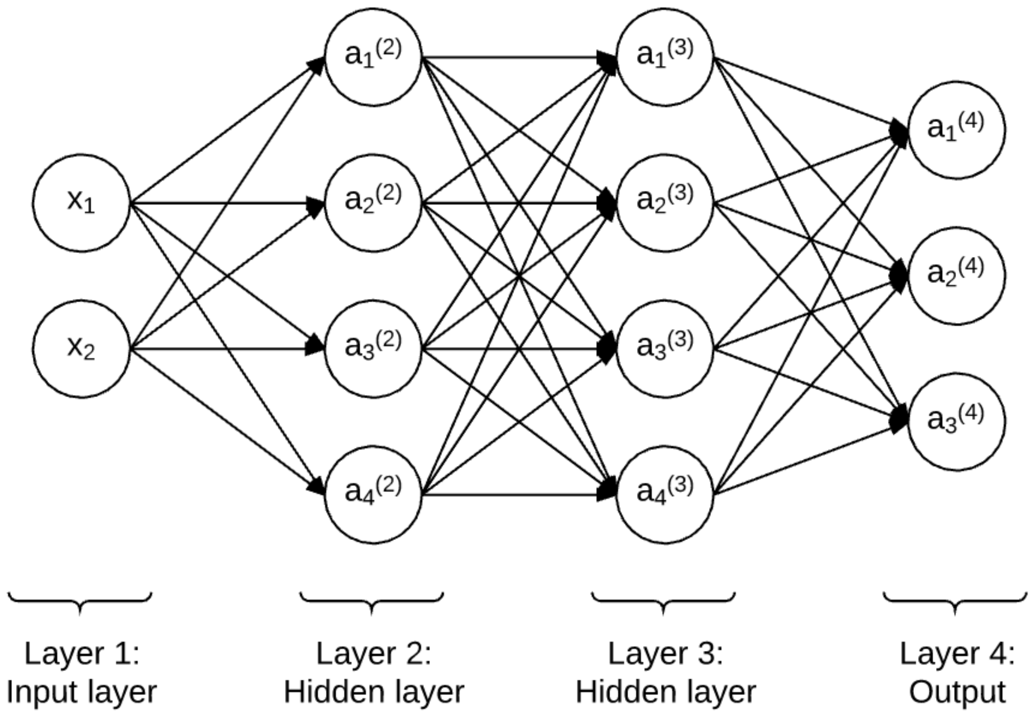

Figure E.1: Example of an artificial neural network with four layers.

A neural network consists of a range of connected *neurons*, as indicated by the circles on figure E.1, in different *layers*. Each neuron, besides those in *Layer 1*, can assume a value of either one or zero, i.e. activated or not, represented by a and the combination of activated and deactivated neurons is used for the prediction. *Layer 1* is known as the *input layer* and each neuron in the input layer represents a feature x. *Layer 4* is known as the *output layer* and represents the possible classes to map the input to. The remaining internal layers are known as *Hidden layers*. The amount of input and output neurons are determined by the amount of features considered and the amount of output classes respectively. In contrast the amount of neurons in each hidden layer and the amount of hidden layers are not fixed and no definitive rules exist to determine how many of each should be present. Furthermore there is no rule specifying that the hidden layers have to have the same amount of neurons, which increases the number of combinations further. Lastly, as indicated by figure E.1 the subscripted number on the a's is the neuron number, i, from the top and the superscripted, parenthesised number on the a's is the layer in which the neuron is, l. Similar notation is used for the parameters, or *weights*, denoted by $\Theta_{ik}^{(l)}$.

Not included on figure E.1 is what is known as the *bias units*. A bias unit is the neuron of a given layer when $i = 0$ and has a constant value of one. Though not shown on the figure, they are included in the calculations.

E.2 Activation functions

To determine the activation of each neuron an *activation function* is required. The property of such a function is to output either 0 or 1 when presented with an input. This can be done by subjecting the result to a threshold as illustrated in the simple case of:

$$f(x) = \begin{cases} 1, & if\ x > TH \\ 0, & if\ x < TH \end{cases} \tag{E.1}$$

with *f(x)* being the activation function, x being the input and *TH* being a threshold. Using only the threshold, the possibilities for the function *f(x)* are endless and the output is discrete. However, for the use in ANN's, other properties are desired. Initially non-linear functions are desired since introducing a non-linearity into the network allows the approximation of non-linear function with networks containing just one hidden layer. Furthermore the function should be continuously differentiable when using gradient-based optimisation methods since the gradient of the activation is required in the calculation, see section E.4.

In the case of this report, two activation functions are used. The first activation function is the *Sigmoid function* and is used on all neurons in the hidden layers of the network. The second activation function is the *Softmax* function which is only used in the output layer.

E.2.1 The Sigmoid function

The Sigmoid function is defined as:

$$g(x_i) = \frac{1}{1 + e^{-x_i}}$$

and its shape is seen on figure E.2.

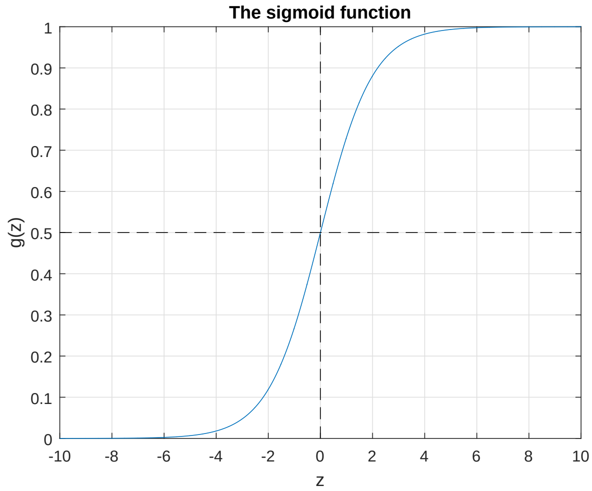

Figure E.2: The shape of the Sigmoid function.

As indicated on figure E.2 the output is finite and lies within the two asymptotes of 0 and 1. Furthermore the function is non-linear and continuous with a gradient given by:

$$g'(x) = g(x)(1 - g(x))$$

which is computationally simple.

E.2.2 The Softmax function

The Softmax function is defined as:

$$Sm(x_i) = \frac{e^{x_i}}{\sum_{k=1}^{K} e^{x_k}}$$

where the total amount of x values, K, are used to calculate the Softmax output of a single input, x_i. The function is used to determine the probability of each input x compared to the total amount of inputs K, i.e. calculate the probability distribution. Being a probability distribution the sum of the probabilities is 1 which is a requirement for the cross-entropy cost function to work. In contrast to the hidden neurons, the error of the output layer is defined through the derivative of the cross-entropy cost function.

E.3 Cross-entropy cost function

The cost function of the optimisation problem is given by the cross-entropy between the probability distribution given by $\mathbf{h}_{\mathbf{\Theta}}(\mathbf{x})$ and the probability distribution given by the labelled outputs, $\boldsymbol{y}$. To understand how this is possible it is necessary to understand the concept of *one-hot encoding*. In this section that concept is introduced and the cross-entropy cost function and its derivative is presented.

E.3.1 One-hot encoding

Faced with the challenge of labelling a set of data, different approaches can be taken. Since the purpose is used in a computational context numbers are used to denote each class which leads to labelling as the two examples given in table E.1.

Class	Sequential	Binary
Pedestrian	1	000
Bicycle	2	001
Scooter	3	010
Car	4	011
Bus	5	100
Truck	6	101
Train	7	110
Other	8	111

Table E.1: Arbitrary classification case with sequential and binary encoding.

Initially, the arbitrary classification case is labelled using sequential numeric encoding. Although each class has a unique digit an unintentional numerical hierarchy is established which may affect the result of the computations at hand. The same problem is experienced in the binary encoding shown in figure E.1 in the amount of 1's the label contains.

To eliminate this problem a so-called one-hot encoding is used. The procedure starts by creating a vector for each data point with the same amount of entries as there are classes. Then the entry representing the correct class is set to 1 while the rest is set to zero. Doing this for the case in table E.1 results in the labelling seen in table E.2.

Class	One-hot encoding
Pedestrian	[1 0 0 0 0 0 0 0]
Bicycle	[0 1 0 0 0 0 0 0]
Scooter	[0 0 1 0 0 0 0 0]
Car	[0 0 0 1 0 0 0 0]
Bus	[0 0 0 0 1 0 0 0]
Truck	[0 0 0 0 0 1 0 0]
Train	[0 0 0 0 0 0 1 0]
Other	[0 0 0 0 0 0 0 1]

Table E.2: Arbitrary classification case with one-hot encoding.

As indicated in table E.2 the hierarchical trend is eliminated. Another aspect of this encoding is that since the sum of the entries of a label vector is always 1, the vector can be considered as a probability distribution where the probability of being the correct class is 100 %. Gathering the label vectors for an entire data set results in a labelled output matrix, $\boldsymbol{y}$, to be used in the definition of the cost function.

E.3.2 The cost function and its derivative

Seeing as the hypothesis outputs a vector containing the probability distribution of predicted classes of the network and the labelled output vector is a vector containing the probability distribution for the actual output being a specific class, cross-entropy can be used. Specifically cross-entropy is based on minimising the negative log-likelihood of a set of weights being able to predict a class I. Using probability theory the likelihood of a given set of weights resulting in a prediction of the correct class of each input can be simplified as follows:

$$\mathcal{L}(\boldsymbol{\Theta}|\mathbf{a}^{(L)},\mathbf{y}) = P(\mathbf{y}|\mathbf{a}^{(L)}) = \prod_{i=1}^{I}(a_i^{(L)})^{y_i}$$

Using this expression the negative log-likelihood is given as:

$$-log(\mathcal{L}(\boldsymbol{\Theta}|\mathbf{a}^{(L)},\mathbf{y})) = -log\left(\prod_{i=1}^{I}(a_i^{(L)})^{y_i}\right) = -\sum_{i=1}^{I} y_i\ log(a_i^{(L)})$$

Summing over the total amount of data point, M, gives the cost function, $J(\boldsymbol{\Theta})$:

$$J(\boldsymbol{\Theta}) = -\sum_{m=1}^{M}\sum_{i=1}^{I} y_{mi}\ log(a_{mi}^{(L)})$$

The equation for calculating the partial derivatives of the last layer in regards to the weights is derived from the cost function. The result is:

$$\frac{\delta}{\delta\Theta_{ik}^{(L)}}J(\boldsymbol{\Theta}) = a_k^{(L-1)}(a_i^{(L)} - y_i)$$

resulting in the overall optimisation problem of:

$$\min_{\boldsymbol{\Theta}} J(\boldsymbol{\Theta}) = \min_{\boldsymbol{\Theta}}\left(-\sum_{m=1}^{M}\sum_{i=1}^{I} y_{mi}\ log(a_{mi}^{(L)})\right)$$

E.4 Training an ANN

In order to train the hypothesis the minimisation problem presented in section E.3.2 is performed using gradient descent. To understand the process of calculating the gradient of the cost function, see section E.3.2, two new terms are introduced - *Forward propagation* and *Backpropagation*.

Forward propagation

In the training process the ANN is subjected to a set of training data. Once a data point $(x^{(m)}, y^{(m)})$ is introduced, the process of forward propagation begins. This is the process of calculating the activation of the neurons in the network starting from the input neurons. In order to do so random initialisation of the weights is performed after which the process can begin. Continuing the case from figure E.1 the vectorised sequential process for one data point is:

[1] $\mathbf{a}^{(1)} = \mathbf{x}^{(m)}$

[2] $\mathbf{z}^{(2)} = \boldsymbol{\Theta}^{(2)}\mathbf{a}^{(1)}$

[3] $\mathbf{a}^{(2)} = g(\mathbf{z}^{(2)})$

[4] $\mathbf{z}^{(3)} = \boldsymbol{\Theta}^{(3)}\mathbf{a}^{(2)}$

[5] $\mathbf{a}^{(3)} = g(\mathbf{z}^{(3)})$

[6] $\mathbf{z}^{(4)} = \boldsymbol{\Theta}^{(4)}\mathbf{a}^{(3)}$

[7] $\mathbf{a}^{(4)} = Sm(\mathbf{z}^{(4)}) = h_{\boldsymbol{\Theta}}(\mathbf{x})$

It should be noted that the bias term is included in the calculation of the activations with the exclusion of the calculation for $\mathbf{a}^{(1)}$.

Backpropagation

Once forward propagation is finished, backpropagation is performed to calculate error terms for the neurons, $\delta_j^{(l)}$. These are calculated to so that the remaining partial derivatives of the cost function can be computed. The process of calculating the error terms is called backpropagation since it starts from the output layer and goes backwards until the input layer is reached. The sequential process is as follows:

[1] $\boldsymbol{\delta}^{(4)} = \mathbf{a}^{(4)} - \mathbf{y}^{(m)}$

[2] $\boldsymbol{\delta}^{(3)} = (\boldsymbol{\Theta}^{(4)})^T \boldsymbol{\delta}^{(4)} \odot g'(\mathbf{z}^{(3)})$

[3] $\boldsymbol{\delta}^{(2)} = (\boldsymbol{\Theta}^{(3)})^T \boldsymbol{\delta}^{(3)} \odot g'(\mathbf{z}^{(2)})$

with $\odot$ being the element-wise multiplication and $g'(z)$ being the derivative of the sigmoid function evaluated at z as presented in section E.2. Note that no error term is calculated for the input layer. From these $\boldsymbol{\delta}$-vectors it is possible to calculate the remaining derivatives of the cost function as:

$$\frac{\delta}{\delta \boldsymbol{\Theta}_{ik}^{(l)}} J(\boldsymbol{\Theta}) = \begin{cases} \delta_i^{(l)}, & if\ l \neq L\ and\ k = 0 \\ a_k^{(l-1)} \delta_i^{(l)}, & if\ l \neq L\ and\ k \neq 0 \end{cases} \tag{E.2}$$

Computing the overall partial derivatives

With the formulae for calculating the partial derivatives of the cost function both for the hidden layers, see section E.4, and the output layer, see section E.3.2, it is possible to perform a non-regularised optimisation of the weights using a data set of one sample. Introducing more data points leads to the introduction of an accumulator used to calculate the partial derivatives of the cost function. This accumulator is denoted Δ and is updated after each back propagation by the following formula:

$$\Delta_{ik}^{(l)} = \begin{cases} \Delta_{ik}^{(l)} + \delta_i^{(l)}, & if\ l \neq L\ and\ k = 0 \\ \Delta_{ik}^{(l)} + a_k^{(l-1)} \delta_i^{(l)}, & if\ l \neq L\ and\ k \neq 0 \\ \Delta_{ik}^{(l)} + (a_i^{(l)} - y_i), & if\ l = L\ and\ k = 0 \\ \Delta_{ik}^{(l)} + a_k^{(l-1)} (a_i^{(l)} - y_i), & if\ l = L\ and\ k \neq 0 \end{cases} \tag{E.3}$$

Once each data point in the training set is run through the forward propagation and backpropagation the overall derivative of the cost function, $\mathbf{D}$, can be calculated as:

$$D_{ik}^{(l)} = \begin{cases} \frac{1}{m} \Delta_{ik}^{(l)}, & if\ k = 0 \\ \frac{1}{m} \left(\Delta_{ik}^{(l)} + \lambda \Theta_{ik}^{(l)} \right), & if\ k \neq 0 \end{cases} \tag{E.4}$$

As shown in the equations regularisation is not performed when $k = 0$ but is introduced when k is one or above. Implementing these equations makes it possible to calculate the gradient of the cost function. Hereby it is possible to perform gradient descent or more advanced optimisation algorithms to minimise the cost in regards to the weights in $\boldsymbol{\Theta}$.

F LabView program

In this appendix the developed LabView program is presented. It consists of a main virtual instrument, henceforth VI, and four sub-VI's. The main VI is shown in figure F.1.

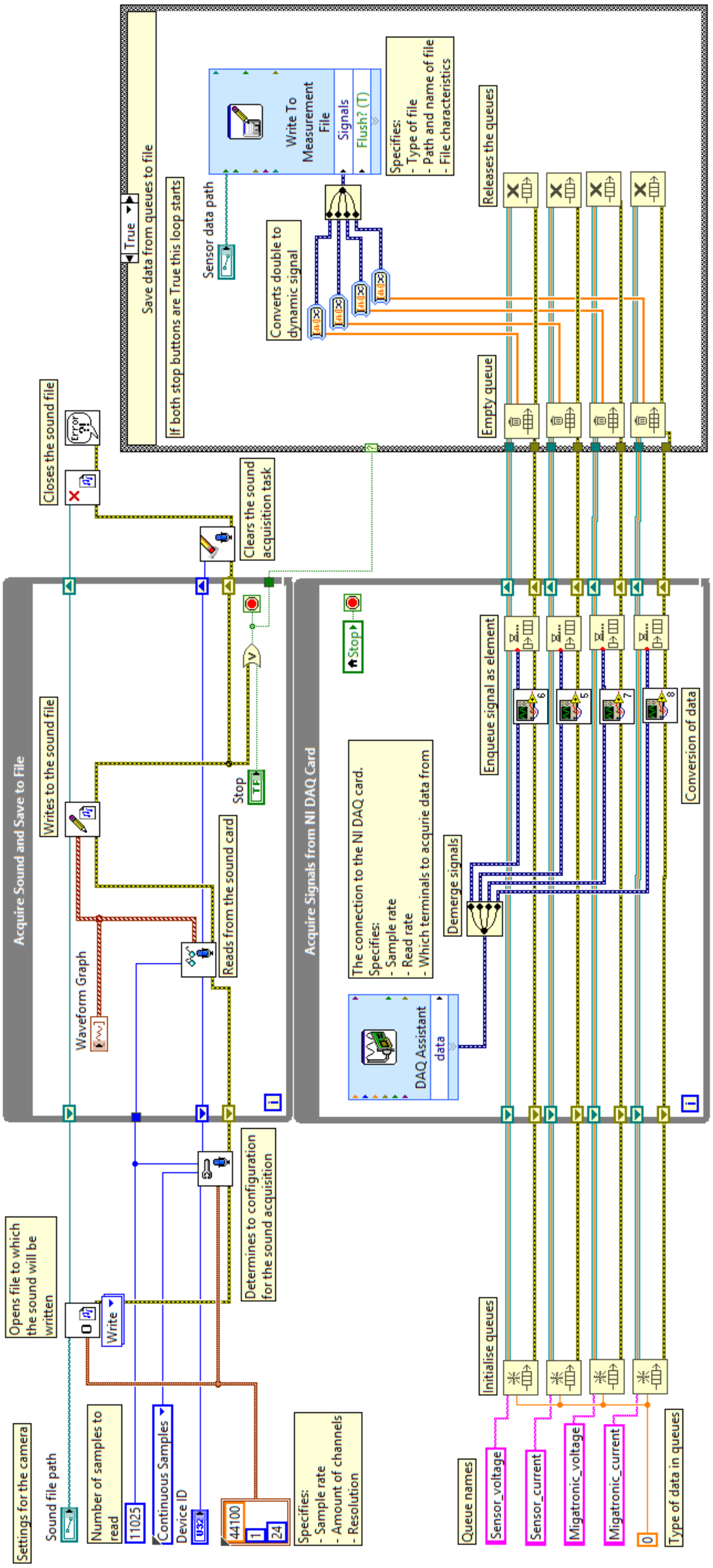

Figure F.1: The primary VI for data acquisition of sound, voltage and current.

The VI should be read from left to right. Three structures are present in the VI:

- Sound acquisition while structure
- Sensor acquisition while structure
- Data saving case structure

The sound acquisition while structure reads data from the sound card and writes it to a wave file until the stop-button is activated. In order to specify how and from what the loop should get the sound data a configuration box is implemented before the loop. This box requires inputs to specify how many data points to read at a time, whether continues or finite sampling is required, the device ID, the sample rate, the amount of channels to capture sound from and the resolution of the signal. In this case it reads 11025 samples at a time, reads data continuously, reads from the EDIROL UA-25 sound card, has a sample rate of 44.1 kHz and captures sound on one channel with a resolution of 24 bit. Once specified it transfers the configuration data into the while loop. Similarly an initiation box for the wave file is required. It specifies the path and name of the file to save the data in and the type of data it will write to the file. Once specified the box opens the file if it exists or creates a new file if it does not. The task is then transferred to the while loop. Once the stop-button is pushed the while loop ends which triggers the program to close the sound file and clear the sound acquisition task.

The sensor acquisition while structure uses the *DAQ Assistant*. This is a sub-VI to read data from a DAQ card and enables the user to specify which terminals to read from and at what rate. In this case the data is sampled at 4 kHz and one data point is read at a time. When the data is read it is outputted as a single signal. Since the signals need different conversions, it is demerged into the four measured signals being *Sensor voltage*, *Sensor current*, *Migatronic voltage* and *Migatronic current* from top to bottom. The signals are transferred into four separate sub-VI's to convert the signals to the actual current and voltage after which the data points are pushed into a queue. Before this acquisition can take place, the four queues need to be initialised. As for the configuration and opening of a sound file for the sound acquisition, the queues are initialised outside the loop. For each queue initialisation box two inputs are needed - the name of the queue and a constant to symbolise the type of data to be stored in the queue. In this case the queues are named *Sensor_voltage*, *Sensor_current*, *Migatronic_voltage* and *Migatronic_current* from top to bottom and are fed a double type constant. The while loop reads and stores data in the queues continuously until the stop button is pressed.

The last structure is the data saving case structure. A case structure has two states - *True* and *False* - and a shift triggers the system inside the structure. In this case the structure is made to empty the queues and write them to a spreadsheet file with the event being that the stop button is pressed. Since no data saving takes place before the stop buttons are activated, the *False* state is an empty structure and therefore not included on figure F.1. The *True* state however, has four boxes to empty the queues and four boxes to release the queues once emptied. The released data is then converted to dynamic signals and fed to a *Write to Measurement File* VI. In this VI the signals are saved to a spreadsheet file with one time column and four data columns corresponding to the four signals acquired.

The VI's to convert each signal to the actual current and voltage are shown on figure F.2.

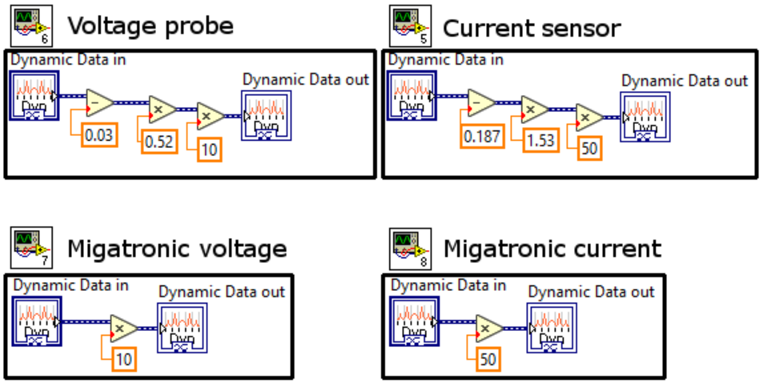

Figure F.2: The conversion VI's for the four acquired signals.

The four VI's refer to the voltage probe signal, the current sensor signal, Migatronic voltage measurement and Migatronic current measurement. The Migatronic conversions are specified in the datasheet, see enclosure A, as 0 - 10 V to 0 - 100 V and 0 - 10 V to 0 - 500 A for the voltage and current measurement respectively. Since the conversions are linear the sub-VI's involve multiplying the acquired signal by a factor of 10 and 50, see figure F.2. The conversions for the implemented sensors are derived in section 9.4. The signal from the voltage probe requires a correction of an offset of 0.03 V followed by multiplication by a factor of 0.52 to have the same value as the Migatronic voltage measurement. After this a factor of 10 is used to convert the signal to the actual voltage based on the reference value from the Migatronic measurement. In the case of the current sensor it is possible to adjust the gain and offset of the signal. To compensate for the settings of the sensor initially the offset, found to be 0.187 V, is subtracted from the signal. To convert the signal to values similar to the Migatronic reference current measurement a factor of 1.53 is found. Since the signal is of the same magnitude as the reference value an additional multiplication by a factor of 50 is implemented to convert the signal to the actual current.

Identifying conversion rates G

In this appendix the experiments required to identify the conversion rates from signal voltage to actual voltage and current from the implemented sensors are documented.

G.0.1 Specification

To determine the conversion rates of the voltage and current signals a range of experiments at different values for voltage and WFS needs to be performed. Since a suitable range for both is used in the experiments for identifying settings for welding defects and transfer modes, see section 9.5, the data from those experiments is used.

From the data a section of the signals where a weld is not being performed is extracted to correct a potential offset while in process data for different values is used to determine a scaling factor.

G.0.2 Results

Example data from the experiments is shown in figure G.1.

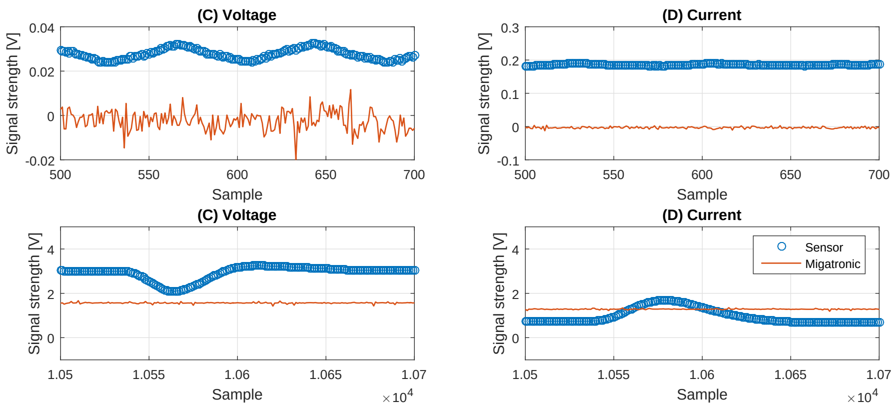

Figure G.1: Comparison of the values acquired from the Migatronic control box and the implemented sensors for voltage and current out of process, (A) and (B), and in process, (C) and (D).

On figure G.1 (A) and (B) the voltage and current are shown out of process. From these graphs it can be derived that an offset of 0.03 V and 0.186 V is present for the voltage and current measurement respectively. On the in process graphs on figure G.1 (C) and (D) the offset is already corrected. By inspection it is derived that scaling the voltage and current signals by 0.52 and 1.53 respectively gives an acceptable result on the example data.

To check that the conversion is linear the conversions are tested on the data from the other experiments. The values for both voltage and WFS are chosen in increments of two while the travel speed is held constant at 1 $\frac{mm}{s}$. The converted signals from the experiments are shown on figure G.2.

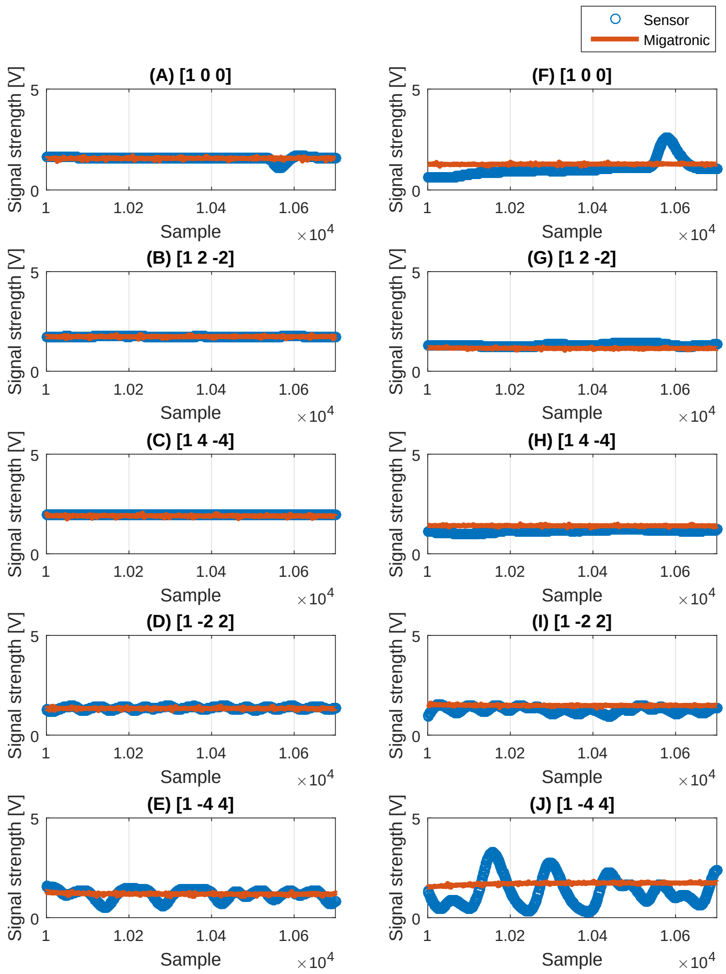

Figure G.2: Comparison of the values acquired from the Migatronic control box and the implemented sensors from various experiments. The titles are of composition: [Travel speed - Voltage adjustment - WFS adjustment].

On graphs (A) through (E) on figure G.2 the converted voltage signal and the signal from the Migatronic control box is compared. Similarly the converted current signal is compared to the signal from the Migatronic control box on figure G.2 (F) through (J). It should be noted that the converted signals seem to follow the measurements from the Migatronic control box which suggests that the conversion is linear and of sufficient precision.

G.0.3 Comments

It is assessed that the conversion rates are of acceptable precision since the aim of the conversion is to approximate the level of voltage and current.

Enclosure A:
Robotcontroller Interface for Flex 4000

Robotcontroller Interface for FLEX 4000

MIGATRONIC

Valid from 0318 50173514

1. The Robotcontroller interface, called RCI, is a general purpose interface for controlling and monitoring the FLEX 4000 by analog and digital signals. The RCI is non-configurable, and no setup is required before use.

2. The RCI communicates with the FLEX 4000 via a CAN-interface and is connected on the rear panel of the FLEX 4000 via a cable, which can be up to 50 meters.

3. The RCI is fully galvanic isolated from the FLEX 4000 except for the powersupply for the RCI, which is taken from the main powersupply in the FLEX 4000. This main powersupply is, however, also galvanic isolated from all other circuits in the FLEX 4000. These galvanic isolations prevents any problems with ground loops and noise interference.

4. The documentations for the RCI consists of the following:
   - Functional description with connections
   - Full schematic for the internal controller board
   - Component layout
   - Equivalent circuits for the analog and digital inputs and outputs
   - Mechanical drawing

Robot interface

Digital inputs

The interface has five digital input with the following functions and specifications:

Functions:

Trigger (start welding)
High level ~ Trigger Off
Low level ~ Trigger On

External error (from the robot)
High level ~ No External Error
Low level ~ External Error

Gas test
High level ~ Gas test Off
Low level ~ Gas test On

Wire inching
High level ~ Wire inching Off
Low level ~ Wire inching On

Pulse Change On / Off
(must be toggled to shift between On and Off)
High level ~ Pulse change Off
Low level ~ Pulse change On

All inputs are galvanic isolated

High input voltage	:	5 - 24 V DC
Low input voltage	:	0 - 2 V DC
Input impedance	:	2 k ohm ±10%
On / Off time	:	max. 5 ms

Digital outputs

The interface has three digital output with the following functions and specifications:

Functions:

Arc detect status
High level ~ Arc Off
Low level ~ Arc On

Common Error (from the Flex 4000)
High level ~ Error Off
Low level ~ Error On

Pulse On / Off Status
High level ~ Pulse Off
Low level ~ Pulse On

All outputs are galvanic isolated and are relais outputs

High output voltage:	+24 V DC ±5% or external supply (from robot)
Low output voltage :	0V
Output load current:	max. 50 mA

Analog inputs

The interface has two analog inputs with the following functions and specifications:

Functions:

Controlling the wirespeed / current
Controlling the voltage / voltage trim

All inputs are galvanic isolated and differential

Input voltage range	: 0 - 10 V DC (0 - 400.0 A / –9.9 - +9.9 V / 0 - 24.0 m/min / 0 - 50 V)
Common mode range	: ±20 V DC
Input resistance	: 400 k ohm
Bandwidth	: 120 Hz / 3 db (third order analog filter)
	: 25 Hz / 3 db
	: (first order digital filter)
Digital resolution	: 10 bit
Gain accuracy	: ±1 %

Analog outputs

The interface has two analog outputs with the following functions and specifications:

Functions:

Readout of actual welding current
Readout of actual welding voltage

All outputs are galvanic isolated

Output voltage range	: 0 - 10 V DC (equals 0 - 500 A / 0 - 100.0 V)
Output resistance	: max. 1 ohm
Load resistance	: min. 2 k ohm
Updating rate	: 1 / sec
Digital resolution	: 10 bit
Gain Accuracy	: ±1 %

Powersupply

The interface is supplied from the FLEX 4000 with + 55 V DC. The interface generates a + 24 V DC (current limit protected to 300 mA), which is brought out external for use in connection with the digital outputs or for any other use.

Connection

Pin 1 :	Arc detect status
Pin 2 :	Common error (from the FLEX 4000)
Pin 3 :	Unused
Pin 4 :	Pulse On / Off status
Pin 5 :	+24 V DC Intern supply
Pin 6 :	Supply for digital outputs
Pin 7 :	Trigger (start welding)
Pin 8 :	External error (from the robot)
Pin 9 :	Gas test
Pin 10:	Wire inching
Pin 11:	Pulse On / Off
Pin 12:	Digital ground (reference to + 24 V DC)
Pin 13:	Controlling Wirespeed / Current (+)
Pin 14:	Controlling Wirespeed / Current (-)
Pin 15:	Controlling Voltage / Voltage trim (+)
Pin 16:	Controlling Voltage / Voltage trim (-)
Pin 17:	Measured welding current
Pin 18:	Measured welding voltage
Pin 19:	Analog ground
Pin 20:	Analog ground

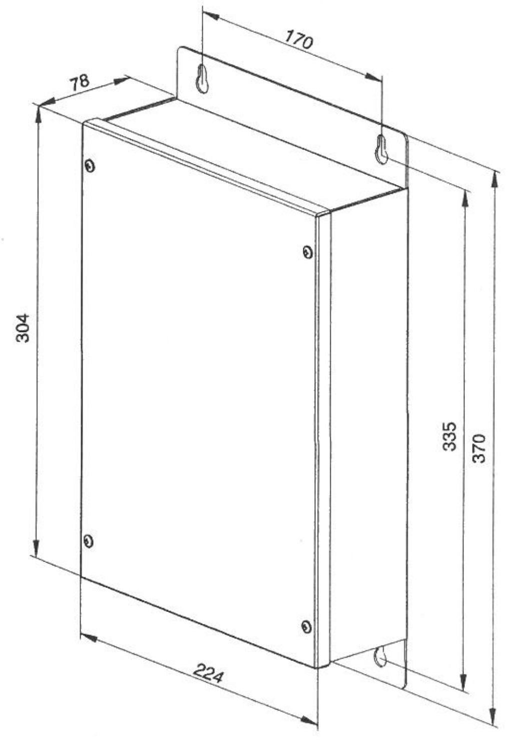

Enclosure B:
Matlab program for feature extraction and ANN training

The complete commented program and sub-functions can be found in "Program.zip"